MECA

Papers Presented to the

SYMPOSIUM ON MARS: EVOLUTION OF ITS CLIMATE AND ATMOSPHERE

July 17-19, 1986

Co-Sponsored by:

LUNAR AND PLANETARY INSTITUTE

SMITHSONIAN INSTITUTION'S NATIONAL AIR AND SPACE MUSEUM

PAPERS PRESENTED TO THE

SYMPOSIUM ON MARS:

EVOLUTION OF ITS CLIMATE AND ATMOSPHERE

Sponsored by:

Lunar and Planetary Institute

Smithsonian Institution's National Air and Space Museum

July 17-19, 1986

Washington, D.C.

Compiled by the

Lunar and Planetary Institute

3303 NASA Road One

Houston, TX 77058

LPI CONTRIBUTION 599

This abstract volume was compiled by the Publications Office, with assistance from Production Services, both of the Lunar and Planetary Institute, 3303 NASA Road One, Houston, TX 77058-4399. The Lunar and Planetary Institute is operated by the Universities Space Research Association under Contract No. NASW-4066 with the National Aeronautics and Space Administration.

TABLE OF CONTENTS

EVIDENCE FOR GLACIATION IN ELYSIUM; Duwayne M. Anderson, Gary W. Brandstrom, Texas A&M University

Evidence for the existence of permafrost and the surface modification due to frost effects and the presence of ice on Mars dates from early observations by Otterman and Bronner (1), Leighton and Murray (2), Anderson et al. (3), Baranov (4) and Anderson and Gatto (5). The Viking landers I and II confirmed the presence of water in the regolith and the periodic occurrance of frost at the surface of Mars, Bieman et al. (6), Anderson (7). Observations from the Viking Orbiters I and II demonstrated the presence of atmospheric water at various concentrations in the atmosphere of the planet (Farmer et al. [8]) and also provided a means of documenting the accumulation and sublimation of frost and ice in the two polar caps and at several other locations on the planet. Later analysis of the Viking Orbiter imagery produced evidence suggesting the former presence of ice sheets that could have played a part in shaping the surface of Mars (Lucchitta et al. [9]). Similarities have been pointed out between a number of streamlined Martian channel features and similar streamlined landforms created by antarctic ice sheet movements.

A study of Viking Orbiter imagery of Granicus Valles and the surrounding terrain in Elysium has produced further evidence of glaciation on Mars. Granicus Valles is located in the Northern hemisphere between 25 degrees and 40 degrees latitude and 220 degrees to 240 degrees longitude. It extends from the Elysium fossae near Elysium Mons to Utopia planitia, the plains where Viking Lander II is located. Granicus Valles has been characterized as an outflow channel (Malin [10], Carr [11]). It is approximately 1100 km long, about 10 km wide at the source, with distributory branches that cover an area approximately 300 km wide. Three distinctly different geological units are involved (Mouginis-Mark [12], Christiansen and Greeley, [13]). Part of the region is characterized as a Complex Vent Area. It is one of the main volcanic centers in Elysium. Another has been referred to as Modified Lava Plain by Christiansen and Greeley (13), and Compound Lava Plains and Erosional Plains by Mouginis-Mark (12). A portion of it was earlier referred to as Channeled Plain by Christiansen and Greeley (13).

Volcanism has played an important role in developing the landscapes of the Elysium region. Two features that strongly resemble terrestrial moberg ridges have been found. These features are ridge shaped, serrated mountains, very similar to the moberg ridges described by Allen (14). Terrestrial moberg ridges form as a result of subglacial, fissure eruptions. The only apparent difference between those observed on earth and these two Martian counterparts is scale; the Martian features are much larger. Because the

size of a moberg ridge is limited by the thickness of ice above the erupting fissure lava, the greater height of the Martian ridges implies a much thicker ice sheet. The height of the moberg ridge near Granicus Valles is about 2.6 km, indicating that the preexisting ice sheet was at least 2.6 km thick. The ground surface surrounding both Martian moberg ridges appears to have two distinct levels; it is lowest at the base of the ridges, rising to a level near the top of the ridges at a distance. A possible explanation is that subsidence occurred during formation of the Martian moberg ridges due to the melting of ground ice near the eruption area while at a distance most of the ground ice in the permafrost is still present and the original elevation has been preserved. Meltwater during and following eruptions might have been suddenly released during subglacial volcanism into Granicus Valles in one case and into Hrad Valles in the other. Fluvial erosion thus could have played a role in shaping both.

Crater size-frequency plots indicate differences in the ages of surfaces from one region to another, ranging from one to three billion years. The presence of a thick ice sheet together with underlying permafrost could help to explain this. A thick mantle of ice would have intercepted and contained many meteoric impacts, shielding the underlying regolith. Subsequent removal of this ice by sublimation or melting would then expose a relatively unmarked surface to subsequent meteoric bombardment. These surfaces, from crater size-frequency plots, would always appear younger than the surrounding, continuously exposed terrains.

Many of the volcanic edifices in Elysium appear to have uncommonly steep slopes at their bases. Many are quite large and probably stood above the hypothetical, pre-existing ice sheet. Volcanic flows and ejecta cascading down slope would have come to rest on the surrounding ice. Later disappearance of the ice would result in the subsidence and redeposition of these materials, helping to explain the abnormally steep basal slopes now evident.

References

1. Otterman, J. and Bronner, F.E. (1966), Martian Wave of Darkening: A Frost Phenomenon?, Science, 153, pp. 56-59.
2. Leighton, R. B. and Murray, B. C. (1966). Behavior of Carbon Dioxide and Other Volatiles on Mars, Science, 153, pp. 136-144.
3. Anderson, D. M., Gaffney, E. S., and Low, P. F. (1967). Frost Phenomena on Mars, Science, 155, pp.319-322.
4. Baranov, I. Ya. (1959). Geographical Distribution of Seasonally Frozen Ground and Permafrost,

Principles of Geocrynology, Part 1. V. A. Obruchev Institute of Permafrost Studies, Academy of Science, U.S.S.R.

5. Anderson, D. M., Gatto, L. W., and Ugolini, F. (1973). An Examination of Mariner 6 and 7 Imagery for Evidence of Permafrost Terrain on Mars. PERMAFROST: The North American Contribution to the Second International Conference, Yakutsk, Siberia. National Academy of Sciences, pp. 499-508.
6. Bieman, K., et al. (1976). Search for Organic and Volatile Inorganic Compounds in Two Surface Samples From the Chryse Planitia Region of Mars. Science, 194, pp.72-76.
7. Anderson, D. M. (1978). Water in the Martian Regolith. Comparative Planetology, Academic Press, Inc., pp. 219-224.
8. Farmer, C. B., et al. (1977). Mars: Water Vapor Observations From the Viking Orbiters. J. Geophys. Res., 82, pp. 4225-4248.
9. Lucchitta, B. K., Anderson, D. M., and Shoji, H. (1981). Did Ice Streams Carve Martian Outflow Channels? Proc. Third Coll. on Planetary Water, Niagara Falls, New York, Nature, 290/5809, pp.759-763.
10. Malin, M. C. (1976). Age of Martian Channels. J. Geophys. Res., 81, pp. 4825-4845.
11. Carr, M. H. (1981). The Surface of Mars, Yale University Press, New Haven.
12. Mouginis-Mark, P. J., et al. (1984). Elysium Planitia, Mars: Regional Geology, Volcanology, and Evidence for Volcano-Ground Ice Interactions. Earth, Moon, Planets, 30, pp. 149-173.
13. Christiansen, E. H., and Greeley, R. (1981). Mega-lahars(?) in the Elysium Region, Mars, (abstract). Lunar Planet. Sci. XII, pp. 138-140.
14. Allen, C. C. (1979). Volcano-Ice Interactions on Mars. J. Geophys. Res., 84, pp. 8048-8059.

NUMERICAL SIMULATIONS OF DUST TRANSPORT INTO NORTHERN HIGH LATITUDES DURING A MARTIAN POLAR WARMING; J.R. Barnes and J.L. Hollingsworth, Department of Atmospheric Sciences, Oregon State University, Corvallis, OR 97331

A beta-plane tracer transport model has been developed and used to carry out numerical simulations of dust transport into northern high latitudes during a polar warming event. Such transport is potentially of considerable significance for the Martian climate system (1). The tracer model is identical, in essential aspects, to that developed by Garcia and Hartmann (2). The model represents tracer transport by the zonal-mean circulation and a single large-scale wave, with a simplified (severely spectrally truncated) latitudinal tracer distribution.

The flow for the tracer transport simulations has been generated using a beta-plane nonlinear dynamical model. Experiments with this model have demonstrated that a polar warming, with essential characteristics like those observed by the Viking IRTM during the 1977 winter solstice global dust storm (3), can be induced by the same basic mechanism responsible for sudden stratospheric warmings on Earth: anomalous amplification of the forcing of vertically propagating, planetary scale waves (4). As discussed by Barnes and Hollingsworth (1), the dynamics of such a polar warming (as well as one not produced by the forced planetary wave mechanism) imply poleward and downward transport of tracers into high latitudes. The so-called residual mean meridional circulation should constitute a good first approximation appropriate for the transport of tracers (5). Figure 1 shows the residual mean meridional velocity (at the center of the beta-plane channel, 60 degrees latitude) for a warming simulation with the nonlinear dynamical model. Very strong poleward flow (up to 7.5 m/s) is present throughout the warming above 20 km. There is weak equatorward flow below 20 km which develops after the peak warming occurs at about sol 10. In conjunction with this the residual mean vertical velocity is strongly downward (up to 5 cm/s) at high latitudes, at all levels, throughout the warming. This residual mean meridional circulation would be expected to produce significant poleward and downward transport of tracers (e.g., dust) which are initially confined largely equatorward of 60 degrees latitude. The extent of such transport might depend fairly strongly on the amounts of the tracer initially present at upper levels (above 20 km) at lower latitudes.

The numerical tracer simulations that have been carried out have been aimed at dust transport during a polar warming, given an initial zonal-mean distribution of dust that could have been produced by the zonally symmetric circulation in the very early stages of a global dust storm (6). The sensitivity of the dust transport to its initial vertical distribution has been examined, as well as the sensitivity to factors which influence the character of the polar warming, such as the zonal wind profile, the radiative damping, and the nature of the wave forcing. An attempt has been made to simulate dust deposition on the surface by incorporating a simple sedimentation term in the tracer transport model.

SIMULATIONS OF DUST TRANSPORT
Barnes, J.R. and Hollingsworth, J.L.

References:

(1) Barnes, J.R., and J.L. Hollingsworth (1986) Implications of a polar warming for dust transport into the north polar region of Mars. Abstracts of the MECA Workshop on Dust on Mars, LPI publication, p. 8-9.
(2) Garcia, R.R. and D.L. Hartmann (1980) The role of planetary waves in the maintenance of the zonally averaged ozone distribution of the upper stratosphere. J. Atmos. Sci., 37, 2248-2264.
(3) Martin, T.Z. and H.H. Kieffer (1979) Thermal infrared properties of the Martian atmosphere. 2. The 15 μm band measurements. J. Geophys. Res., 84, 2843-2852.
(4) Barnes, J.R. and J.L. Hollingsworth (1985) Dynamical modeling of a Martian polar warming. Bull. Amer. Astron. Soc., 17, 3:733.
(5) Holton, J.R. (1981) An advective model for two-dimensional transport of stratospheric trace species. J. Geophys. Res., 86, 11,989-11,994.
(6) Haberle, R.M., C.B. Leovy and J.B. Pollack (1982) Some effects of global dust storms on the atmospheric circulation of Mars. Icarus, 50, 322-367.

Figure 1: The residual mean meridional velocity at the center of the beta-plane channel (60 degrees north) for a wavenumber 1 polar warming simulation. The velocity is in m/s and the contour interval is 1 m/s; shaded regions represent equatorward flow. The vertical axis is height in km, and the horizontal is time in sols.

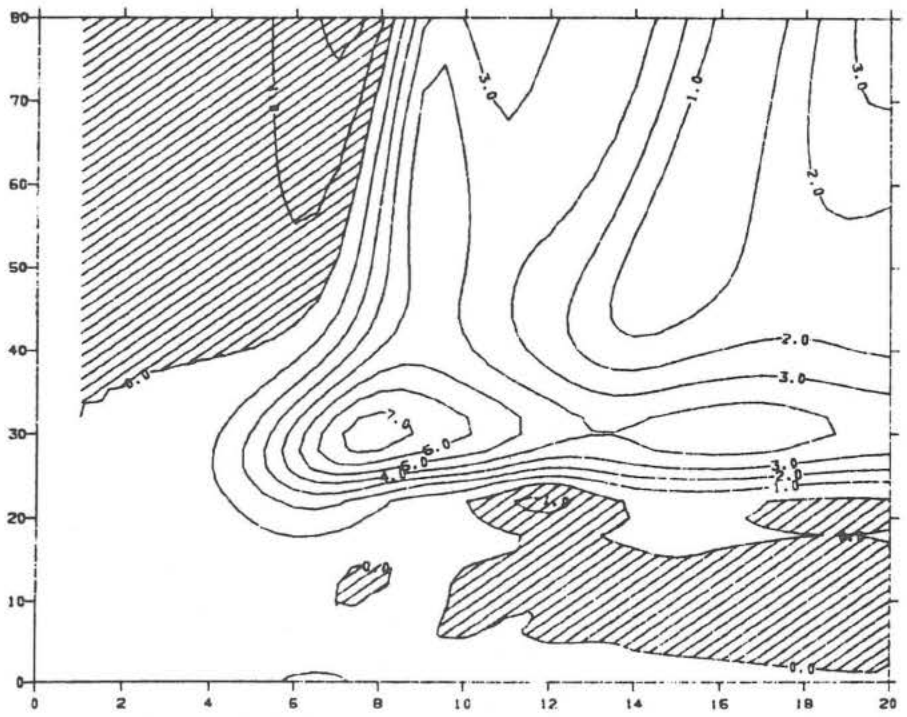

THE PALEO-OCEAN OF MARS; John E. Brandenburg
Mars Research

The hypothesis that Mars once had an ocean filling the low northern plains to the 0 kilometer elevation contour is based on four observations:

1. The upper limits on Mars' original inventory of water are large enough to permit oceans (a 200 meter layer covering the planet's surface (1)).
2. The presence of myriad water channels of varying age suggests that liquid water exist and flow on the surface during some period or periods in Mars' past (2).
3. The dichotomy separating the low northern plains from older, higher terrain appears to coincide approximately with the 0 kilometer elevation contour around their entire boundary.
4. The present distribution of water vapor on Mars appears strongly asymmetric, with an apparent strong source concentration in the north but little in the south (3).

The resemblance of the northern plains to an old ocean bed was noted by Mutch et. al. (4) and the possibility of a Paleo-ocean was discussed by Chandler (5) and in a paper given at the Case for Mars II conference (6).

I. Extent and Evolution:

If such an ocean had existed it would have represented approximately ¼ of the planets surface filled to a depth of 1.5 km. Following this pattern two smaller seas would have filled Argyre and Hellas Planitia in the south with another small sea in the south polar depression. The amount of water required would have covered the entire surface of Mars to a depth of 400 meters. This figure is only twice the upper limit on water inventory inferred by McElroy (1).

Dating of the Viking landing sites, both on the floor of the Paleo ocean, suggests the ocean existed until 1 to 1.5 Gy ago. Such an ocean would have formed early in the history of Mars when its atmosphere was dense and warm, accompanying a period of intense outgassing. The loss of atmosphere and its accompanying greenhouse effect would have caused a rapid spread of ice across the oceans surface from the northern polar cap. The ocean would have formed an ice sheet covering a mud layer that slowly sublimated from its surface. The water vapor would then be lost to space via ultra violet photolysis. Assuming that the early period of liquid ocean lasted long enough, a weather cycle would have operated in the northern hemisphere of Mars, transporting water by precipitation to the surrounding highlands and forming a water table of depth corresponding to the present 0 kilometer line. This "charged aquifer" could

have provided the source for catastrophic floods later in martian history as the ocean - ice sheet receded and allowed a large hydrostatic pressure head to develop between the aquifers surrounding the ocean basin and the emptying basin itself. The concentration of water in the lowest elevation of Mars during a period when water could run downhill would be preserved as the atmospheric pressure and temperature dropped. The water concentrations would be largely immobilized with transport confined to sublimation and loss to space.

II. Comparison With Other Data

The general absence of cliffs or beaches indicating an old shoreline was noted by Masursky et. al. (2), however, both a sharp cliff line, punctuated by chaotic terrain, and a delta-like deposit occur where Shalbatana Vallis enters the Chryse basin at the 0 kilometer line. A similar delta like feature occurs at the 0 kilometer line in Hrad Vallis in Utopia. The appearance of polygonal ground, ubiquitous on the northern plains and attributed to thick permafrost (7), is roughly coincident with the 0 kilometer contour in the Cydonia Mensae region. Such a layer would seem consistent with a muddy, frozen sea bed. The existence of "pedestal craters" on the northern plains has also been attributed to meteor impacts into ice saturated soil.

The Viking landing sites were both on the floor of the hypothesized Paleo-ocean. Does the 'ground truth' available at these sites support this hypothesis? The soil at the landing sites appeared similar to smectite ocean clays (8) found on earth and was covered by a duricrust containing concentrations of water soluble sulphates, carbonates and salt. However, the soil also matched well with plagonites formed by basaltic lava - ice interactions and the duricrust is found in terrestrial deserts.

The chief problem with the hypothesized Paleo-ocean is its long life. If an ocean and later ice sheet covered the northern plains until 1.5 billion years ago the presently observed rate of water loss is insufficient to account for its disappearance by at least two orders of magnitude. Percolation of the water into the regolith, another loss mechanism, would seem inconsistent with a stable ocean bed.

THE PALEO-OCEAN OF MARS;
Brandenburg, J.E.

References:

(1) McElroy, M.B., T.Y. Kong, and Y.L. Yung - J. Geophys. Res., 82, 4378, 1977.

(2) Harold Masursky, J.B. Boyce, A.L. Dial, G.G. Schaber and M.E. Strobell - J. Geophys. Res., 82, 4625, 1977

(3) C.B. Farmer et. al., Science, 194, 1339, 1976.

(4) Mutch, Thomas; Arvidsen, Raymond; Head, James III; Jones, Kenneth; and Saunders, R. Stephen. "The Geology of Mars", Princeton N.J., Princeton University Press, 1976.

(5) David L. Chandler, "Life on Mars", E.P. Dutton, New York, New York, P. 74.

(6) William Beatty et. al., "The Preliminary Findings of the Independent Mars Investigation Team, New Thoughts on Unusual Surface Features", Case For Mars II Conference, Boulder, Colorado, July 1984.

(7) Micheal H. Carr and Gerald G. Schaber - J. Geophys. Res., 82, 4039, 1977.

(8) Priestley Toulmin III et. al. - J. Geophys. Res., 82, 4625, 1977.

MARS: A WATER-RICH PLANET: Michael H. Carr, U. S. Geological Survey, Menlo Park, CA 94025.

Mars is estimated to have outgassed 0.5-1 km of water, 10-20 bars of CO_2, and 0.1 to 0.3 bars of N_2. These estimates are significantly larger than most previous estimates but are consistent with what is known of the geology of the surface, the composition of the atmosphere and the chemistry and mineralogy of SNC meteorites. Some of the strongest evidence for large amounts of water is from the cratered uplands. In both the northern and southern hemispheres the character of the cratered uplands changes at roughly the 30° latitude. Fretted terrain (Sharp, 1973) and terrain softening (Squyres and Carr, 1986) both suggest the presence of significant amounts of ice within 2 km of the surface at the higher latitudes. In the fretted terrain, presence of abundant ground ice is suggested by its latitudinal distribution, the mobility of debris flows, the presence of closed depressions, and tunneling (Sharp, 1973; Lucchitta, 1984, Squyres, 1978). Terrain softening is best explained by the presence of ice near the surface in sufficient quantities to reduce the effective viscosity of the near-surface materials. Extreme softening in the 30-55° latitude band and less softening in the 55-90° latitudes is consistent with the changing viscosity of ice at the mean temperatures at these latitudes (Lucchitta, 1984). The amount of ice required to change the viscosity and to cause the features of the fretted terrain is unknown but, by analogy with terrestrial features, is believed to be in excess of the porosity, estimated to be at least 10 percent by volume.

Fretted terrain, terrain softening, and debris flows are absent from the cratered uplands at low latitudes (<30°). This suggests that ice, or water, have not been present in the near-surface materials in sufficient quantities to affect their mobility since the geologic record emerged 3.8 billion years ago. Talus was produced on steep slopes as within craters, but it has not had the mobility to flow away from the slopes to produce the variety of flow features seen in the 30-55° latitude bands. Although the surface materials have not flowed, the branching valley networks provide convincing evidence for the presence of groundwater, at least during the early history of the planet. The presence of the networks, coupled with the lack of flow of the near-surface materials, suggests that the water was interstitial, that is, it was present in amounts less than the porosity. Thus, as early as when the geologic record emerged 3.8 billion years ago, a latitudinal contrast had developed between the water content of the near surface materials at high and low latitudes. At high latitudes water was present in amounts that exceeded the porosity; at low latitudes water was present in amounts less than the porosity.

The deep megaregolith has a substantial water-holding capacity (Carr, 1979; Clifford, 1981), the difficulty is knowing the extent to which the capacity is filled. Many of the large outflow channels may have formed through eruption of groundwater under high pressure from the megaregolith beneath the permafrost, which is estimated to have been about 1 km thick. (Carr, 1979). A lower limit on the amount of water involved in formation of the outflow channels can be derived by assuming that the volume of water that flowed through the channels had to be at least as large as the volume of materials eroded to form the channels. This is equivalent to assuming that all the water that flowed through the channels carried the maximum sediment

load (Komar, 1980). The total volume eroded to form the circum-Chryse channels is estimated to be 5×10^6 km^3, or 35 meters averaged over the entire planet. The area over which the megaregolith was drained to form these channels is unknown but reasonable limits are the summit of the Tharsis ridge to the west, the center of the Tempe plateau to the north, and to the south and east the limits of chaotic terrain. This area is 1.6×10^7 km^2 or roughly one tenth of the planet's surface. If we further assume that the water content of the megaregolith in this region was no different from that in other parts of the planet then we conclude that the megaregolith, below one 1 km, planet-wide, contained no less than 350 meters of water. Implicit in this assumption is that the outflow channels are located in the Chryse region not because the megaregolith here contained more water, but because relief was present to create the hydrostatic head needed to drive the water through the permfrost cap to the surface. The assumption of a generally uniform distribution of water in the surface is supported by the uniform distribution of valley networks in the cratered uplands (Clow and Carr, 1981). To the 350 meters must be added the 50-100 meters estimated to be present in the upper 1 km of the cratered uplands at high latitudes, to give a total inventory of 400-450 meters. This is a conservative number in that the assumption that the volume of water that flowed through the cirum-Chryse outflow channels equals the volume of the channels is very conservative. Moreover the megaregolith is unlikely to have been drained dry in the process of making the channels. Finally, the 400-450 meters represents only unbound water. Significant amounts of water may be bound in weathered debris and in primary minerals. In excess of 500 meters of water is thus believed to have been outgassed from the planet.

As indicated above, the contrast between high and low latitudes had already been partly established when the impact rates declined around 3.8 billion years ago, with the near-surface materials containing less water than those at high latitudes. After the impact rates declined, depletion of the low latitudes continued by groundwater seepage, formation of floods and simple diffusion. That lost during large floods appears to have mostly pooled in low-lying areas at high latitudes where numerous features that have been attributed to the presence of ground ice are observed (Carr and Schaber, 1977; Rossbacher and Judson, 1981; Lucchitta, 1981). That lost through formation of valley networks and by diffusion may be presently in the polar layered deposits. Since the impact rates declined much of the surface has been overplated by water-poor, mantle-derived volcanics of which we have representated in the SNC meteorites.

Outgassing of over 0.5 km of water is consistent with the geochemical evidence. Low water inventories estimated by Anders and Owen (1977) and Rasol and LeSergeant (1977) were based on the assumptions that all the argon outgassed from Mars is still present in the atmosphere, and that the ratio of the non-radiogenic noble gases to other volatiles on Mars is the same as on Earth. Both these assumptions are now suspect. Noble gases could have been lost from the early atmopshere by impact erosion or hydrodynamic escape, and the noble/non-noble gas ratio is demonstrably not the same on Venus as on Earth, so the assumption that Mars should be the same as the Earth is

questionable. Although nitrogen isotopes may be used successfully to derive the nitrogen content of the early atmosphere (McElroy and Yung 1976), their utitilty in deriving the total volatile inventory is more doubtful because of uncertainties in the amounts of nitrogen fixed in the ground. SNC meteorites suggest that Mars is richer than the Earth in moderately volatile elements (Dreibus and Wanke, 1984), as is expected from models of planetary accretion (Lewis, 1974), but they contain little evidence on abundances of the more volatile atmosphilic elements.

REFERENCES

Anders, E., and Owen, T., Science, 198, 453-465, 1977; Carr, M. H., J. Geophs. Res., 84, 2995-3007, 1979; Carr, M. H., and Clow, G. D., Icarus, 48, 91-117, 1981; Carr, M. H. and Schaber, G. G., J. Geophys. Res., 82, 4039-4065, 1977; Clifford, S. M., Proc. 3rd Int. Colloq. on Mars, Pasadena, CA, 46-48, 1981; Dreibus, G., and Wanke, H., Proc. 27th Int. Geol. Congr., Moscow, 11, 1-11, 1984; Komar, P. D., Icarus, 42, 317-329, 1980; Lewis, J. S., Sci. American, 230, no. 3, 50-65, 1974; Lucchitta, B K., Icarus, 45, 264-303, 1981; Lucchitta, B. K., J. Geophys. Res., 89, B409-B418, 1984; McElroy, M. B., and Yung, Y. L., J. Geophys. Res., 82, 4379-4388, 1976; Rasool, S. I., and LeSeargeant, L., Nature, 266, 822-823, 1977; Rossbacher, L. A., and Judson, S., Icarus, 45, 25-38, 1981; Sharp, R. P., J. Geophys. Res., 78, 1045-1049, 1973; Squyres, S. W., Icarus, 34, 600-613, 1978; Squyres, S. W., and Carr, M. H., Science, 231, 249-252, 1986.

MARTIAN VOLCANISM: A REVIEW. Michael H. Carr, U. S. Geological Survey, Menlo Park CA 94025

Volcanic activity was widespread on Mars when the geologic record emerged around 3.8 Ga ago but became progressively more restricted with time such that the most recent activity has been largely confined to the large Tharsis shields (Scott and Carr, 1978). Two man types of activity are recognized: formation of lava plains, presumably as result of fissure eruptions, and accumulation around central vents to form roughly circular volcanoes. Both types appear to have been dominated by effusion of low viscosity lava that has formed a variety of landforms such as lobate flow fronts, leveed channels and sinuous rilles, that are familiar from terrestrial, and lunar basaltic terranes.

Lava plains probably constitute the bulk of the volcanic products. Three main types can be recognized (Carr, 1981; Greeley and Spudis, 1981). (1) On flow plains individual flows can be readily identified, and ridges like those on the lunar maria are generally absent. Flow plains are common in central Tharsis, central Elysium, around Alba Patera, in Solis Planum and Syria Planum and on the south of Hellas. The size of the flows suggests that effusion rates were extremely high compared with typical terrestrial rates. (2) On ridged plains flows are rarely observed but ridges similar to those on the lunar maria are common. Ridged plains are found mainly in Chryse Planitia, Lunar Planum, eastern Syria Planum, and Hesperia Planum, and small areas occur locally throughout the cratered uplands. The plains are presumed to be volcanic largely on the basis of their resemblance to lunar maria. Most ridged plains are older than the flow plains. (3) Pitted plains are present in some areas, particularly in Isidis Planitia. These are characterized by lines of small <1 km diam.) cones, that may merge to form ridges with slotted central vents (Frey and Jarosewich, 1982). The ridges resemble spatter ramparts, such as occur along the Hawaiian rift zones. Not all plains fall into these three types. Extensive areas of plains have a variety of characteristics that are difficult to reconcile with a simple volcanic origin. Many of their features have been attributed presence of ground ice or the result of interaction of volcanics with ground ice (Carr and Schaber, 1977; Lucchitta, 1981; Allen, 1979). These plains, in which the volcanic component is unclear, include Amazonis Planitia, the peripheral regions of Elysium Planitia, and most of the plains in the high northern latitudes.

The central-type volcanoes provide the most obvious manifestations of martian volcanism. Several types are recognized (Greeley and Spudis, 1981). (1) Shield volcanoes typically have large summit calderas and gently sloping flanks on which are numerous long linear flows. The three large shields of central Tharsis appear to have gone through a similar growth cycle - the building of a radially symmetric shield to a height of about 25 km above the Mars datum was followed by eruptions from the NE and SW flanks which caused embayments in the shields, buried their lower flanks, and covered extensive areas of the surrounding plains. Growth of Olympus Mons was more symmetric. The lithosphere appears to have deformed under the weight of the large shields. Estimates of the thickness of the elastic lithosphere from its flexure range from 20 km under Arsia and Ascreaus Mons to 150 km under Olympus Mons (Comer et al., 1985). All the large Tharsis shields have terraced flanks, possibly the result of thrusting caused by compression of the edifice.

as the lithosphere flexes under the volcano load (Morris, personal comm.). Large central calderas suggest the volcanoes incorporate or overlie magma chambers that are large compared with those under terrestrial shield volcanoes (Wood, 1984). Several small shield volcanoes in Tharsis and Elysium are partly buried by lavas that form the surrounding plains. (2) Domes or Tholi generally have smaller diameters and steeper slopes than the shield volcanoes. The group also includes some small shields, but includes some volcanoes that are distinctively different from shields. Hecates Tholus and Ceraunius Tholus have densely pitted flanks with numerous roughly radial channels. The summit of Hecates Tholus is muted as though blanketed with debris. All these features have been ascribed to pyroclastic activity (Reimers and Komar, 1979; Mouginis-Mark et al., 1979; Greeley and Spudis, 1981). Whether the explosive activity is the result of a distinctive composition of the lavas or interaction of basaltic lava with groundwater is unclear. (3) Patera is a term applied to volcanoes with very little vertical relief, but the various paterae have little in common other than low relief. The largest patera, Alba Patera, is over 1500 km across and has flanks that slope less than 1°. From the features on its flanks it appears to have been built almost entirely of low viscosity lava. In contrast, Tyrrhenna Patera appears to be surrounded by deeply eroded horizontal sheets of debris, as though formed mainly by ash flows.

Comparison of the martian volcanic features with those of the Earth and the Moon suggests that the volcanism has been dominantly basaltic. Such a composition is consistent with the available spectroscopic data (Singer et al., 1979;), and interpretation of analyses of debris from the Viking landing sites (Toulmin et al., 1977). The SNC meteorites suggest that the martian mantle is more iron rich than the Earth's and richer in moderately volatile elements such as Na, K, and Rb (Dreibus and Wanke, 1983). Modeling of planetary accretion also suggests that the Mars mantle is more iron-rich than the Earth's (Lewis, 1972, 1974; Ringwood and Clark, 1971). These models of composition of the Mars mantle are consistent with a mantle density of 3.44 gm cm^{-2} estimated from the planet's mean density and moment of inertia factor (Goettel, 1983). The intercumulus melts from Shergotty liquid yield liquids with viscosities around 200 poise as compared with values of 400-1000 poise typical of terrestrial basalts (McSween, 1985). Thus the properties of the lavas inferred from surface morphology, surface reflectivity, SNC meteorites and the bulk planet properties are all consistent.

REFERENCES

Allen, C. C., J. Geophys. Res., 84,, 8048-8059, 1979; Carr, M. H., The Surface of Mars, Yale University Press, 1981; Carr, M. H., and Schaber, G. G., J. Geophys. Res., 82, 4039-4065, 1977; Comer, R. P., Solomon, S. P., and Head, J. W., Rev. Geophys., 28, 61-92, 1980; Dreibus, G., and Wanke, H., Proc. 27th Int. Geol. Congr., Moscow, 11, 1-11, 1984; Frey, H., and Jarosewich, M., J. Geophys. Res., 87, 9867-9879, 1882; Goettel, K. A., Carnegie Inst. Year Book, 82, 363-366, 1983; Greeley, R., and Spudis, P., Rev. Geophys. Space Phys., 19, 13-41, 1981; Lewis, J. S., Earth and Planet. Sci. Lett., 15, 286-290, 1972; Lucchitta, B. K., Icarus, 45, 264-303, 1981; McSween, H. Y., Lunar and Planet. Sci. XVI, 546-547, 1985; Mouginis-Mark, P. J., Wilson, L., and Head, J. W., J. Geophys. Res., 87, 9890-9904, 1982; Reimers, C. E., and Komar, P. D., Icarus, 39, 88-110, 1979; Ringwood, A. E.,

and Clark, S. P., Nature, 234, 89-92, 1971; Scott, D. H., and Carr, M. H., U. S. Geological Survey, Misc. Inv. Map I-1083, 1978; Singer, R. B., McCord, T. B., Clark, R. N., Adams, J. B., and Huguenin, R. L., J. Geophys. Res., 84, 1979; Toulmin, P., Baird, A. K., Clark, B. C., Keil, K., Rose, H. J., Christian, R. P., Evens, P. H., and Kelliher, W. C., J. Geophys. Res., 82, 4625-4634, 1977; Wood, C. A., J. Geophys. Res., 89, 8391-8406, 1984.

COMETS, VOLCANISM, THE SALT RICH REGOLITH AND CYCLING OF VOLATILES ON MARS; Benton C. Clark, Planetary Sciences Laboratory, Martin Marietta Denver Aerospace, Denver, CO 80201.

Many independent estimates of the total volatile inventory in the surface and near-surface of Mars have been made based upon noble gas measurements and analogies with terrestrial and/or meteorite data. As compiled in Table I, volatile inventory models range from 1100 to over 24,000 g/cm^2 for the elements C, H, O, and N (the "CHON" group). Of this, H_2O is estimated variously to comprise 46% to 80% of the total. The spread in the CO_2 component is much larger, from 5% to 53%, while N is consistently estimated at less than 1% of the total for the CHON group. The predictions for the ratio C/N (weight/weight) vary from 4 to 28. Two other elements, S and Cl, are often found at significant concentration in volcanic and fumarolic gases. Inventory predictions for these two elements are less common, but as discussed below, they may drastically alter the fate of molecules incorporating the CHON elements.

Table I. Volatile Inventories

	A	B	C	D	E	F	G
Total CHON (g/cm^2)	16-27	300 to 30,000	1108	2021	9423	18,058	24,000
H_2O	0.02%	0.5-10%	53%	47%	80-94%	74%	66-86%
CO_2	96%	0-10%	46%	52%	5-11%	26%	13-33%
N	2.6%	0-10%	0.7%	0.5%	0.2%	0.3%	1%
Reference	Atmos.	Regolith	1 RHK	2 A & O	3 C & B	4 MKY	5 P & B
C/N ratio	10	-	18	28	7-15	24	4-9

The role of comets. From remote observations, it has been known for some time that comets contain abundant H_2O as well as organic compounds and N-containing molecules, particularly HCN. The total predicted volatile inventories for Mars could be produced by the impact with only 10^4 to 10^5 comets, following the primary accretion of the planet.

During the recent flyby of Comet Halley, a variety of organic molecules in the gas phase were apparently detected, although the CO_2/H_2O ratio inferred for the ices was less than 0.035 [6]. Particle composition analysis discovered grains with C and S, as well as grains with CHON composition [7]. If cometary material is of the same overall average composition (including both ices and dust grains) as the sun, the ratios will be C/N=4 and S/Cl=102. Further analysis of the Giotto and Vega measurements may permit reasonably accurate estimates of these ratios, irrespective of the complexity of the distribution of these elements among various chemical phases. The results published so far are not inconsistent with these predictions.

As listed in Table I, the current Mars atmospheric ratio for C/N is

10. Allowing for a relatively large loss in N due to exospheric escape [4], the starting ratio could have been as low as 2. On the other hand, virtually all authors predict large amounts of "missing" CO_2, which apparently is stored in the regolith. Such storage, either as carbonate minerals or as cryo-adsorbed gas, is much easier than with N because of the greater problem of formation of the nitrates and the lower partial pressure and adsorption energy of N_2 gas from the atmosphere. Whether the C/N ratio can be used as a discriminator for or against a major contribution by cometary material to the volatile inventory on Mars must await more definitive results on the chemical composition of cometary nuclei and accurate information on the C and N-bearing molecular components in the martian soil.

Use of H or O in constructing discriminating atomic ratios is almost certainly more difficult because of the distribution of O among many chemical phases, the incorporation of H_2O and OH into the regolith, and the uncertain magnitude of the losses of H by escape during the history of the planet.

More useful should be the S/Cl ratio, which on earth is only 0.3, but is 4 in the martian soil [8], still some 25 times lower than predicted for comets on the basis of solar and chondritic meteorite abundances. Clearly, only if comets are found to be anomously halogen-rich can they be the major source of these volatile elements, and presumably the others as well, on Mars. Their effect, however, could be to raise the S/Cl ratio if planetary outgassing mimics the terrestrial proportion; about a 3-4% contribution to the volatile inventory would be sufficient. An equivalent cometary contribution to the 30x higher inventory on earth would be undetectable.

The salt-rich regolith. At both Viking lander sites, the fines contain abundant S and Cl, almost certainly as sulfate and chloride salts, respectively. Based upon spectroscopic limits for active gases in the atmosphere, more than 99.999% of the S and Cl inventories reside in the regolith of Mars.

Likewise, all estimates of volatiles place the majority of the CHON materials in the regolith fines, since the atmosphere and polar cap reservoirs are demonstrably too small. Neither the Viking XRFS nor the GCMS instruments were capable of detecting carbonates or nitrates, although it was often suggested during development of the latter that soil acidification be added to the experiment. Remote-mapping infrared spectroscopy has placed some upper limits on these minerals, but unambiguous and quantitative detection by this means probably must await the Mars Observer mission. Thermal adsorption processes could be the primary mechanism for uptake of the C and N gases; quantitative predictions are extremely model dependent because of the wide range in properties of the silicate minerals which may or may not be present.

Whichever salts are present, they are sure to be hygroscopic when the temperature and H_2O partial pressure are appropriate. Modeling of climatic cycling of water through the regolith has generally avoided this consideration because the rates of the hydration reactions at low temperatures are presumably not well knwon. In addition, the ubiquitous duricrust can, in principle, form a relatively impermeable barrier by virtue of salt-filling of pore spaces, although the Viking duricrusts are

surprisingly friable. Of special interest in this connection is the recent deduction that the duricrust in the vicinity of the Viking sites is unusually "thin" with respect to the other widespread occurrences on Mars [9].

The roles of volcanism. The worldwide eruptive emissions of volcanoes combine to add gases to earth's atmosphere at an average S/Cl ratio of about 5-to-1 [10], a value quite close to the observed ratio in soil on Mars, as previously noted [8]. Furthermore, these gases are chemically very active; even in the cold, dry environment of Mars it has been shown that SO_2, for example, rapidly and quantitatively destroys carbonates and nitrates [11]. Thus, with every volcanic eruption, these minerals will be forced to release C and N (in gases) to the atmosphere. Additional carbonates and nitrates may form, via very slow reactions under contemporary conditions [12], with unreacted igneous minerals in the soil. Even at one-tenth the terrestrial rate [10], some 660 g/cm^2 of SO_2 would be released over geologic time, adequate to recycle much or all of the CO_2 at least once.

Volcanic activity can also serve to irreversibly remove volatiles by sealing over regolith deposits with lava flows. Although some volatiles may be thermally released at the contact zones, this will be small compared to the amounts buried. Without tectonic subduction or aqueous errosion processes, it is unlikely these volatiles can ever be recycled to the atmosphere. Impact blanketing can similarly bury volatile-rich sediments.

Note on returned sample handling strategies. Most sample return studies have focused on the rocks of Mars. The enormously pivotal question of the history of the climate hinges upon the fine-grained component of the regolith. For it is here that the chemically and physically trapped volatiles will be found. Perturbations of the sample during the sampling process will be much more likely than with the taking of rock. Relatively small deviations from the ambiant temperature and vapor conditions could destroy key mineral phases and cause the loss of adsorbed volatile species. On-site studies, such as of thermally-induced gas release, combined with experiments on earth, such as measurement of adsorption isotherms and their hysteresis characteristics, may help resolve such problems. Nonetheless, the preservation of the physico-chemical state of regolith cores should receive the highest priority.

References

1. Rasool S. I., et al., Physics Today (July 1977) 23-32.
2. Anders E. and Owen T. (1977) Science, 198, 453-465.
3. Clark B. and Baird A. K. (1979) Geophys. Res. Lett., 6, 811-814.
4. McElroy M. B. et al. (1977) J. Geophys. Res., 82, 4379-4388.
5. Pollack J. B. and Black D. C. (1979) Science, 205, 56-59.
6. Krankowsky D. et al. (1986) Nature, 321, 326-329.
7. Kissel J. et al. (1986) Nature, 321, 336-7.
8. Clark B. C. and Baird A. K. (1979) J. Geophys. Res., 84, 8395-8403.
9. Jakosky B. M. and Christensen P. R. (1986) Icarus, 66, 125-133.
10. Cadle R. D. (1975) J. Geophys. Res., 80, 1650-1652.
11. Clark B. C. et al. (1979) J. Molec. Evol., 14, 91-102.
12. Kahn R. (1985) Icarus, 62, 175-190.

MARS: CRUSTAL PORE VOLUME, CRYOSPHERIC DEPTH, AND THE GLOBAL OCCURRENCE OF GROUNDWATER; Stephen M. Clifford, Lunar and Planetary Institute, 3303 NASA Rd. 1, Houston, TX, 77058.

There is considerable photogeologic evidence which indicates that Mars, like the Moon, underwent an early period of intense bombardment, producing a "megaregolith" of crater ejecta, interbedded volcanics, weathering products, sediments, and intensely fractured basement, that is likely to extend to considerable depth (1,2). Evidence in support of this conclusion comes from the seismic propagation characteristics of the outer layer of the lunar crust, where P wave velocities increase with depth until they reach a local maximum at about 20 km (3,4,5). This behavior is consistent with a reduction in crustal porosity with increasing lithostatic pressure. The transition between fractured and coherent lunar basement is believed to coincide with the beginning of the constant velocity zone at a depth of 20 km, where lithostatic pressure is thought to be sufficient (>1 kbar) to completely close all fracture and intergranular pore space (3,4,5).

Binder and Lange (5) argue that the seismic properties of the lunar crust are best explained by an exponential decline in porosity with depth (to less than 1% at 20 km). Thus, at a depth z, the porosity is given by

$$\Phi(z) = \Phi(0) \exp(-z/K) \qquad (1)$$

where $\Phi(0)$ is the porosity of the crust at z=0 and K is the porosity decay constant. Given that the density of the martian crust is comparable to its lunar counterpart, the inferred value of the lunar porosity decay constant (6.5 km) can be gravitationally scaled to find the value appropriate for Mars (2.82 km) (5,6,7).

Applying Eq. (1) to Mars, two potential porosity profiles of the crust are illustrated in Figure 1. The first is based on a surface porosity of 20%, the same value assumed for the Moon by Binder and Lange (5). This model yields a self-compaction depth (the depth at which crustal porosity falls below 1%) of approximately 8.5 km, and a total pore volume of roughly 7.8×10^7 km^3. This pore volume is sufficient to store a global layer of water approximately 0.54 km deep. In the second profile, a surface porosity of 50% is assumed, a value that may be appropriate given a significant degree of weathering. The self-compaction depth predicted by this model is roughly 11 km, while its total pore volume is approximately 2×10^8 km^3, a volume equivalent to a global ocean some 1.4 km deep. Of course, it is doubtful that weathering will affect more than the upper 1-2 km of the martian crust; therefore, below this depth, the porosity profile will most likely resemble the gravitationally scaled lunar curve.

The fraction of the total pore volume of the martian crust that exists at a temperature below freezing, places an upper limit on the amount of H_2O that can be stored within the crust as ice. This "ground ice capacity" is easily calculated by combining the porosity profiles discussed above with a simple thermal model of the crust (7).

The martian cryosphere has been defined as that region of the crust where the temperature is below the freezing point of water (8). Assuming a solute-free freezing point of 273 K, this condition is satisfied everywhere at the martian surface, thus defining the cryosphere's upper bound. The depth to the cryosphere's lower bound can be calculated from the steady-state one-dimensional heat conduction equation:

$$d = k\,(T_{mp} - T_{ms})/Q_g \qquad (2)$$

where k is the thermal conductivity of the crust, T_{ms} is the mean annual surface temperature, T_{mp} is the melting point temperature, and Q_g is the geothermal heat flux (1,8). Based on a melting point temperature of 273 K, and reasonable estimates of thermal conductivity (8×10^4 erg cm^{-1} s^{-1}) and geothermal heat (30 erg cm^{-2} s^{-1}), the depth to the melting isotherm will vary from approximately 1 km at the equator to slightly in excess of 3 km at the poles (Table 1) (1,8). Of course, given the presence of salt in the regolith, the possibility exists that the freezing point of H_2O could be depressed well below 273 K (9,10). For example, saturated solutions of NaCl and $CaCl_2$ have associated freezing points of 252 K and 218 K respec- tively (10). Clearly, the presence of such potent freezing point depressors could reduce the depth to the melting isotherm significantly (Table 1).

Estimates of the total pore volume of the cryosphere can be obtained by integrating the porosity profiles in Figure 1 down to the melting isotherm depths presented in Table 1 for all latitudes. For the variety of possible permutations, the total pore volume of the cryosphere is found to lie within the range of 1.0×10^7 - 9.6×10^7 km^3; while the quantity of H_2O required to saturate this pore volume is equivalent to a global layer of water approx- imately 70 - 670 meters deep (Table 2).

Given a quantity of H_2O sufficient to fill the available pore volume of the cryosphere, how much additional H_2O is required to produce an aquifer of global proportions? Groundwater will drain to saturate the region of lowest gravitational potential; therefore, the volume of water required to produce an aquifer of a given thickness is calculated by integrating the pore volume of the region between the self-compaction depth and the water table. For example, a quantity of water equivalent to a global layer 10 meters deep is sufficient to saturate the lowermost 0.85 km of the porosity profiles seen in Figure 1; while a quantity of water equal to a 100 meter layer would create an aquifer nearly 4.3 km deep (Figure 2). These figures assume that Mars is a perfect sphere whose porosity profile is everywhere described by Eq. (1). In reality, the self-compaction depth undoubtedly exhibits a high degree of variability. Therefore, because groundwater will collect in the lowermost porous regions of the crust, the actual areal coverage of an aquifer may be substantially less than 100%.

The above calculations suggest that if the planetary inventory of outgassed H_2O on Mars exceeds by more than a few percent the quantity required to saturate the pore volume of the cryosphere, then a subpermafrost groundwater system of substantial proportions will necessarily result (7). This condition may be satisfied by an H_2O inventory as small as 100 m, however, in no event does it appear that it would require more than 700 m. The presences of such a system may have a significant impact on the long-term cycling of H_2O on Mars (7).

REFERENCES:

1) Fanale, F. P. (1976) Icarus 28, 179-202.
2) Carr, M. H. (1979) J. Geophys. Res. 84, 2995-3007.
3) Toksoz, M. N. (1979) Rev. Geophys. Space Phys. 17, 1641-1655.
4) Binder, A. B. (1980) J. Geophys. Res. 85, 4872-4880.
5) Binder, A. B. and M. A. Lange (1980) J. Geophys. Res. 85, 3194-3208.
6) Clifford, S. M. (1981) Third Int. Colloq. on Mars, LPI Cont. 441, 46-48.

7) Clifford, S. M. (1984) PhD dissertation, Univ. of Mass., 286 pp.
8) Rossbacher, L. A. and S. Judson (1981) Icarus 45, 39-59.
9) Brass, G. W. (1980) Icarus 42, 20-28.
10) Clark, B. C. and D. C. Van Hart (1981) Icarus 45, 370-378.

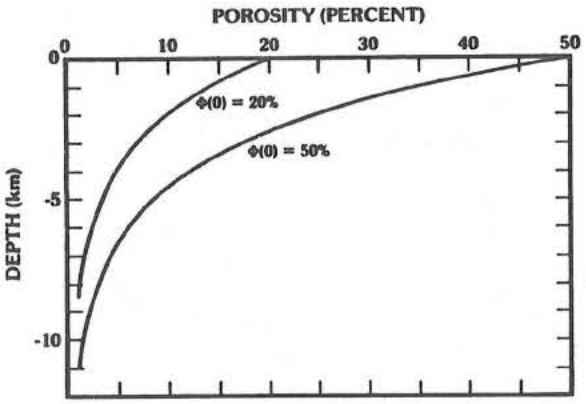

Figure 1

Table 1. Latitudinal variation of cryosphere thickness.*

Latitude	Mean annual surface temperature (K)	Cryosphere depths (km) T_{mp} = 273 K	252 K	218 K
0°	225	1.28	0.72	0.0
10°N/S	222	1.36	0.80	0.0
20°N/S	218	1.47	0.91	0.0
30°N/S	215	1.55	0.97	0.08
40°N/S	205	1.81	1.25	0.35
50°N/S	185	2.35	1.79	0.88
60°N	170	2.75	2.19	1.28
60°S	173	2.67	2.11	1.2
70°N	155	3.15	2.59	1.68
70°S	170	2.75	2.19	1.28
80°N	146	3.39	2.83	1.92
80°S	163	2.93	2.37	1.47
90°N	142	3.49	2.93	2.03
90°S	160	3.01	2.45	1.55

*After Fanale (1976) and Rossbacher and Judson (1981).

Table 2. Pore volumes of cryosphere for various surface porosities and melting isotherm temperatures.

Melting Isotherm (K)	Pore volume ($\times 10^7$ km^3)		Equivalent layer of H_2O (m)	
	Φ(0)=20%	Φ(0)=50%	Φ(0)=20%	Φ(0)=50%
218	1.01	2.53	70	175
252	2.90	7.26	200	500
273	3.86	9.64	270	670

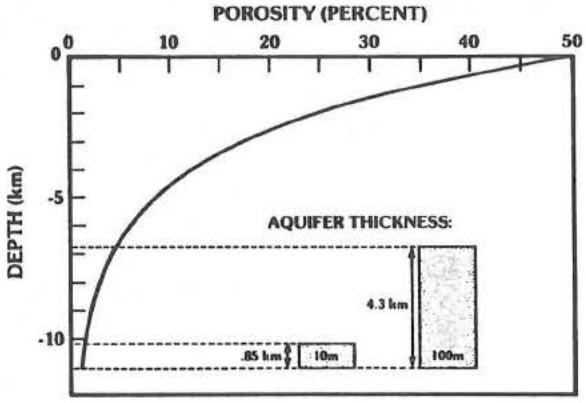

Figure 2

IS REGOLITH ADSORBTION THE EXPLANATION FOR THE TRANSITION FROM EARLY TO PRESENT MARS CLIMATE?; F.P. Fanale, S. Postawko, A.P. Zent, and J.R. Salvail, Planetary Geosciences Division, Hawaii Institute of Geophysics, University of Hawaii, Honolulu, Hawaii.

The total degassed CO_2 inventory on Mars is currently thought to be the equivalent of ~ 1.0 bar or less (1). Using the highest of these estimates, several radiative transfer models for early Mars have been advanced (2) proporting to show that a significant greenhouse effect could have characterized the early Mars environment, possibly explaining the intense channeling of the most ancient Mars terrain. However virtually all the available CO_2 would be needed in the atmosphere to achieve a significant greenhouse effect (3).

We have reexamined those models with regard to the effect that regolith adsorption may have had. In our model, we take into account: 1) the atmospheric greenhouse effect, 2) the existence, mass and temperature of any cap and 3) the partition of CO_2 between the atmosphere-cap system and the regolith as required by the latitudinal temperature distribution and 4) atmospheric heat transport.

We solve simultaneously for all these interdependent variables for cases involving realistic <u>total</u> CO_2 inventories (< 2 bar equivalent), a variety of published greenhouse models, and both current and lower solar constants.

To describe regolith adsorption properties we use the mineralogically insensitive adsorption relationship developed by Zent et al. (4), which is based on laboratory measurements on palagonite, nontronite, and basalt, and which is normalized to be consistent with observed surface properties of Viking-sampled soil (5). We should point out that adsorption is relatively more effective under current Martian conditions than at the higher temperature and pressure conditions that may have characterized the early Martian environment. However the regolith currently has adsorbed 10-100 times the atmospheric CO_2 inventory, whereas in most models, the removal of only half the original atmospheric CO_2 inventory would be sufficient to destroy the strong greenhouse effect.

Resulting scenarios fall into several classes. Either: 1) The greenh ouse effect is so weak that a cap exists throughout the period of growth of several hundred meters of regolith; in this case the surface environment is essentially unaffected by the development of any reasonably postulated regolith; or 2) A cap exists initially, but is sufficiently small that the growth of >100 m or so of regolith causes a significant repartitioning of CO_2 molecules among the three parts of the system and the equilibrium solution finally involves no cap. In this case the regolith has no effect on the atmospheric pressure and resulting temperatures <u>until</u> the cap disappears. However, once the cap disappears the effect of further regolith growth is to dramatically lower atmsopheric pressure and hence surface temperatures; or 3) A substantial greenhouse effect exists initially, and there is no cap initially. In this case also, regolith growth to a depth of a few hundred meters dramatically lowers atmospheric pressures and surface temperatures, and the effect of the regolith is important from the outset.

In other words, <u>in all realistic scenarios in which surface temperatures are both higher than at present and dependent on high CO_2 pressures</u>,

high pressure and temperature conditions are truncated by the growth of only a few hundred meters of regolith, ultimately leading to present Mars conditions. It might be argued that while the development of a regolith a few hundred meters thick in early Mars history is likely in view of the existence of the ancient cratered terrain, it is unreasonable to postulate a much lower regolith thickness at the very outset. We point out, however, that it is not literally the thickness of the regolith that is the critical parameter, but rather its total surface area. Weathering products such as palagonites and nontronites typically exhibit specific surface areas for CO_2 adsorption of tens to hundreds of square meters per gram whereas basalts typically exhibit specific surface areas of a fraction of a square meter per gram to several square meters per gram. Thus, although we represent the "regolith growth" as a physical thickening (keeping the specific surface area equal to the Viking derived value), the actual case involves the product of both actual thickening and a great increase due to an increased abundance of weathering products. While the precipitation of carbonates has probably been an important process during Mars history (6), the rates at which this process could have taken place under early Mars conditions would have dropped sharply once liquid water was fairly scarce. Furthermore, conditions under which liquid water was available may have involved efficient recycling of carbonate so that steady state conditions rather than irreversible CO_2 removal prevailed. In contrast, the growth of regolith surface area demands corresponding and predictable CO_2 removal from the atmosphere cap system and is, as shown here, fully capable of terminating any enhanced temperature regime on early Mars in the absence of any other effects. To put it another way, total degassed CO_2 inventories of < 2 bar and the existence of substantially higher temperatures than present are compatible; total degassed CO_2 inventories of < 2 bar, substantially higher temperatures than present, and a regolith qualitatively comparable to the present one are not compatible.

REFERENCES: (1) Pepin, R.O. (1985), MECA Workshop on the Evolution of the Martian Atmosphere, 14-15; (2) Hoffert, M.I., et al., (1980), Icarus, 47, 112-129; (3) Toon O.B., et al., (1986), Icarus, 44, 552-607; (4) Zent, et al., (1986), Symposium on Mars: Evolution of its Climate and Atmosphere, in press; (5) Ballou, E.V., et al., (1978), Nature, 271, 644-645; (6) Kahn, R. (1985), Icarus, 62, 175-190.

MARTIAN SURFACE PHYSICAL PROPERTIES TO BE DERIVED BY RADAR ALTIMETER ON THE MARS OBSERVER SPACECRAFT

Garvin J. B.[#], F.T. Ulaby[@], D.E. Smith[#], H.V. Frey[#], S. Solomon[$], and H. J. Zwally[#]

[#]NASA/Goddard, Greenbelt, MD 20771; [@]Radiation Lab, Univ. Michigan, Ann Arbor, MI 48109; $Dept. Earth and Planetary Sci., MIT, Cambridge, MA 02139.

Two of the primary objectives of the Mars Observer (MO) mission are global monitoring of those surface physical properties which can be linked with the recent climatic history of Mars, as well as characterization of planet-wide surface composition and mineralogy. While the main emphasis in orbital radar altimetry is quite naturally the determination of the topography of the planet, information concerning meter-scale roughness and the dielectric properties of the upper surface layer can be inferred from analysis of doppler and time-delay altimeter waveforms. In addition, it is relatively straightforward to use the time between altimeter pulse trains for passive microwave radiometry from which complementary data concerning surface emissivity (and hence dielectric properties) and roughness can be derived. The Pioneer Venus (PV) radar altimeter (17 cm wavelength), although in a highly elliptical orbit, was able to acquire valuable information concerning the roughness, radar reflectivity (r), and emissivity (e) of the venusian surface at coarse spatial resolution (30-100 km) for virtually all of the planet [1-3]. A 13.6 GHz (Ku-band or 2.2 cm wavelength) radar altimeter/radiometer (RAR), a candidate instrument for the Mars Observer [4], is capable of providing approximately 10 km resolution data on the surface roughness (C), microwave brightness temperature (Tb), emissivity (e), Fresnel reflectivity (r), and dielectric permittivity (k') for the entire martian surface. The complete waveform resulting from spreading of the altimeter pulses is saved (after being compressed) and used to derive the properties mentioned above by means of both a Hagfors scattering model (e.g. as used by Pettengill [1] and colleagues for PV, and to be used for Magellan altimetry), and an empirical scattering law (based upon the solution of an inverse scattering matrix problem as proposed by Tyler and Simpson for Magellan [5]).

As the MO is planned to be in a 360 km circular polar orbit, the derived altimeter surface properties can be obtained for the entire planetary surface at least three times (on the basis of the mapping orbit groundtracks), and thus seasonal effects can be directly assessed. This may shed new light on the proposition that seasonal variations in radar reflectivity (observed from Earth) in certain regions of Mars (e.g. Solis Lacus) are caused by the presence of liquid water on or near the surface [6,7]. Figure 1 is a theoretical volume mixing model approach for considering how much liquid water would be required to cause the observed seasonal variation in the radar reflectivity (i.e. a factor of 2) [8,9]. The model assumes that the water would occur as either grain coatings (as in clays) or as a pore fluid in the regolith or bedrock, and applies in general to radar reflectivity observations above 1 GHz [8,9]. As can be seen from the mixing curves (one for each type of surface, from very porous regolith to dense basalt [porosity less than 8 %]), between 8 to 10 vol. % liquid water would be required to cause the observed reflectivity variations. While regolith porosities of 8-10 % may be quite reasonable, saturation of the regolith by liquid water may not be

feasible on Mars except in regions where surface permafrost is dominant. For average porosity igneous and sedimentary rocks, between 1 and 5 vol. % liquid water would be required to account for the observed variations; thus, low vesicularity basalts with a few vol. % pore water could explain the increase. It should be noted however, that a few vol. % of a high permittivity phase such as ilmenite, rutile, pyrite, or even simple hematite could cause the observed reflectivity magnitudes [2,3,9]. For instance, 5-10 vol. % hematitic coating on average regolith grains (perhaps basaltic ash) would easily lead to reflectivities above 0.16 (the maximum observed), although a seasonal variation would not be expected. Perhaps the deposition and subsequent removal of porous eolian material (low permittivity) from a surface of lower porosity and greater enrichment in alteration products (e.g. hematite or pyrite) would serve as an alternate explanation to the seasonally varying reflectivity. Whatever the case, surface-layer permittivities derived from radar altimeter measurements on a seasonal basis should provide new insights on temporal electrical property variations (and porosity?), and perhaps on the activity of liquid water, especially if visual-IR mapping spectrometry can distinguish iron oxides from "wet regolith".

The surface properties derived from a Ku-band RAR in circular martian orbit are complementary and synergistic with other synoptic MO datasets such as thermal emission spectroscopy, Visual-IR mapping spectrometry, ultra high-resolution imaging (e.g. 1 m resolution), mm-wave radiometry, and HF-VHF sounding radar (to be flown on the PHOBOS mission in 1988 [10]). The depth penetration capabilities of 2.2 cm radar depend on the loss properties of the upper surface layer (and hence porosity and composition), but for Mars should vary from about 2 cm to 30 cm (for loss tangents between 0.1 and 0.001). More interesting is the possibility of detecting high permittivity regions which could be associated with near-surface concentrations of liquid water (as mentioned above and illustrated in Fig. 1), or to deposits of metallic-oxides or sulfides perhaps resulting from volcanism or weathering (or even to very high Ti basalts such as those discovered on the Moon). The multi-temporal seasonal coverage should permit some separation of mechanisms responsible for high permittivity surfaces to be established. The radiometer mode , as with PV, will help to refine estimates of the magnitude of high dielectric properties [2].

Surface physical/electrical properties derived from a RAR instrument on MO are a potentially important global and seasonal dataset which will complement measurements from other MO experiments (TEMS, VIMS, MOC etc.), and lead to a better understanding of the interaction of geological and climatological processes on the surface of Mars. This report merely illustrates some of the possibilities for answering fundamental questions with such measurements.

REFERENCES:

[1] Pettengill G. et al. (1980) JGR 85, 8261. [2] Ford P. and G. Pettengill(1983) Science 20, 1379. [3] Garvin J. et al.(1985) JGR 90, 6859. [4] Smith D. et al.(1985) A Radar Altimeter for the Topography and Surface Properties of Mars, Proposal to NASA for AO no. OSSA-2-85, the Mars Observer. [5] Pettengill G. et al.(1985) Magellan Sci. Expt. Plan, 19-22. [6] Zisk S. and P. Mouginis-Mark (1980) Nature 288, 735. [7] Roth L. et al.(1985) LPSC XVI, 712. [8] Sen P. et al.(1981) Geophys. 46, 781. [9] Garvin J. and J. Head (1986) LPSC XVII, 255. [10] Armand N. (1986) NASA TM-88413, 30 pp. (translation of "Performance data on the Soviet PHOBOS mission "GRUNT" radar".

FIGURE 1: Theoretical volume mixing model curves [8,9]; see text for detailed explanation.

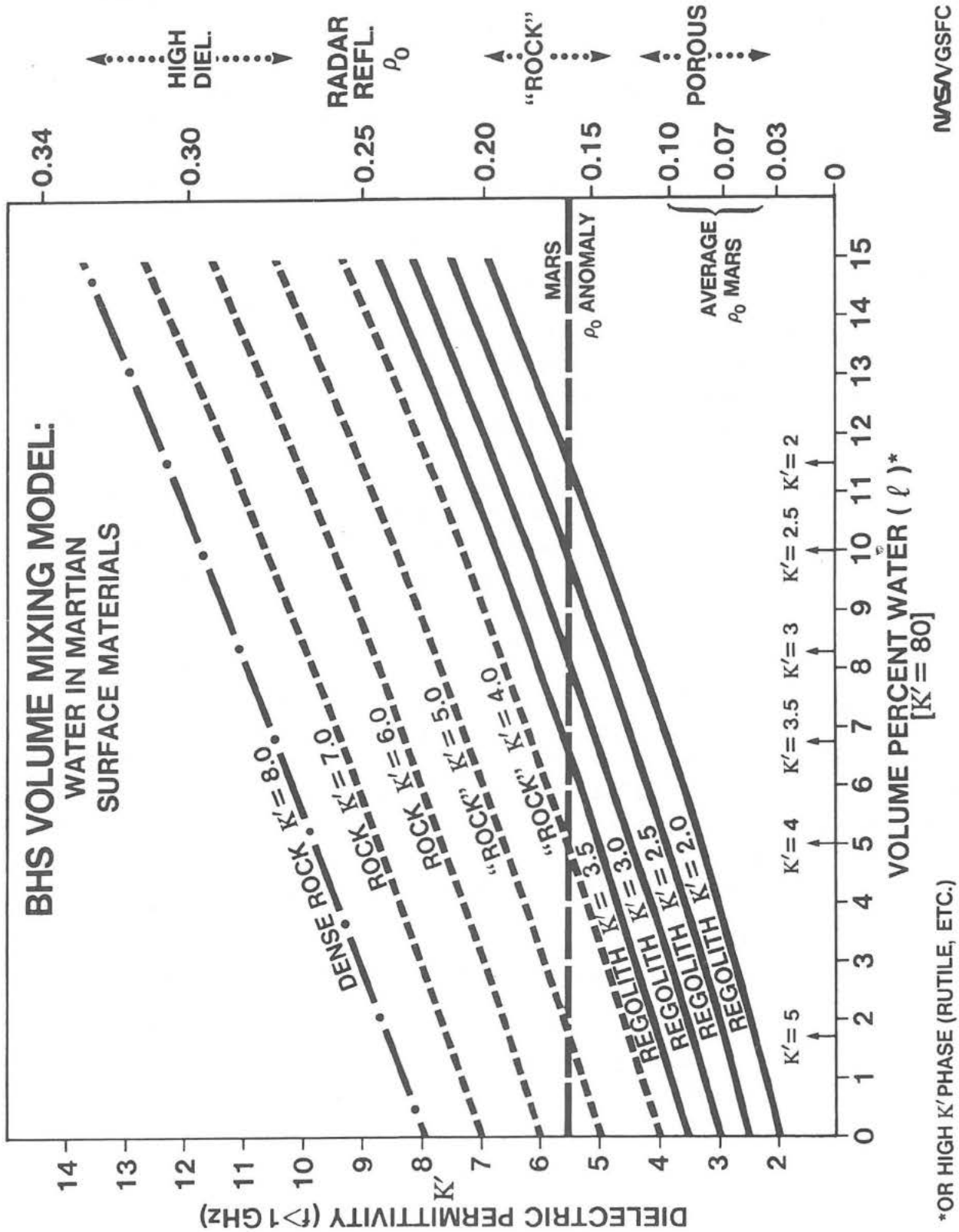

RELEASE OF MAGMATIC WATER ON MARS: ESTIMATED TIMING AND VOLUMES; *R. Greeley, Department of Geology and Center for Meteorite Studies, Arizona State University, Tempe, AZ 85287*

The amount of water and other volatiles on and near the surface of Mars and their effects on the climate history have been the focus of the MECA (Mars: Evolution of its Climate and Atmosphere) Project, and the subject of considerable debate and interest (1). As reviewed by Wanke and Dreibus (2) and others, estimates of the total volume of water on Mars have been based on modelling of the distribution of elements in the inner solar system, considerations of the SNC meteorites, and analysis of results from the Viking landers. Estimates of the total amount of water released on Mars based on these various approaches range from <1 m to >50 m for a water layer covering the planet. However, few of these estimates consider the rate or timing of volatile release to the surface of Mars from the interior. The results presented here are inferred from the amounts of volatiles released in association with volcanic eruptions that have occurred during the evolution of Mars, as derived from geological mapping.

Table 1 shows the amount of water released via volcanism during each major interval of the martian geologic time-scale. It is based on: (a) mapping of volcanic units on Mars and estimates of their volumes, (b) crater-count ages of the units, and (c) estimates of the volatile-release associated with the eruption and emplacement of the volcanic units. Mapping of volcanic units was derived from manuscript versions of recently completed 1:15 M-scale geological maps of Mars (3,4,5), supplemented by reviews of martian volcanism (6,7,8). Although a wide variety of volcanic units occur on Mars, for simplicity, a two-fold classification was used here: (a) materials forming central volcanoes (which include all units derived from central vents, such as shield volcanoes) and (b) plains-forming lavas (includes both *flood lavas* presumably fed from fissures, and complex *plains lavas,* involving thin, multiple flows). Volumes of the volcanic materials are difficult to obtain; however, estimates of flow thicknesses, derived by DeHon (9,10), were used for some plains, such as Herperia Planum. In other volcanic plains areas, an average thickness of 1 km was used, based on the thickness of flood lavas in the Columbia River Plateau, which can be considered a terrestrial analog for martian flood-lava provinces. Volumes of the central volcanoes were estimated from their topography. Geological ages for the volcanic units are taken from the mapping (3,4,5), supplemented by data from other crater counts (11). In addition, the paleogeographic sequence for the Tharsis area derived by Scott and Tanaka (12) enabled estimates to be made for the volumes and timing of volcanic units for this part of Mars.

Although magmatic water is commonly released to the atmosphere during volcanic eruptions, the amounts as a function of composition, style of eruption, etc. are poorly known. Most volcanic units on Mars appear to be mafic (6). Using a value of 1.0 percent by weight of water associated with terrestrial basaltic eruptions as a guide (J. Holloway, personal communication) an approximation can be made for the volumes of water released in association with the volcanic units identified from the geological mapping. The total volume released is >10 m, consistent with previous estimates. Although the central volcanoes, such as Olympus Mons, tend to dominate general perceptions of martian volcanism, by far the plains units contain the greatest volume of volcanic materials and made the greatest contribution to the water budget.

The development of the valley networks occurred early in martian history, during the Noachian Period; yet the amount of water released in association with volcanism is relatively small.

This suggests either (a) other sources of water early in martian history (such as cometary contributions), (b) unidentified volcanic units of an early age, or (c) that the valley networks are erroneously dated. Of these, (b) seems most likely. Most of the ancient martian crust has been degraded or buried and, thus, its origin cannot be ascertained. However, by analogy with the Moon, the martian crust probably developed by magmatic differentiation and extrusion of flood lavas. Thus, although few traces of this earliest volcanism are visible in present data, substantial water may have been released early in martian history. The greatest volumes of volcanic materials--and by inference the greatest volumes of water--were emplaced in Mars "middle-life" and coincide with the development of the large out-flow channels. Photogeologic evidence shows that the formation of outflow channels was episodic and extended over a long interval of martian history, a reflection of the availability of large volumes of water at or near the surface.

It is noted that the volumes of water inferred in this study involve only those derived from volcanism as interpreted from surface features. The greatest uncertainties involve the thicknesses of units and the amounts of water associated with different types of volcanic units. Future work will address some of these uncertainties through use of better geochemical models for Mars and additional analysis of high resolution Viking Orbiter images for volcanic units.

TABLE 1. Inferred water released in association with volcanic units through time on Mars. Values given are for equivalent thickness of water layer in meters covering entire surface of planet.

GEOLOGIC PERIOD		PLAINS	CONSTRUCTS
Young	Late Amazonian	0.28 m	0.53 m
↑	Middle Amazonian	0.94	0.21
	Early Amazonian	2.64	0.34
	Late Hesperian	1.22	0.05
	Middle Hesperian	2.68	0.17
↓	Early Hesperian	0.84	0.17
Old	Noachin	0.26	0.00
	Totals	8.58 m	1.47 m

REFERENCES

1. Greeley, R. and K. Burke (1984). Water on Mars (abs.), *Trans. Amer. Geophys. Union, 65*, 979.
2. Wanke, H. and G. Dreibus (1985). Volatiles on Mars (abs.), *Workshop on water on Mars,* Lunar and Planetary Institute, Tech. Rpt. 85-03, 90-93.

3. Scott, D. and K. Tanaka (1986). Geology of the western equatorial region of Mars, *U.S. Geol. Survey Misc. Inv. Map I-1802 A*.
4. Greeley, R. and J.E. Guest (1986). Geology of the eastern equatorial region of Mars, *U.S. Geol. Survey Misc. Inv. Map I-1802 B*.
5. Tanaka, K. and D. Scott (1986). Geology of the polar regions of Mars, *U.S. Geol. Survey Misc. Inv. Map I-1802 C*.
6. Greeley, R. and P. Spudis (1981). Volcanism on Mars, *Rev. Geophys. Space Phys., 19,* 13-41.
7. Greeley, R. and P. Spudis (1978). Volcanism in the cratered terrain hemisphere of Mars, *Geophys. Res. Lett., 5,* 453-455.
8. Albin, E.F. and R. Greeley (1986). Mars: Volcanic plains in the cratered uplands and possible tectonic associations, *Lunar Planet. Sci., XVII*, 7-8.
9. DeHon, R.A. (1982). Thickness and distribution of volcanic materials on Mars: A progress report, Repts. Planetary Geology Program, *NASA Tech, Mem., TM-85127*, 129-131.
10. DeHon, R.A. (1984). Thickness of ridged plains material in Hesperia Planum, Mars, Repts. Planetary Geology Program, *NASA Tech. Mem., TM-87563*, 242-244.
11. Tanaka, K. (1986). The new stratigraphy of Mars, submitted to *Icarus*.
12. Scott, D.H. and K.L. Tanaka (1981). Mars: Paleostratigraphic restoration of buried surfaces in Tharsis Montes, *Icarus, 45*, 304-319.

THE MARTIAN DUST CYCLE: A PROPOSED MODEL; *Ronald Greeley, Department of Geology and Center for Meteorite Studies, Arizona State University, Tempe, AZ 85287*

Martian dust storms have long been held in fascination. Yet, despite more than a decade of study, many of their characteristics and associated processes remain enigmatic, including the mechanisms for dust raising, mode(s) of settling, and the nature of dust deposits. However, observations of Mars dust, considerations of terrestrial analogs, theoretical models, and laboratory simulations permit the formulation of a ***Martian Dust Cycle Model*** (Fig. 1) which consists of three main processes; (a) suspension threshold, (b) transportation, and (c) deposition; two associated processes are also included: (d) dust removal and (e) the addition of "new" dust to the cycle. Although definitions vary, "dust" includes particles <4 to ~60 μm in diameter, which by terrestrial usage includes silt, loess, clay, and aerosolic dust particles.

Suspension threshold. Perhaps the least understood aspect of martian dust storms is the mechanism(s) for putting dust into suspension (1). Because of the low density atmosphere, extremely high winds are required to raise loose dust of the size inferred for martian dust. Although some dust may be raised by these high winds, most investigators invoke other threshold mechanisms. Dust devils may be one such mechanism; laboratory experiments show that vortical wind shear is very efficient in raising particles (2). With the discovery of dust devils on Mars (3) this possible mode of dust-raising is enhanced. Outgassing of volatiles (CO_2 or H_2O) from the regolith in response to changes in atmospheric temperature/pressure has also been suggested as a means of injecting dust into the atmosphere (4,5). Although slow outgassing does not cause dust injection, it can lead to surface fracturing and fissuring, which may be important in the "aggregate" mode of dust-raising discussed below.

Because sand-size grains are more easily moved than dust, it has been suggested that saltating sands could act as "triggers" to set dust into suspension (6,7). Laboratory experiments show this to occur, although in some circumstances, the saltating sands merely "indent" the surface without dislodging the dust (1). Sand "triggering" has been proposed for dust-raising in Australia in reference to "***parna***", which may be an analog to martian dust deposits. Parna is an aboriginal word meaning "sandy and dusty ground", used by Butler (8) for the extensive deposits that mantle parts of southeast Australia. The deposits consist of two components, dust (~2 μm) and large grains (~100 μm) termed as ***companion sand*** (9). Field studies show prevailing winds when the deposits were formed, possible source regions, and particle size distributions as a function of transport distance. Butler proposed that parna was transported in suspension as aggregates equal in size to the companion sands. Multiple layered deposits suggest climatic cycles in which clay was produced by chemical weathering during humid periods and redistributed by winds during more arid periods. Pre-existing sand dunes served as one source for the parna. Dust within the sand dunes was mobilized by triggering of the sand, which then became the "companion" component. Westerly winds then transported the aggregates in suspension more than 650 km where they settled as a uniform blanket over all terrain features--an aspect cited as evidence for transport via suspension. Once deposited, the pellets disaggregated, forming a matrix containing evenly-distributed sand grains. As discussed previously (10), parna may be an analog for the threshold, transportation, and deposition of some martian dust.

The third general mechanism of dust-raising involves ***aggregates*** (11) ("dust"-size grains collected into sand- and larger-size clumps). In addition to parna, four other sources of aggregates may occur on Mars: (a) deposits settled from the atmosphere as part of the dust cycle, (b) ancient lake bed deposits, similar to clay pellets derived from playas on Earth, (c) aggregates derived from frothy/crusty surfaces generated by fluctuations of saline ground water, and (d) crusty/cloddy weathering surfaces which may be disrupted, as by outgassing (discussed above). Aggregate strength is variable, depending on mode of bonding. Because the wind speeds on Mars required to set particles into motion are high, Sagan et al. (12) proposed that holocrystalline grains would be pulverized into fine grains by the "kamikaze" effect. If aggregates were involved,

the destruction would be even more effective because of their low strength. Wind tunnel experiments with aggregates show that as they lift above the surface, they rupture into dust clouds (1). Thus on Mars, disaggregation may occur via "kamikaze dust explosions".

Transportation. The movement of dust in both local clouds and as global transport is documented through earthbased and spacecraft observations. Pollack et al. (13,14) and Haberle (15) have developed models to predict the patterns of transport and provide the key to this part of the dust cycle.

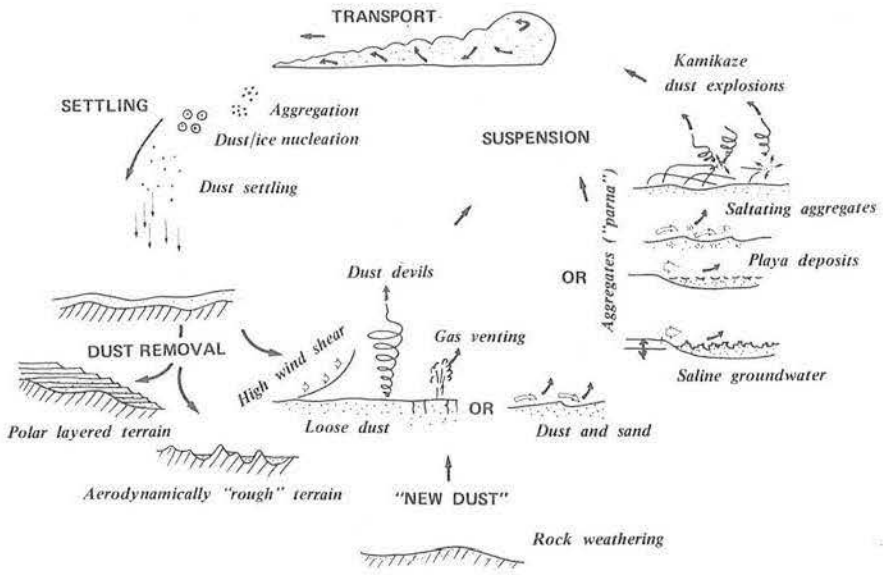

Fig. 1. Diagram of proposed Martian Dust Cycle.

Deposition. With a decrease in driving energy for dust clouds, in time particles settle from the atmosphere. However, because of possible "feedback" mechanisms (14), one of the problems in the dust cycle is how to shut-down dust storms. One mechanism involves the accretion of ice on dust grains (13). Aggregation of grains may also occur via electrostatic bonding, a mechanism demonstrated in laboratory experiments (11) and observed in volcanic dust clouds. Lee has shown (16), however, that the settling rate of larger grains (either ice/dust or dust/dust) is a function of the grain density and diameter, both of which change during accretion.

With settling and deposition, the cycle may be completed and the stage set for dust-raising to initiate the next cycle. However, in addition to the dust threshold, transport, and deposition components of the cycle, dust may be removed from the cycle, and "new" dust may be added.

Dust removal. On Earth, the largest "sinks" for dust removal are the oceans. Although these sinks are lacking on Mars, there are other areas where dust may be removed from the cycle. These include the polar regions (layered deposits) and surfaces that are aerodynamically rough such as impact ejecta fields, terrain that has been severely fractured by tectonic and other processes, and some lava flows. Once deposited on these surfaces, the dust would be difficult to remove until the roughness elements were effectively buried.

"New" dust. Dust may be added to the cycle by a variety of mechanisms on Mars, including chemical and physical weathering (clays are the normal end product of weathering on Earth), impact cratering, volcanism, and tectonism.

In summary, the proposed Martian Dust Cycle inter-relates many of the previously proposed aspects of martian dust, and introduces some new concepts, such as "kamikaze dust explosions".

References

(1) Greeley, R., 1985, Dust storms on mars: Mechanisms for dust-raising, *in* Workshop on Dust on Mars, *LPI Technical Report No. 85-02*, 3-5.
(2) Greeley et al., 1981, *Geol. Soc. Amer. Sp. Pub. 186,* 101-121.
(3) Thomas, P. and P.J. Gierasch, 1985, Dust devils on Mars, *Science, 230,* 175-177.
(4) Greeley, R. and R. Leach, 1979, *NASA TM 80339,* 304-307.
(5) Hugnenin, R. et al., 1979, *NASA Conf. Pub. 2072,* 40.
(6) Peterfreund, A.R., 1981, *Icarus, 45,* 447-467.
(7) Christensen, P.R., 1983, Eolian intracrater deposits on Mars: Physical properties and global distribution, *Icarus, 56,* 496-518.
(8) Butler, B.E., 1956, *Austral. J. Sci. 18*, 145-151.
(9) Butler, B.E. and J.J. Hutton, 1956, *Austral. J. Agric. Res. 7*, 536-553.
(10) Greeley, R., 1986, Martian dust: The case for "parna", *in* MECA Workshop on Dust on Mars II, 25-27.
(11) Greeley, R., 1979, Silt-clay aggregates on Mars, *J. Geophys. Res., 84,* 6248-6254.
(12) Sagan, C., D. Pieri, P. Fox, R. Arvidson, and E. Guinness, 1977, Particle motion on Mars inferred from the Viking lander cameras, *J. Geophys. Res., 82,* 4430-4438.
(13) Pollack, J.B., 1979, Climatic change on the terrestrial planets, *Icarus, 37,* 479-553.
(14) Pollack, J.B., C.B. Leovy, P.W. Greiman, and Y. Mintz,1981, A martian general circulation experiment with large topography, *J. Atmosph. Sci. 38,* no. 1, 3-29.
(15) Haberle, R.M., 1986, The development of global dust storms on Mars: The role of the mean meridianal circulation, *in* MECA Workshop on Dust on Mars II, 28-29.
(16) Lee, S.W., 1984, Influence of atmospheric dust loading and water vapor content on settling velocities of martian dust/ice grains: Preliminary results, *in* Workshop on Dust on Mars, *LPI Technical Report No. 85-02,* 51-52.

INTERANNUAL VARIABILITY OF GLOBAL DUST STORMS ON MARS; R.M. Haberle, NASA-Ames Research Center, Moffett Field CA 94035

Global dust storms on Mars occur in some years but not in others. In years with global dust storms, dust is raised in the southern hemisphere and spread over much of the planet by an intensified Hadley circulation. In years without global dust storms, dust is raised in the northern hemisphere by relatively active midlatitude storm systems, but does not spread globally. In both cases the dusty season is winter in the north. It is shown from numerical simulations that a northern hemisphere dust haze weakens the intensity of the cross-equatorial Hadley circulation and the contribution it makes to the surface stress in the southern hemisphere. This, in turn, reduces the possibility of global dust storm development. The interannual variability is the result either of a competition between circulations in opposite hemispheres, in which case the variability has a random component; or it is the result of the cycling of dust between hemispheres, in which case the variability is related to the characteristics of global dust storms themselves.

CHEMICAL FROST WEATHERING OF OLIVINE: EXPERIMENTAL STUDY AND IMPLICATIONS; S.L. Harris, R.L. Huguenin, Geology/Geography, University of Massachusetts, Amherst, MA 01003.

It has been proposed that chemical frost weathering of silicates may occur in the contemporary Mars surface environment (1,2) Exposure of olivine and other mafic silicates to H_2O at frost temperatures was proposed to result in the incorporation of H^+ into the crystal, converting oxide ions to hydroxide ions. Incorporation of electrons (derived from OH^- in the frost), at positive defects (e.g. Fe^{3+} substituted for Fe^{2+}) was proposed to restore charge balance and convert OH^- to H_2O_2. Production of H_2O_2 was observed experimentally (2,3).

A new experiment has been performed to test the proposal that H^+ reacts with O^{2-} to form OH^- during the frost weathering of olivine. The olivine used is the same as that in (2) and has composition Fo_{86}. The olivine was placed in an atmosphere and temperature controlled chamber. The sample chamber pressure was maintained at $\approx$ 760 torr N_2, except during initial frost formation and desorption. Frost was formed on the olivine by cooling the sample below -10^o C with a flow of H_2O saturated N_2 gas into the sample chamber. Frost desorption was accomplished by cycling the temperature below 0^o C with a cold trap in the system and the vacuum pump running. Reflectance spectra of the olivine samples were taken before, during, and after frost formation. Band positions were extracted from spectra using the Bands Data Analysis System described by (4).

The penetration of H^+ into the crystal structure during weathering should be observable from spectra. The H^+ should react with O^{2-} in the crystal to produce structural hydroxyl. The structural hydroxyl absorption bands would occur at wavenumber positions that are close to those of absorbed H_2O and surface hydroxyl ions, thus they would not be uniquely indicative of structural hydroxyl found by penetration of H^+ into the lattice. With the H^+ that has been proposed to migrate to cation vacancies (3), a more diagnostic spectral signature is a shift in the Fe^{2+} absorption band positions arising from a change in the crystal field splitting parameter Dq. Dq is defined as Dq $\approx Q/R^5$ where Q is the charge on the ligands and R is the metal-ligand interatomic distance (5). Since Dq is proportional to Q, a change in Q from 2 (O^{2-}) to 1 (OH^-) should produce a decrease in Dq.

Huguenin (3) found that approximately 9 x 10^{19} H^+ were incorporated into a 1 gm sample after exposure to frost. The number of $Mg^{2+} + Fe^{2+}$ cations in a 1 gm sample of olivine is approximately 4.8 x 10^{21}. If the H^+ were incorporated at or adjacent to the cation sites, then there would be a predicted 1.9 % decrease in Dq.

Absorption bands in the olivine spectra are due to electronic transitions and charge transfers by the d shell electrons in Fe^{2+}. The wavelength position of the band centers depend on the charge of the ligands and on the dimensions and symmetry of the Fe^{2+} site. In a perfect octahedral site the five d-shell orbitals are split into a triply degenerate, t_{2g}, set and a doubly degenerate, e_g, set due to the presence of the surrounding six O^{2-} ligands. The $d_{x^2-y^2}$ and d_{z^2} orbitals, which point directly to coordinating ligands, are raised in energy to the e_g set. The d_{xy}, d_{xz} and d_{yz} orbitals lie between the ligands and are lowered in energy to the t_{2g} set. Fe^{2+} has six d electrons, five of which have parallel spin directions in the ground state. The sixth electron occupies the lowest energy level with its spin in the opposite direction. Absorption occurs when the sixth electron is moved from the ground state energy level to one of the higher energy levels. The energy separation between the t_{2g} and e_g orbitals is termed the crystal field splitting and, it is denoted by Dq or $\triangle o$ (5,6).

The crystal structure of olivine contains 2 six-coordinated sites; a centrosymmetric M(1) site and a non-centrosymmetric M(2) site. There is no site preference so that Mg^{2+} and Fe^{2+} are randomly distributed between the sites (6,7). Thus, there are contributions from Fe^{2+} in both M(1) and M(2) sites in absorption spectra. Burns (6,7) has assigned the absorption bands occurring around 11,700 and 9,000 cm^{-1} to the M(1) site and the absorption band at $\approx$ 9540 cm^{-1} to the M(2) site.

The experimental results showed an average decrease of $400cm^{-1}$ in the olivine M(2) site band position upon frost weathering. Shifts in M(1) site band position were not apparent, although a small shift may have escaped detection. Burns (6) gives a Dq value of $8330cm^{-1}$ for Fe^{2+} in the M(2) site of an Fo_{88} olivine. The observed shift in the M(2) site band position would correspond to a shift in Dq of $\approx$ 4.8 %. This is somewhat larger than the predicted shift, but it generally supports the proposed model.

The observed shift in band position has two implications. First, it supports the proposed frost weathering model and its occurrence on Mars. It was predicted that 10^0 - 10^3 meters of H_2O may have been lost to weath-

ering over the planets history, and the results here support that prediction. Second, it suggests that frost-weathered olivine may have absorption band positions that are lower in energy than the

$$\frac{Fe^{2+}}{Fe^{2+} + Mg^{2+}}$$

ratio would predict. This would have significant impact on interpretation of the Fe^{2+} content of olivines on Mars from their absorption band positions.

Acknowledgment: This research was supported by NASA grants NSG 7405 and NAGW 570.

References

(1) Huguenin, R.L., (1986) Icarus, 28 p.203-212.
(2) Huguenin, R.L., Miller, K.J. Harwood, W.S. (1979) J. Mol. Evol.,14 p.103-132.
(3) Huguenin, R.L., (1982) J. Geophys. Res., 87 p.10,069-10,082.
(4) Huguenin, R.L., Jones, J.L., (1986) J. Geophys. Res. in press.
(5) Basolo, F., Pearson, R.G., (1967), Mechanisms of Inorganic Reactions - A Study of Metal Complexes in Solution, J. Wiley & Sons Inc. N.Y. 701p.
(6) Burns, R.G., (1970) Mineralogical Applications of Crystal Field Theory, Cambridge Univ. Press, 224p.
(7) Burns, R.G., (1974) Am. Min., 59 p. 625-629.

MARS LOW ALBEDO REGIONS: POSSIBLE MAP OF NEAR-SURFACE H_2O; R.L. Huguenin, Geology/Geography, University of Massachusetts, Amherst, MA 01003.

It has been proposed that dust storms on Mars that develop during pre-dawn hours may be triggered by a freeze/thaw dust injection process (1). The model was based on a phenomenon that was observed during the Viking Gas Exchange experiments on Mars, in which adsorbed gas was catastrophically desorbed from soil samples when exposed to humidification at $\sim 5^0$C. Similar conditions may develop at mid-latitude locations on Mars near perihelion, and a similar humidification-driven desorption process might occur in the soil column. If soils are dampened during humidification, desorbed gases in confined pore spaces could possibly reach 8.6 bar. Diurnal freezing may cause H_2O to crystallize within the pores, producing cohesive soil failure, release of the trapped gas, and explosive injection of freeze-dried powdery overburden dust into the atmospheric column. The process could potentially occur at 5-20 cm depth, and the freeze/thaw dust injection event may initiate after 10:00 p local time (20^0S latitude). Dust would be injected at velocities approaching 450 m/s and it would remain in the atmosphere for at least several hours before settling out. The plumes could potentially regenerate diurnally until the growing atmospheric dust load produced sufficient dampening of the diurnal thermal wave to prevent freeze/thaw. Seasonal replenishment of H_2O could potentially occur by upward migration from depth during the period between 150 sols and 475 sols after perihelion. The model was experimentally tested and the results were in good agreement with predictions, although a factor of 14 times more gas evolved from the laboratory samples than from the Viking samples. Most of the characteristics of the pre-dawn major storms could be adequately explained by the freeze/thaw injection model, including 1) pre-dawn onsets; 2) post-perihelion seasonal occurrence; 3) daily recurrence during the initial phases of the storms; and 4) generation of blue clouds (H_2O ice) at the storm sites (1).

While the proposed mechanism specifically addressed the large pre-dawn storms which initiated in Solis Lacus, Noachis-Hellespontus, and the Syrtis Major border regions (1), the process may be more widespread. The storms at those sites were the most spectacular events, expanding to global proportions. Large numbers of smaller events occur during the season of maximum local soil temperature at a variety of low-latitude locations, however. Many of these storms could possibly be the result of freeze/thaw dust injection, due to the presence of H_2O ice in the near-surface soil column.

H_2O ice is probably not restricted to Solis Lacus, Noachis-Hellespontus, and the Syrtis Major border regions. Although perhaps it may be more abundant in those regions, H_2O ice may be relatively widespread in the near layer. At the Utopia Viking lander site there was evidence for greater H_2O abundance than at the Chryse site, and within the sampling area at Utopia there was more H_2O under rocks than in the exposed soils (2,3). The concentration under rocks supports the possibility of upward migration/condensation of H_2O from a subsurface source, and the source could possibly be widespread (4).

It was argued by Farmer and Doms (5) that during the colder portions of the year H_2O ice would be stable in the regolith at latitudes poleward of +30 and -35^0, and that during the warmer times of the year some of the H_2O would tend to sublime away. At lower latitudes H_2O ice would be unstable at all times of the year, and it would continually tend to sublime away. If there were subsurface sources of H_2O such as described by Clifford (4), it

would be possible that significant tempofrost deposits could accumulate seasonally poleward of $+30^0$ and -35^0 and extend close to the surface. With expected heterogeneities in regolith thermophysical properties, it is possible that the edge of the tempofrost zone could deviate somewhat from $+30^0$ and -35^0 latitude. In locales where thermal cycles are more extreme, it is reasonable that the tempofrost zone could possibly extend equatorward to $\pm 15^0$ or more, since water vapor abundances over these latitude bands could be seasonally at saturation levels with only a few degrees drop from the modeled regolith temperatures. With the latitude of maximum solar insolation extending close to the latitude of seasonal tempofrost emplacement, it is possible that conditions for the freeze/thaw dust injection process could thus be widespread along the $+15^0$ to $+30^0$ and -15^0 to -35^0 latitude belts.

Although it is not proposed here that the freeze/thaw dust injection process is the only mechanism for generation of the mid-latitude storms, most non-polar plumes occur in the southern hemisphere in a latitude band between -15^0 to -35^0 (e.g., 6). This is the latitude band into which the edge of the zone of seasonal ground ice accumulation (tempofrost) may extend, and it is the zone of maximum solar insolation during the dust cloud events. In the northern mid-latitudes the sites of most frequent occurrence were the Syrtis Major border regions, Cerberus, and Chryse. Again, these regions were in the $+15^0$ to $+30^0$ latitude band of the proposed edge of seasonal ground ice accumulation. Consequently, many of the mid-latitude local storms may possibly occur under conditions that are favorable for the freeze/thaw dust injection process, and the process could possibly be relatively widespread in these latitude bands.

If the humidification-induced dust injection process is widespread in the mid-latitude bands during the period of maximum insolation, these latitude bands would be zones of preferential seasonal dust entrainment. If true, then this latitude band may possibly be subjected to preferential removal of dust by wind transport, since the transport of dust in the rarefied Mars atmosphere should be rate-limited by the entrainment processes. This would suggest that the regions of preferential humidification-induced dust injection could possibly have relatively lower abundance of dust than regions of minimal entrainment. By contrast, the regions of minimum dust injection activity might, neglecting other entrainment processes, be possible sites of preferential dust deposition. If true this would suggest the possibility that the regions where humidification-induced entrainment occurs may have lower albedo than other regions, since the mobile dust component is apparently higher in albedo than the more coarse-grained rocks and soils (7). If the differences in dust content are sufficient, the zones of preferential dust removal could also have higher thermal intertia, since the unconsolidated fine-grained dust would have relatively low thermal intertia (8). Indeed, the regions of preferential dust cloud occurrence have moderate-to-high thermal intertia and moderate-to-low albedo. Dust clouds rarely originate in regions of high albedo and low thermal intertia (6), which is consistent with the predictions.

The latitude band which is predicted to have the maximum freeze/thaw dust entrainment activity, i.e., 15^0-35^0S latitude, contains most of the permanent low albedo regions of the planet. If the model proposed here is viable, the dark areas within this latitude band may correspond to areas of seasonal ice emplacement and humidification-induced dust entrainment activity. Low albedo regions in the northern mid-latitudes may have similar origin.

One aspect of the proposed model for formation and preservation of the low-albedo features that might appear inconsistent is the fact that the

sites of dust clouds are sites of proposed minimum dust deposits. Associated with this is the apparent possible inconsistency that the dust injection event is proposed to occur within 5-20 cm deposits of fines in regions that are supposed to be relatively dust-free. These observations are not necessarily inconsistent, however, the dust plumes probably contain at most a few millimeters equivalent of dust in the atmospheric column (e.g., 6). If the dust originated from cracks, voids, and other fine-scale topographic traps, most of the surface could be dust-free.

Several-centimeter-thick layers of dust could potentially be injected from only a few percent of the surface area to produce the inferred atmospheric dust loads within the plumes. Turbulence from the injection event and regional winds could potentially combine to keep the exposed surface rocks relatively free from settled dust deposits, confining the dust primarily to the cracks and other traps and potentially preserving the low albedo.

Another aspect of the model that might appear inconsistent with the observations is the lack of water vapor anomalies at the sites of proposed freeze/thaw injection. This was discussed in detail by Huguenin and Clifford (9), where it was shown that the amount of vapor that would be injected would have been undetectable by the Viking Mars Atmospheric Water Detector Experiment. The vapor would be injected during the predawn hours, form ice, and slowly sublime, producing negligible additions to the background vapor abundances. Abundant ice fogs and frosts were observed, however, after each of the major predawn storms, consistent with the release of $\sim$1 mg/cm^{-2} of H_2O from the fines (9). Clouds and fogs are the most sensitive indicators of H_2O vapor anomalies in the Mars environment, and there are preferential occurrences of the clouds and fogs in the low albedo regions (9).

The origin and preservation of low albedo markings has been a subject of considerable interest since the time that Mars was first studied, and it continues to be a focus of study at the present (10). The fact that dust storms and blue cloud activity were more frequent in the dark areas has also been of considerable interest (9). The model proposed here that the low albedo markings in the mid-latitude belts are the possible result of seasonally emplaced ground ice and humidification-induced dust entrainment may possibly provide a reasonable explanation for many of the characteristics of these features.

Acknowledgement. This research was supported by NASA Grants NSG7405 and NAGW570 to the University of Massachusetts.

References.

1 Huguenin, R.L., Harris, S.L., and Carter, R. (1986) Icarus, in press.
2 Biemann, K., et al (1977) J. Geophys. Res., 82, p.4641-4658.
3 Oyama, V.I. and Berdahl, B.J. (1977) J. Geophys. Res., 82, p.4669-4671.
4 Clifford, S.M. (1984) Ph.D. Dissertation, U Massachusetts.
5 Farmer, C.B., and Doms, F.E. (1979) J. Geophys. Res., 84, p.2881-2888.
6 Peterfreund, A.R. (1985) Ph.D Dissertation, Arizona State University.
7 Singer, R.B., McCord, T.B., Clark, R.N., Adams, J.B., and Huguenin, R.L., (1979) J. Geophys. Res., 84, p.8415-8426.
8 Kieffer, H.H., Martin, T.Z., Peterfreund, A.R., Jakosky, B.M., Miner, E.D., and Palluconi, F.D. (1977) J. Geophys. Res., 82, p.4249-4291.
9 Huguenin, R.L. and Clifford, S.M. (1982) J. Geophys. Res., 87, p.10227-10251.
10 Mutch, T.A., Arvidson, R.E., Head, J.W. III, Jones, K.L., and Saunders, R.S. (1976) The Geology of Mars, Princeton Univ. Press, Princeton, NJ, Chapter 1.

PHOTOCHEMICAL WEATHERING AND CONTEMPORARY VOLATILE LOSS ON MARS.
R.L. Huguenin, Geology/Geography, University of Massachusetts, Amherst, MA 01003.

In an earlier series of papers by the author it was proposed that photochemical weathering of Fe^{2+} in magnetite (1,2) and in mafic silicates (3) may be occurring in the contemporary surface environment with a resultant loss of O_2 from the atmosphere (4):

$$2FeO_{surface} + \tfrac{1}{2}O_{2atmosphere} + h\nu \rightarrow Fe_2O_{3surface} \quad (1)$$

It was estimated that a net loss of 10^{25}-10^{28} molecules cm^{-1} could have occurred over geologic time. If the O_2 were lost at the expense of H_2O, this would correspond to a loss of 10^0- 10^3m of ice over geologic time (4). Several lines of evidence from Viking lander and orbiter measurements as well as Earth-based telescopic observations support the occurrence of such a contemporary process on Mars. (5).

Morris and Lauer(6) challenged the photochemical weathering model, proposing that oxidation by radient heating rather than UV photoelectron-emission-induced oxidation may have dominated in our experiments. They based this on an experiment whereby unfiltered radiation was able to produce nearly complete oxidation of their samples, while IR-filtered xenon radiation produced no observable oxidation. Their unfiltered radiation produced very high temperatures, while the filtered radiation did not. The authors stated that the filtered and unfiltered irradiances were similar to within a factor of two at 350nm, and they deduced that the high temperatures of the unfiltered radiation drove the reaction.

Subsequent laboratory studies of photochemical weathering of magnetite described here support the original proposal that UV illumination can indeed drive the oxidation of magnetite under contemporary Martian surface conditions. The negative results of the Morris and Lauer (6) study can now be explained.

Samples of reagent grade precipitated magnetite (0.5g) from Fisher Scientific and Pfizer were used for the new experiments. The former sample was cation deficient and the latter was close to stoichiometric, as discussed by Morris and Lauer (6). Samples were placed in an environmental chamber consisting of a hollowed out (1¼" diameter x 3/8" depth) 2 3/4" Varian Conflat blank flange coupled to a 2 3/4" Varian Conflat Sapphire View Port flange using a copper compression gasket. Thermocouples, cooling and heating cartridges, and gas lines were fitted into the chamber, which was interfaced to a Varian ultrahigh vacuum system. The chamber provided horizontal sample orientation to minimize physical disturbance of the exposed sample surface throughout the experiment. The sample chamber was fitted to a sample port at the base of a prototype 3" integrating sphere within a Perkin Elmer 330 dual beam spectrophotometer (185-2600 nm). References and the integrating sphere coating were both Halon.

Samples were illuminated using a PRA Model 6100C microsecond pulsed UV source, which has a thyratron-gated 1.5μs pulse width (FWHM) and programmable pulse frequency. The output spans from 200-2000 nm with peak power at 300 nm (40% of total power output is at 200-500 nm). Samples were illuminated through selected Oriel Optics band pass and long pass filters. Samples were illuminated at pulse frequencies of 2.7 or 4.5 pulses per second (p/s), depending on the experiment, and reflectance spectra of the samples were measured periodically every 1-3 days. Peak pulse power varied depending on the filters used. The unfiltered source had 3kW peak power per pulse, which corresponded to 12.1 mW/cm^2 at 2.7 p/s and 202.2 nW/cm^2 at 4.5 p/s. A long pass filter with a 50%

transmission cut-on wavelength at 530 nm (Oriel Model 5130) yielded 1.3kW peak power per pulse. A UV band pass filter with a center at 325 nm and band width (FWHM) of 200 nm (IR-blocked) (Oriel Model 5165) yielded a peak power of 0.68kW per pulse. At 4.5 p/s pulse frequency, the UV filter produced 4.6 mW/cm^2 average power.

By using narrow pulse widths (1.5μs) and low pulse frequencies, the thermal component of incident radiation was low (flux at 1100 nm is ∿10% the flux at 350 nm) and samples could cool to near-ambient surface temperatures between pulses.

In situ reflectance spectra of the illuminated sample surface provided a sensitive means of detecting and monitoring oxidation. Spectra were periodically measured, and the spectra were divided by the starting (pre-illumination) spectrum to reveal changes. As discussed originally (1,2), a sensitive measure of oxidation of magnetite is provided by a reddening of the spectrum over the 350-750 nm wavelength range. By keeping the sample undisturbed physically, only the UV-illuminated surface layer is measured and surface scattering properties are held constant. A layer of Fe_2O_3 less than 1 micrometer thick can be detected.

Exposure of the Fisher Scientific (Lot 724199) magnetite sample to unfiltered radiation in ambient laboratory air at 20^0C revealed a systematic reddening of the sample that became visible in the ratio spectra (scaled to 1.0 at 350 nm) between the fifth and eighth days of exposure. In a second experiment, using a fresh 0.5 g sample from the same lot, but this time inserting the UV filter, reddening again occurred to the same extent after a similar exposure period, i.e., after 6-9 days. A third fresh sample from the same lot was illuminated using the long pass filter, and this time there was no detectable reddening after 49 days of illumination, at which point the experiment was terminated. The three experiments were repeated and the results were confirmed.

A second set of experiments were performed using samples of the Pfizer (Lot E1531) magnetite. As for the Fisher Scientific samples, the unfiltered radiation and radiation using the UV filter both produced detectable significant reddening after similar illumination periods. The length of time required to produce the equivalent reddening, however, was approximately six times longer than for the Fisher Scientific sample, viz. 32-54 days, using the same pulse frequency (4.5 p/s).

In these experiments, illumination through the UV filter was 85-95% of the intensity of the unfiltered radiation over the 200-330 nm wavelength range. Between 330 nm and 400 nm attenuation was appreciable, reaching 10^{-5} at 400 nm. Overall power was reduced, using the UV filter, to 23% of the power of the unfiltered radiation. Illumination through the long-pass filter, by contrast, attenuated total power by only a factor of 2.3 (42% of the power of the unfiltered radiation), with greater than 92% transmission at wavelengths longer than 550 nm. At wavelengths shorter than 520 nm, however, attenuation was total ($<10^{-5}$% transmission) with the long-pass filter. The fact that the illumination through the UV filter produced apparent oxidation at approximately the same rate as unfiltered radiation, while illumination through the long-pass filter produced no observable change after 5-8 times longer illumination, suggests that the reaction was probably controlled by radiation in the 200-330 nm range. This supports the original findings that the reaction is driven by UV illumination at wavelengths shorter than ∿350 nm.

An independent investigation was recently carried out by M. Schaefer (unpublished) at MIT. A magnetite sample was illuminated using a low-power 2.5 watt source, of which the sample intercepted 4 mW. If all the power were

absorbed with 100% efficiency, the maximum sample temperature that would have been possible was 29°C, well below the thermal oxidation threshold. Oxidation was observed to occur after 30 h of illumination (photon flux of 5×10^{15} photons/s intercepting the sample as λ = 253.7 nm line). About 1% of the sample was observed to oxidize to Fe_2O_3, using Mossbauer spectroscopy as the detection technique. In addition to providing independent evidence that the oxidation proceeded non-thermally, the quantum yield was determined to be $\sim$0.1, which was in good agreement with the quantum yield proposed by Huguenin et al (9) for radiation at that wavelength.

Another critical test was performed by a separate laboratory at MIT (8), and independently confirmed by a team at IBM Research Labs (9). The original study (1,2) deduced from the kinetics that photoelectron emission from the Fe^{2+} was occurring as a critical step in the process. It was argued that it occurred with a work function of 3.8-4.2 eV and a quantum yield of $\sim$0.1 electron/photon at 195 nm. This was the first time that photoemission of electrons was proposed to occur from Fe^{2+} in magnetite, and it was deduced to be the most critical and unique step in the process. Poole (8) designed an experiment to detect photoelectron emission from Fe^{2+} in minerals, and he experimentally confirmed that photoelectron emission did indeed occur with magnetite with a work function of 3.9 $\pm$0.1 eV. The quantum yield was also in agreement with predictions. Bagus et al (9) similarly determined a photo-threshold of 3.9$\pm$0.3 eV in a combined photoelectron-spin-polarization (ESP) and UV and far-UV photoemission spectroscopy (UPS and FUPS) study of magnetite.

These independent studies support the findings reported here, and suggest that photochemical weathering of magnetite can be UV-induced as originally proposed (1,2,3). The findings are in disagreement with the conclusions of Morris and Lauer (6), and two factors can be cited that may account for the disagreement.

The most important factor seems to be that Morris and Lauer may have not irradiated the samples long enough with the unfiltered radiation to produce detectable oxidation. In particular, examination of the spectral curves for the filtered and unfiltered radiation revealed that the flux differences were greater than claimed by Morris and Lauer. The spectral radiances were published by Morris and Lauer. The wavelengths significant for photooxidation are 195 nm - 350 nm (1,2). Inspection of their figure shows that only at 350 nm are the fluxes of the filtered and unfiltered radiation within the factor of 2 claimed by Morris and Lauer. By 230 nm the fluxes are different by a factor of 60. Extrapolations to 200 nm indicate that filtered fluxes were > $\sim$100 times lower than the unfiltered fluxes. The shorter wavelengths produce the more significant quantum yields for photooxidation ($\sim 10^{-7}$ at the 350 nm threshold to $\sim 10^{-1}$ at 200 nm) (7). Scaling the irradiation periods needed to produce oxidation with unfiltered radiation to these lower fluxes would require irradiation periods that were longer than those used by Morris and Lauer with the filtered radiation.

A second factor is the low sensitivity of their oxidation detection technique. To detect oxidation there would need to be a minimum of between 3% and 15% conversion to Fe_2O_3 (1 standard deviation of $J_S(t)/J_S(o)$ for hematite and maghemite, respectively). With the technique used here, only 0.1% (<1 micrometer thick oxidation layer on a millimeter thick layer of magnetite) conversion was required. To produce >3-15% oxidation would have required 30-150 times longer irradiation periods than required for the detection of 0.1% conversion, and under the conditions of the Morris and Lauer experiment irradiation times would again not have been long enough.

We think that these two factors explain the differences between the Morris and Lauer (6) results and the results reported here. The potential loss of H_2O by this process on Mars over geologic time would be a factor of 10^0-10^3 times greater than the amount predicted to have been lost by exospheric escape. It may be the principal reservoir for H_2O that has been released to the atmosphere over geologic time.

Acknowledgement. This research was supported by NASA Grants NSG7405 and NAGW570 to the University of Massachusetts.

References.

1 Huguenin, R.L. (1973) J. Geophys. Res., 78, p. 8481-8493.
2 Huguenin, R.L. (1973) J. Geophys. Res., 78, p. 8495-8506.
3 Huguenin, R.L. (1974) J. Geophys. Res., 79, p. 3895-3905.
4 Huguenin, R.L. (1976) Icarus, 28, p. 203-212.
5 Huguenin, R.L. (1982) J. Geophys. Res., 87, p.10,069-10,082.
6 Morris, R.V. and Lauer, H.V. Jr. (1980) Geophys. Res. Lett., 7, p. 605-608.
7 Huguenin, R.L., Prinn, R.G., and Maderazzo, M. (1977) Icarus, 32, p.270-298.
8 Poole, C. (1977) Thesis, MIT Dept. Physics.
9 Bagus, P.S., Brandle, C.P., Chuang, T.J., and Wandelt, K. (1977) Phys. Rev. Letters, 39, p. 1229-1232.

INTERANNUAL DIFFERENCES IN THE REGRESSIONS OF THE POLAR CAPS OF MARS

K. Iwasaki, Y. Saito, Kwasan Observatory, University of Kyoto, Kyoto 607, and T. Akabane, Hida Observatory, University of Kyoto, Kamitakara, Gifu 506-13, JAPAN.

Analyses of the behavior of the Martian polar caps in the recent spacecraft and ground-based observations seem to reveal the existence of year to year variations on their regressions(i.g. James et al. (1), James and Lumme (2), Iwasaki et al. (3), for the south polar cap; Iwasaki et al. (4), James (5), Iwasaki et al. (6), for the north polar cap).

In order to investigate the interannual differences in the regressions of the polar caps, we reexamined the earlier data by Fischbacher et al.(7), which were based on the measurements of the large number of high-quality photographic plates and films collected from 1905 to 1965 at the Lowell Observatory. Their data, consisted of the cap edge latitudes for each longitudes, are now projected onto a plane tangent to the pole of Mars using a polar stereographic projection in units in which the planetary radius is set as 0.5 after James and Lumme (2). Each circle, which shows the polar cap boundary, is derived by least squares fitting to these data points.

In figure 1, the south polar cap radius is plotted against the areocentric longitude of the sun, Ls. The regression data show a significant difference from year to year and the maximum difference occurs near Ls=250°. The best fit circles for the south polar cap boundaries of recorded years are shown in figure 2. The centers of the circles do not differ so much, but the radii are different significantly. We therefore conclude that there is an interannual difference in the regression of the south polar cap.

James et al. (1) reported that the 1977 dust storms seemed to have a significant effect on the south polar retreat. We examined the relation between the interannual difference in the regression of the south polar cap and dust

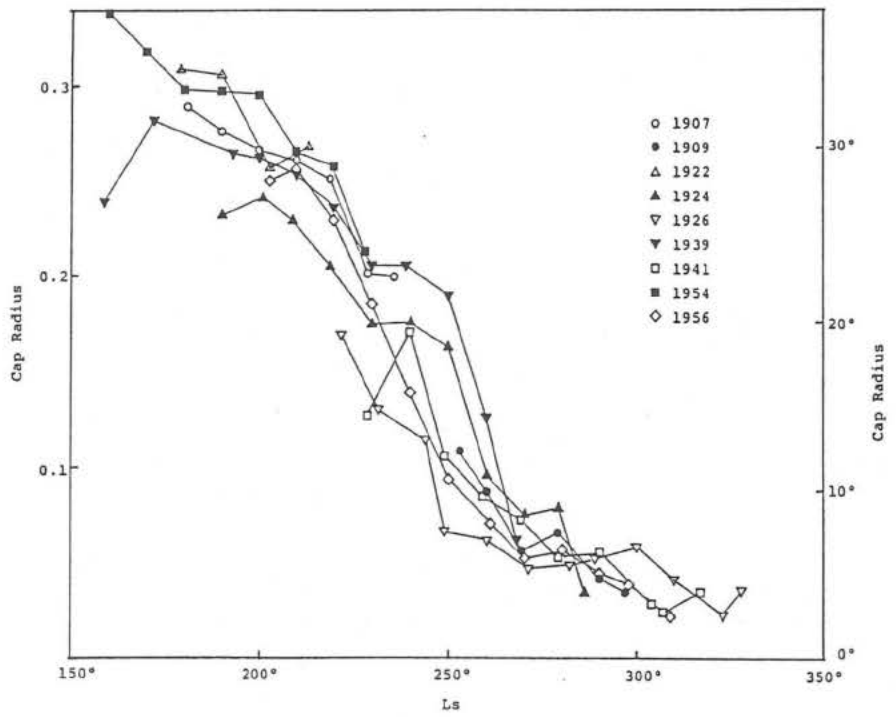

Fig. 1. The south polar cap radius (Mars diameter=1) as a function of Ls.

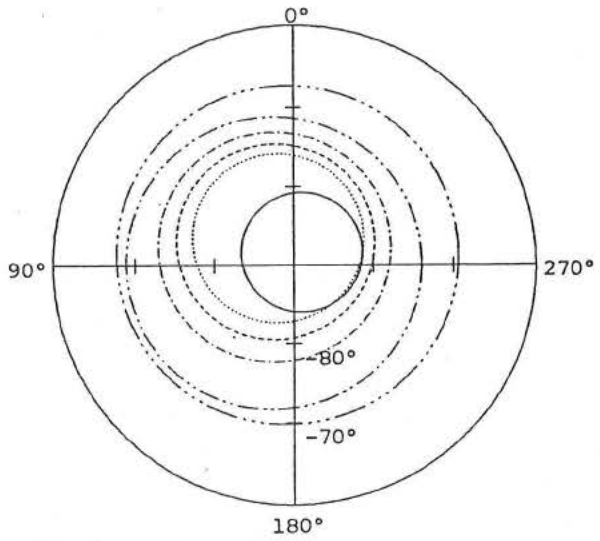

Fig. 2.
South polar cap boundaries at Ls=245°-254°.

------ 1909 ·—·—· 1924 ——— 1926
···—— 1939 ·—·—· 1941 ····· 1956

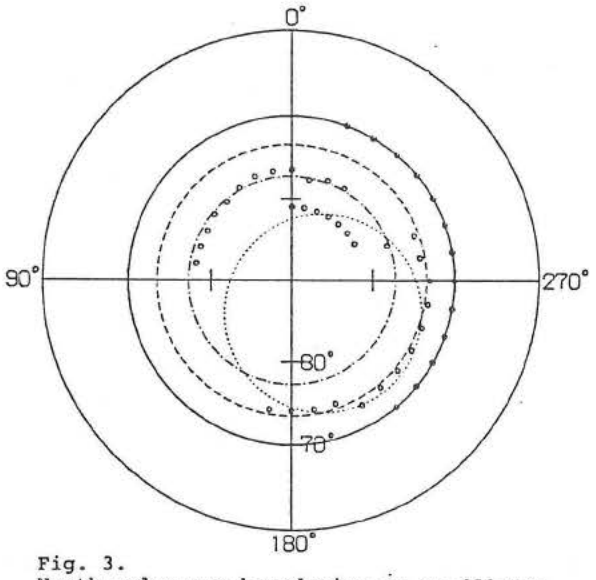

Fig. 3.
North polar cap boundaries at Ls=65°-74°.

——— 1916 ------ 1948
----- 1950 —·—·— 1965

storms, and found that the dimension of the south polar cap near Ls=250° tends to be larger in the year when the first dust storm occurs near Ls=200°.

In figure 3, the best fit circles of the north polar cap boundaries of observed years are shown. In figure 4, the north polar cap radius is plotted against the Ls. The mean regression curves for the north polar cap and south polar cap, obtained from our reexamination, are also shown for comparison. The regression data for the north polar cap also show a significant difference from year to year. The maximum interannual difference occurs near Ls=70° before the period of the permanent north polar cap.

As is seen in figure 4, the accumulation of the data is poorer for the north polar cap because the observational data must be obtained while the planet is near the aphelion of its orbit. But we can clearly see the smaller north polar cap and the standstill in its recession before Ls=40°, when compared with the south polar cap before Ls=220°. Also we see the larger north remnant cap after Ls=100°, when compared with the south remnant cap after Ls=280°. Comparing figure 1 and 4, we can say that the maximum interannual difference occurs in the same season in each of the polar caps. However, the maximum interannual difference of the latitude of the north polar cap (8°) is smaller than that of the south polar cap (14°). This smallness seems to be related to the difference of the distance from the sun. That is, in the season of the regression of the north polar cap, Mars is farther away from the sun and receives weaker energy from the sun. Great dust storms do not occur and the atmosphere is relatively clear and quiet. Therefore the interannual difference of the north polar cap seems to be smaller than that of the south polar cap. The mean regression curves of the north polar cap and the south polar cap are compared with the theoretical regression curves by James and North (8). The theoretical regression curves show that the north polar cap is always smaller than the south polar cap. On the contrary, in our reexamination of the observational data the north polar cap is larger than the south polar cap during the period of Ls=40°-77°.

Acknowledgments: We gratefully acknowledge the hospitality of the Planetary

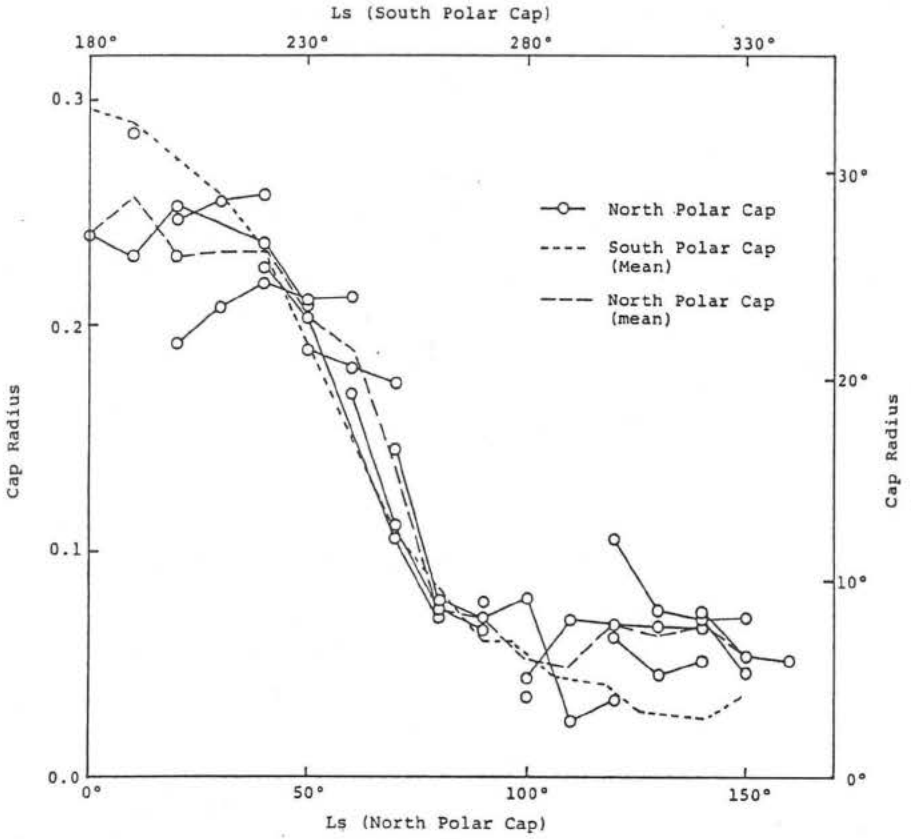

Fig. 4. The cap radius (Mars diameter=1) as a function of Ls.

Research Center of Lowell Observatory in supplying Mars data used in this study.

References

1. James P. B., Briggs G., Barnes J., and Spruck A. (1979) J. Geophys. Res., 84, p. 2889-2922.
2. James P. B., and Lumme K. (1982) Icarus, 50, p. 368-380.
3. Iwasaki K., Saito Y., and Akabane T. (1986) Publ. Astron. Soc. Japan, 38, P. 269-277.
4. Iwasaki K., Saito Y., and Akabane T. (1982) J. Geophys. Res., 87, p. 10265-10269.
5. James P. B. (1982) Icarus, 52, p. 565-569.
6. Iwasaki K., Saito Y., and Akabane T. (1984) Publ. Astron. Soc. Japan, 36, p. 347-356.
7. Fischbacher G. E., Martin L. J., and Baum W. A. (1969) Report under JPL Contract No. 951547, Planet. Res. Center, Lowell Obs., Flagstaff.
8. James P. B., and North G. R. (1982) J. Geophys. Res., 87, p. 10271-10283.

THE OBSERVED DAY-TO-DAY VARIABILITY OF MARS WATER VAPOR.

Bruce M. Jakosky[1], Michael R. LaPointe[1], and Richard W. Zurek[2]. [1]Laboratory for Atmospheric and Space Physics, University of Colorado, Boulder, CO 80309. [2]Jet Propulsion Laboratory, California Institute of Technology, Pasadena, CA 91109.

Introduction. Analyses of observations of water vapor in the Mars atmosphere have centered on the gross spatial and seasonal variation (e.g.,1,2). Although variations on timescales short compared to the martian seasons have been observed (3,4), there has been no systematic analysis of such variability. We have examined the variations of water vapor which occur from day to day within a given season using Viking Mars Atmospheric Water Detector (MAWD) data. This will allow us to understand short-term variations and observational effects which may play an important role in our understanding of the seasonal cycle of water.

Both real variations in water vapor and observational effects may result in an observed day-to-day variation of water vapor. Real effects include atmospheric transport of water vapor and ice or possible surface sources or sinks of water vapor active on short timescales. Observational effects that would produce an apparent day-to-day variability include variations of cloud or dust opacity, variable viewing geometry with some aerosol present, or variations in the vertical distribution of water vapor within the atmosphere (due to the uniform vertical profile assumed in the data inversions).

Data Analysis. Three distinct stages were involved in the data analysis. Initially, the entire MAWD database was re-inverted under a constant set of assumptions. Each raster, consisting of five radiance measurements which are the average of fifteen individual field-of-view measurements, was inverted to obtain the column water vapor abundance, assuming a constant effective temperature and an effective pressure of half of the (seasonally and spatially varying) surface pressure. All further analysis was done using this reduced data set. This approach is distinct from that used earlier (1,2,3), where values were averaged over 10° of latitude and longitude and 15° of L_s; our approach is more appropriate for examining day-to-day variations in column water abundance.

In the second step, daily averages of water vapor were obtained by averaging over 10° of latitude and longitude. These averages were used to construct maps of the day-to-day variability over 15° of L_s; the variability was calculated as the standard deviation of the daily averages, normalized to the average water value within this bin. Finally, these maps were examined, and selected locations (in space and season) were chosen for further study. This final stage took the form of constructing plots of the raster-level data (such as water vapor versus local time of day or observed brightness) in order to constrain those processes which might be producing the observed variability of water.

Results. Figure 1 shows a zonally-averaged plot of the water vapor variability as a function of latitude and season for the bulk of the Viking mission. Systematic trends in the variability are, in fact, seen. Increased variability is seen at the start of the two 1977 global dust storms (at L_s 205° and 275°); this variability is due to the effects of obscuration of the water vapor by airborne dust. High variability is seen along the edge of the retreating north polar seasonal cap during the northern spring season (L_s 0-60°); clouds were observed here at these seasons (5,6), and the MAWD data indicate that the variability is an observational effect due to their presence. Finally, high variability is seen in the northern spring season in

the Tharsis and Lunae Planum regions. The water vapor data here indicates a large apparent dependence on local time of day and a correlation with the observed brightness that suggests that morning and afternoon clouds combined with the day-to-day variations of the observing geometry are responsible.

There is a remarkable correlation of the seasonal and spatial trends of the water vapor variability with the occurrence of moderate and thick diffuse hazes in the atmosphere as mapped by Kahn (6). Much of this observed variability is probably an artifact of the variable viewing geometry. Due to the nature of the Viking orbit, which was most often asynchronous, a location on the surface that is observable for many consecutive days will be seen first near one limb, then near the center of the disk, then near the other limb. Scattering by aerosol will reduce the apparent column water vapor abundance, producing an apparent time-of-day or day-to-day variability of water (3,7). Superimposed on this apparent variation with time of day is an additional time-of-day dependence due to the diurnal variations of atmospheric temperature and the tendency for clouds to form preferentially near dawn and dusk.

Conclusions. Analysis of the day-to-day variability of water vapor in the martian atmosphere suggests that the observations are, at certain locations and seasons, significantly affected by the presence of water-ice hazes. Because such effects are generally limited to specific locations, such as Tharsis, Lunae Planum, and the polar cap edge during the spring, the seasonal and latitudinal trends in water vapor that have been previously reported are not significantly affected.

References. (1) Farmer and Doms, J.G.R., 84, 2881, 1979. (2) Jakosky and Farmer, J.G.R., 87, 2999, 1982. (3) Farmer et al., J.G.R., 82, 4225, 1977. (4) Davies and Wainio, Icarus, 45, 216, 1981. (5) Christensen and Zurek, J.G.R., 89, 4587, 1984. (6) Kahn, J.G.R., 89, 6671, 1984. (7) Davies, J.G.R., 84, 2875, 1979.

Figure 1: Zonally-averaged normalized day-to-day water vapor variability in the martian atmosphere.

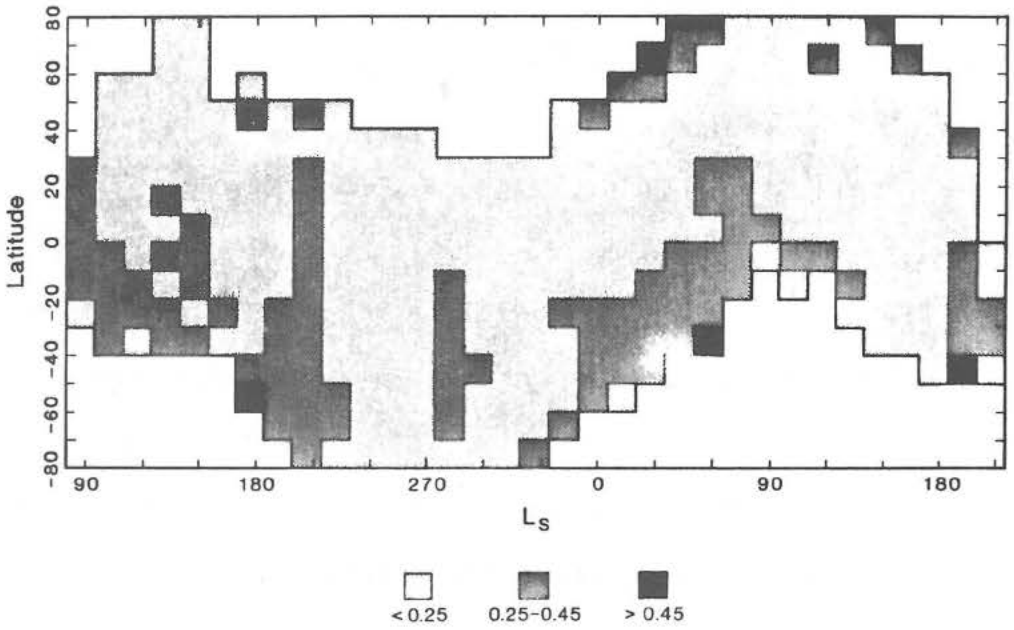

THE DIRECTION OF WATER TRANSPORT ON MARS: A POSSIBLE PUMPING MECHANISM.

P. B. James, Physics Department, University of Missouri-St. Louis, St. Louis, MO 63121.

William Herschel (1) first recognized that a seasonal volatile cycle was revealed by variations of the martian polar caps which, by analogy with Earth, he assumed were composed of water ice. Leighton and Murray (2) demonstrated that carbon dioxide was a more likely candidate for the polar volatile, and this was confirmed by the infrared observations of Mariner 7 (3). Surface pressure measurements by Viking landers (4) as well as accurate polar cap measurements from Viking orbiter images (5) have afforded the opportunity to quantitatively model the CO_2 cycle thereby constraining the physical mechanisms which play a role in the martian climate system.

Viking data also revealed an active hydrologic cycle on Mars through observations of a water ice residual north polar cap (6) and vapor in the atmosphere (7). The surface ice and atmospheric water vapor abundances observed by Viking experiments are quite asymmetric in their latitudinal distributions. This has raised the interesting question of the direction of net water transfer on Mars at the present time; is water transferred from north to south or from south to north when integrated over an entire seasonal cycle? Jakosky (8) has correctly noted that transfer should be in the direction of the negative gradient of the net vapor distribution if no pumping mechanisms are present. Scavenging of vapor by the cold CO_2 permanent cap in the south should also cause a north to south transfer.

A mechanism which can "pump" water from south to north on Mars does exist for the current orbital parameters of Mars. It is provided by the asymmetric seasonal temperature distribution produced by the eccentric

martian orbit and by the associated seasonal asymmetry in the carbon dioxide cycle. The alternating condensation and sublimation of CO_2 at the poles produces condensation winds (9) which, in turn, contribute to the meridional transport of water vapor. For the current values of orbital elements, the phasing of these asymmetric condensation winds with the surface temperatures is such as to provide net south to north transport during the seasonal cycle (10). This pumping action is strong enough to overcome the tendency of vapor to diffuse down the gradient and can maintain the asymmetric water distributions observed. The question of long term entrapment of water by a permanent CO_2 cold trap in the south is less clear cut; the pumping mechanism will reduce the rate of condensation, but long term effects depend on the long term stability of the residual south cap, which is not certain.

Research supported by NASA Grant No. NAGW 742.

1. Herschel, William (1784). Philosophical Transactions lxxiv, 233-273.
2. Leighton, R. B. and B. C. Murray (1966). Science 153, 136-144.
3. Neugebauer, G., G. Munch, H. Kieffer, S. Chase, and E. Miner (1971). Astron. J. 76, 719-749.
4. Ryan, J. A., R. Henry, S. Hess, C. Leovy, J. Tillman, and C. Walcek (1978). Geophys. Res. Lett. 5, 717-718.
5. James, P. B., G. Briggs, J. Barnes, and A. Spruck (1979). J. Geophys. Res. 84, 2889-2922.
6. Kieffer, H. H., S. Chase, T. Z. Martin, E. D. Miner, and F. D. Palluconi (1976). Science 194, 1341-1344.
7. Jakosky, B. M. and C. B. Farmer (1982). J. Geophys. Res. 87, 2999-3019.
8. Jakosky, B. M. (1983). Icarus 55, 19-39.
9. Hess, S., R. M. Henry, and J. Tillman (1979). J. Geophys. Res. 84, 2923-2927.
10. James, P. B. (1985). Icarus 64, 249-264.

CLIMATIC EFFECTS OF ENHANCED CO_2 LEVELS IN MARS' EARLY ATMOSPHERE; James F. Kasting, Space Science Division, MS 245-3, NASA Ames Research Center

The existence of branching valley networks in ancient, heavily cratered Martian terrain probably implies a much warmer and wetter Martian climate in the past (1,2). The most likely mechanism for bringing this about is greatly enhanced atmospheric CO_2 pressures. Calculations of the amount of CO_2 necessary to warm the early climate have been made previously using 1-D, radiative-convective models. For present solar luminosity, Pollack (3) predicted that about 2 bars of CO_2 would be required to elevate Mars' average surface temperature (T_s) above the freezing point. Cess et al. (4) repeated the calculation with what they claimed was a more sophisticated radiative model and concluded that only about 0.7 bar of CO_2 would be required to bring T_s above freezing. Their model also predicted warmer temperatures for early Earth than did other 1-D climate models (5,6,7). Subsequently, Cess et al. have discovered that their original model contained an error that caused their predicted surface temperatures to be too high (V. Ramanathan, private communication, 1985). New calculations described here confirm Pollack's earlier results and show that the climatically plausible range of CO_2 pressures for early Mars is 1 to 5 bars.

The radiative-convective model used here is described in references (8) and (9). Absorption coefficients for H_2O and CO_2 in 55 different spectral intervals were derived by fitting synthetic spectra generated from the AFGL tape (10). Band models (Goody model for H_2O, Malkmus model for CO_2) were used in the infrared; exponential sum fits were used in the visible and near-IR. Approximate Doppler corrections were applied to the band models, and the effective broadening pressure was modified to account for the increased efficiency of collisions involving H_2O or CO_2. The absorption coefficients used here are particularly appropriate for modeling the dense early Martian atmosphere because they were derived for CO_2 column densities as high as those on Venus. A δ 2-stream scattering approximation was used to calculate solar energy deposition. Rayleigh scattering cross sections were calculated by the method of Vardavas and Carver (11). The Rayleigh scattering coefficient for CO_2 is a factor of 2.5 times higher than that of air; this is climatically important because it enhances the planetary albedo and provides a negative feedback on surface temperature at high CO_2 levels.

Other parameters in the model were treated in the following manner: The moist adiabatic lapse rate was used in the troposphere. The tropospheric relative humidity was assumed to follow a Manabe/Wetherald (12) profile, with a surface value of 0.77. Above the convective region, the relative humidity was allowed to increase upwards, provided that the water vapor mixing ratio did not increase with altitude. Clouds were assumed to be absent in all cases. The surface albedo was fixed at 0.215; this choice produced a planetary albedo of 0.212 for the present Martian atmosphere, in good agreement with the measured value of 0.214 (13). The present solar flux was assumed to be 0.43 times the flux at Earth's orbit; the surface gravity was set at 373 cm s^{-2}; and the present surface pressure (p_s) was assumed to be 6 mbar.

Calculated surface temperatures (T_s) and planetary albedos (A_p) for different surface pressures and present solar flux are shown in Figure 1. Both T_s and A_p increase slowly at first as p_s is increased, then more rapidly at pressures exceeding a few tenths of a bar. The surface pressure

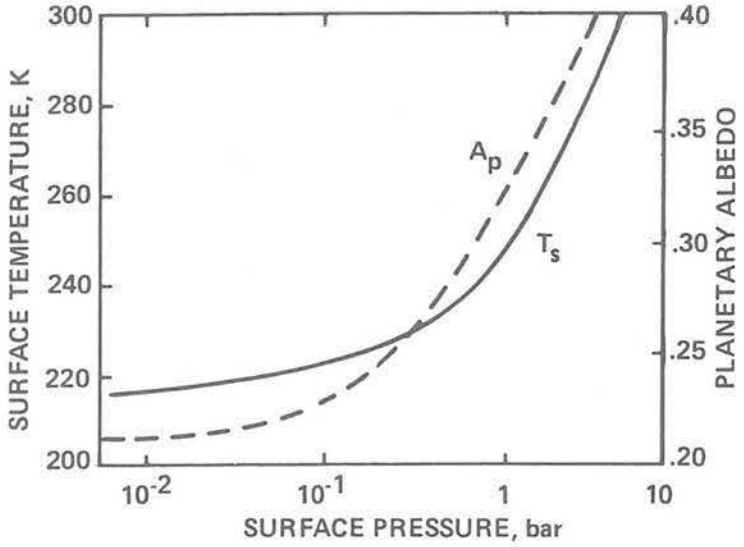

Fig. 1 Calculated surface temperature T_s and planetary albedo A_p as a function of surface pressure. A pure CO_2 atmosphere and present solar flux are assumed.

required to elevate T_s above freezing is 2.2 bars, in agreement with Pollack's earlier prediction (3). The calculated planetary albedo is in rough agreement with that predicted by Cess et al. (4), except that it does not exhibit the decrease near p_s = 1 bar caused by the large amount of water vapor in their model.

This calculation does not directly tell us about early Mars because the solar flux (S_o) was lower in the past by 25 to 30% (14,15). For a 30% reduction in S_o, the CO_2 pressure required to elevate Mars' average surface temperature above freezing is about 5 bars (Fig. 2). On the other hand, Mars' orbit is highly eccentric (e = 0.093); thus, at perihelion the incident solar flux is enhanced by some 22%. At Mars' maximum eccentricity of 0.14 (16), the enhancement in S_o at perihelion would be 35%. Furthermore, the equatorial regions are more strongly heated than the planet as a whole by about 40%. Thus, under favorable conditions (at the equator during perihelion), the local irradiation in certain areas on early Mars could have been as much as 30% higher than the present flux. The CO_2 pressure required to push T_s above freezing in this case is just 1 bar (Fig. 2). This value could be even further reduced to 0.8 bar if the surface albedo of (an unoxidized) early Mars was as low as 0.1 (dashed curve, Fig. 2).

In conclusion, Mars could have had surface temperatures above freezing in the past if the CO_2 pressure was above ~1 bar. Approximately 2 to 5 bars of CO_2 would have been required for widespread liquid water to exist. More detailed (3-dimensional) climate models could refine this prediction to some extent; however, large uncertainties would still remain because of the possible presence of other greenhouse gases and of clouds.

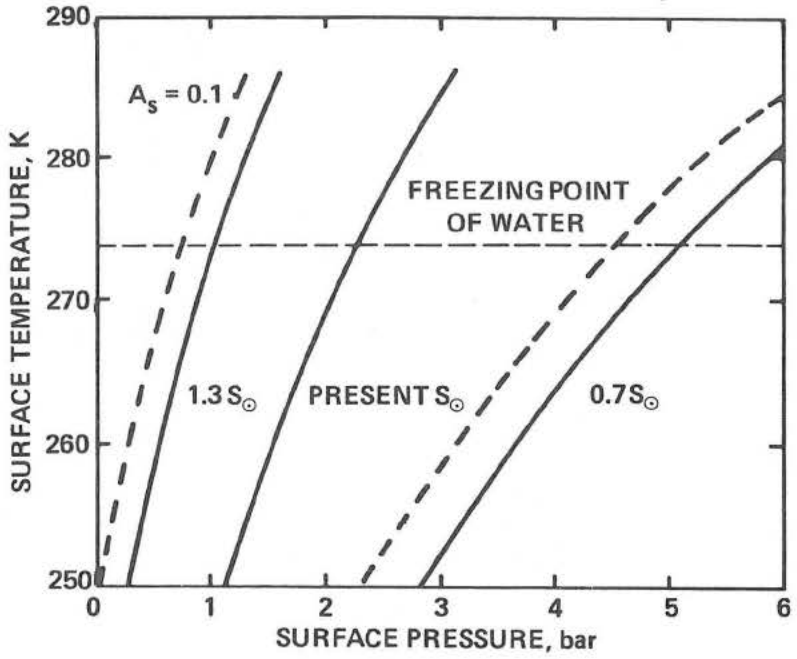

Fig. 2 Surface temperature as a function of surface pressure for different values of the incident solar flux. Solid curves are for a surface albedo A_s of 0.215; dashed curves are for A_s = 0.1.

References

1. Sagan, C., Toon, O.B., and Gierasch, P.J. (1973) Science, 181, 1045-1049.
2. Masursky, H., Boyce, J.M., Dial, A.L., Schaber, C.G., and Strobell M.E. (1977) J. Geophys. Res., 82, 4016-4038.
3. Pollack, J.B. (1979) Icarus, 37, 479-553.
4. Cess, R.D., Ramanathan, V., and Owen, T. (1980) Icarus, 41, 159-165.
5. Owen, T., Cess, R.D., and Ramanathan, V. (1979) Nature, 277, 640-642.
6. Kuhn, W.R. and Kasting, J.F. (1983) Nature, 301, 53-55.
7. Kasting, J.F., Pollack, J.B., and Crisp, D. (1984) J. Atmos. Chem., 1, 403-428.
8. Kasting, J.F. and Ackerman, T.P. (1986) Manuscript in preparation.
9. Ackerman, T.P., Kasting, J.F., and Pollack, J.B. (1986) Manuscript in preparation.
10. McClatchey, R.A., Fenn, R.W., Selby, J.E.A., Volz, F.E., and Garing, J.S. (1971) Tech. Rept. AFCRL-71-0279, Bedford, Mass.
11. Vardavas, I.M. and Carver, J.H. (1984) Planet. Space Sci., 32, 1307-1325.
12. Manabe, S. and Wetherald, R.T. (1967) J. Atmos. Sci., 24, 241-259.
13. Kieffer, H.H., Martin, T.Z., Peterfreund, A.R., and Jakosky, B.M. (1977) J. Geophys. Res., 82, 4249-4292.
14. Newman, M.J. and Rood, R.T. (1977) Science, 198, 1035-1037.
15. Gough, D.O. (1981) Solar Phys., 74, 21-34.
16. Murray, B.C., Ward, W.R., and Yeung, S.C. (1973) Science, 180, 638-640.

AREAL AND TIME DISTRIBUTIONS OF VOLCANIC FORMATIONS ON MARS

G.N.Katterfeld and V.I.Vityaz
Section of Planetology, Astronomical Society, the USSR Academy of Sciences

The analysis of igneous rock distribution has been fulfilled on the basis of the Geologic-morphological map of Mars at scale 1 : 5 000 000 compiled by G.N.Katterfeld (1972 - 85) according to the data obtained from interpretation of 1 : 2 000 000 scale pictures of „Mariner 9", „Mars 4", „Mars 5", „Viking 1 and 2". The following areological eras or groups have been distinguished as the stratigraphic basis for a martian time scale: I.Pre-Hellassian (PH), II.Hellassian (H), III.Elysian (E), IV.Amazonian (A), V.Olympian (O) /1, 2/. These 5 eras are subdivided into 14 periods (systems): 1. Ancient (PH_1), 2. Eridanian (PH_2), 3. Newtonian (PH_3); 4. Amphitritian (H_1), 5. Keplerian (H_2), 6. Phaethontian (H_3); 7. Acheronian (E_1), 8. Tharsidian (E_2); 9. Korolevian (A_1), 10. Alban (A_2), 11. Arcadian (A_3); 12. Arsian (O_1), 13. Pavonian (O_2), 14.Ascraean (O_3). These periods are, in turn, subdivided into more detailed epochs (sections), for example, early, middle and late Alban A_2^1, A_2^2, A_2^3; early, middle and late Arcadian A_3^1, A_3^2, A_3^3 /3/. The latest - Olympian era is crowned with the Modern epoch, represented by light rayed craters, barchan and dunes fields, and polar glacial depositions.

The area of volcanic eruptions and the number of eruptive centers are calculated on 10 x 10° cells and for the each areological eras: PH, H, E, A, and O. The largest area of eruptions happening at different times is related with Tharsis tectonic uplift. The summary area of martian basalts is 47 %, including 15 % for eruptive volcanic formations; the sum total of eruptive centers is 154 volcanoes. Almost half of igneous rocks area and of number of volcanoes dates from the Pre-Hellassian and Hellassian eras. The areas of Amazonian and Olympian volcanic formations are about 25 % each, and number of mapped eruptive centers for Olympian era is 14 (37 % from common number). The area of Elysian volcanic formations is more 1 %, and number of eruptive centers is 6 % from common number on Mars.

The study of distribution of igneous rock area and volcanic centers number on 10° sectors and zones revealed the concentration belts of volcanic formations. There are the greatest prevalence belts of volcanogenous formations along 108° W (meridian of major axis of triaxial martian ellipsoid) and 15°N, also the five meridional and three zonal belts along 5°, 65°, 95°, 245°, 295° W, and 35°N, 15°S, 65°S. The spaces between adjacent active belts are 30 ± 10°, 60 ± 10°, and 110°.

The most number of eruptive centers are observed in the sector of meridian 120° and in zone of parallel 65°S which coincide practically with „extremal" meridian 108°W and parallel 62° S /4, 5, 6/.

Maximum area of igneous rocks of Olympian era is coincided with sector of meridian 135°W and zone of parallel 15°N.The most area of Amazonian volcanites are along meridian 115°W and parallel 45°N. The igneous formations of Hellassian era are concent-

rated in the South hemisphere and subequatorial zone of planet. The maximum area of volcanic rocks of Hellassian is observed in sector of meridian 65°W and zone of parallel 62°S.

The belts of maximum prevalence of volcanic formations in course of areological time moved from the East to the West and from subpolar regions to equator. I.e., favourable for volcanic eruptions tectonic conditions for the early stages of planetary evolution taked place in subpolar regions of relatively tectonic contraction, but the volcanites of late stages are formed mainly in subequatorial zone with relatively tectonic expansion of planet (canal Agathodaemon = rift valleys Marineris).

Noteworthy, the 20° equatorial zone itself is characterized as belt with the moderate areal disposition of volcanic rocks and eruptive centers.

The planetary area of Olympian volcanic formations with the NW and NE orientations is connected with Tharsis tectonic uplift. The major tectonic and volcanic heights of Mars (and of all planetary solar system, at all) are linked to Tharsis. The Tharsis mountain massif and framing regional tectonic structures are as framework control for disposition of the major volcanic regions of planet. There are here the characteristic zonal-concentric pattern of volcanic rocks disposition, and typical Radial System of disjunctive dislocations, including major faults, rift valleys and lineaments. The Tharsis is volcanic-tectonic Radial-Concentric System of Mars, with periodical activity. In Hellassian era Tharsis was as large, relatively unamplitude positive structure with the vast display of volcanic processes. The differentiation with decrease of uplift area but with increase of uplift hights is happened in the following epochs of volcanic-tectonic activization. In Olympian era taked place the intensification of volcanic activity on the background of contrasting uplift of tectonic systems and volcanic centres of Tharsis that reached the hights of 27 km.

REFERENCES

1. Beneš K., Galibina I.V. and Katterfeld G.N.(1975). Trends in evolution of the terrestrial planets.-Proceedings of the USSR Acad.Sci.,Geol.Ser.,No 5,p.5-33,(in Russian).Intern. Geol.Rev.,1978,vol.20,No 1,p.1-25, (in English).
2. Katterfeld G.N. (1977). Principles of the geologic mapping of planets. - Problems of Planetology, vol.2 (Tectonics and Volcanism of Planets), Leningrad-Yerevan, p. 47 - 60, (in Russian); ibid. Yerevan, p. 49 - 64, (in English).
3. Katterfeld G.N. and Shmouratko V.I. (1986). Planetological comparison of Mars and the Earth. - Modern Geology, New York - London - Paris - Montreux - Tokyo, (in press).
4. Katterfeld G.N. (1958). Basic regularities of planetary relief. - Transactions of Leningrad Pedagpgical Institute,vol. 151, p.101 -134 + 2 Tabl., (in Russian).
5. Katterfeld G.N. (1962). The Face of the Earth and its Origin, Moscow,152 pp.,(in Russian); NASA,Langley,1968,(in English).
6. Katterfeld G.N. and Shmouratko V.I. (1983). Planetological differences and similarities of the Earth and Mars. - Proceedings of the Armenian Acad.Sci., Geosciences, vol.36, No 6, p.62-73, Yerevan, (in Russian).

INFLUENCE OF POLAR-CAP ALBEDO ON PAST AND CURRENT MARTIAN CLIMATE; Hugh H. Kieffer (U.S Geological Survey, Flagstaff AZ 86001) and David A. Paige (Jet Propulsion Laboratory, Pasadena CA 91109)

The bolometric reflectance of the Martian polar caps is a significant term in the annual heat budget of the caps and, in turn, in the current seasonal climate. The albedos of the polar caps were observed by the Viking Orbiters to vary significantly with time and location (1,2): albedos of the two caps differ, but generally increase with insolation intensity. Possible contributing "micromechanisms" include grain growth through metamorphism, floating away or sinking of included dust grains, subsurface sublimation and surface recondensation of CO_2, and surface concentration of frozen H_2O. Although the importance of each of these mechanisms is still uncertain, seasonal-cap models that incorporate the observed albedo variation and the hemispheric difference in polar topography correspond better than other models to the observed annual surface-pressure cycle. Observations by the Mars Observer could distinguish among many of these micromechanisms.

Frost metamorphism is expected to result in grain growth on the order of 100 μm diameter in half a Martian year and would yield a decrease in albedo through the spring and summer. Stokes "floating" is predicted for dust grains of diameters less than 10 μm that reach the cap surface under typical polar summer conditions; this process would yield a constant albedo for dust that initially was uniformly mixed. Radiative transfer in dusty CO_2, which includes sinking motion of individual grains relative to the subliming surface (due to their greater absorption of insolation), has been modeled and does demonstrate the observed brightening. This model also predicts subsurface sublimation and surface frost growth due to the smaller extinction coefficient for thermal versus solar wavelengths. The concentration effect of H_2O frost grains depends upon relative grain size, but it is unlikely to be significant because of the similarity between CO_2 and H_2O single-scattering albedos. The magnitudes of these micromechanisms will vary in different ways with the astronomical variation of insolation.

The variability of CO_2 frost albedo will be important for long-term climate models; the frost albedo will depend upon the dustiness of the atmosphere, and hence upon the atmospheric surface pressure and dynamics. In models that include both the polar caps and the regolith as volatile reservoirs, the free (atmosphere + cap) volatile inventory depends largely on the soil albedo and the obliquity; however, the surface atmospheric pressure is still controlled by the vapor pressure of a perennial polar cap (3). This mutual dependence of surface pressure, amount of atmospheric dust, frost albedo, and stability of the polar caps make predictions at different obliquities quite uncertain. The variation of obliquity is the dominant term in the astronomical control of Martian climate (4,5); yet, the total range of obliquity is equivalent to an albedo range of 0.65 to 0.88, a range readily accomplished by dusty and clean CO_2 frosts. In Martian climate models, polar-frost albedo has commonly been assumed to be constant; this simplifying assumption about a major parameter in the annual volatile cycle brings into question at least the quantitative aspects of such models. An understanding of the processes governing current Martian

climate is required before reliable extrapolations can be made to other conditions.

Another challenge for climate models is to distinguish between the effects of the precessional hemispheric asymmetry, which probably controls the season of the dust storms and has a cycle of 50,000 years, and the topographic hemispheric asymmetry, which may influence the global circulation patterns and which perseveres over the astronomical insolation cycles.

References

(1) Kieffer H. H. (1979) J. Geophys. Res., 84, p. 8263-8288.
(2) Paige D. A. (1985) Thesis, California Institute of Technology.
(3) Fanale F. P., Salvail J. R., Banerdt W. B., and Stevens R. S. (1982) Icarus, 50, p. 381-407
(4) Ward W. R. (1974) J. Geophys. Res., 79, p. 3375-3386.
(5) Ward W. R., Murray B. C., and Malin M. C. (1974) J. Geophys. Res., 79, p. 3387-3410.

REGIONAL SOURCES AND SINKS OF DUST ON MARS: VIKING OBSERVATIONS OF CERBERUS, SOLIS PLANUM, AND SYRTIS MAJOR;

Steven W. Lee, Department of Geology, Arizona State University, Tempe, AZ 85287

Seasonal variability of classical martian albedo features has long been noted by terrestrial observers [1,2]. Spacecraft observations of such features have shown them to be related to aeolian transport of bright dust into and out of regions, primarily in association with major dust storms [cf. 3,4]. Investigation into the amount and direction of dust transport related to variable features can reveal regions which, at present, act as either sources (net erosion of dust from an area) or sinks (net deposition) [5,6].

A study of seasonal variations of albedo features in the Cerberus, Solis Planum, and Syrtis Major regions has been based on Viking Orbiter data obtained over more than one complete martian year. Contour maps of Lambert albedo and single-point thermal inertia have been constructed from the Infrared Thermal Mapper (IRTM) experiment data, and Orbiter images have been used to determine the pattern and variability of regional winds (inferred from wind streak orientations). Coupled with ground-based radar data, these data sets allow the regional sediment transport direction, surface properties (texture, morphology, and roughness), and the implications of the observed seasonal and longer term dust redistribution, to be investigated. The results of this study are outlined below.

Solis Lacus, the most prominent dark albedo feature in Solis Planum, extends over approximately 20° of longitude and 10° of latitude (centered at 25°S, 85°W), and contains and is surrounded by a conspicuous pattern of bright and dark wind streaks. The albedo feature is highly variable in extent and contrast with its surroundings, generally being most distinct during southern spring and summer (minimum Lambert albedo ~0.13) and less distinct during southern fall and winter (minimum albedo ~0.16). The regional thermal inertia values (~8-10 x 10^{-3} cal/cm^2/sec$^{1/2}$/°K) are indicative of a surface covered by particles larger than ~100 μm [7]. A seasonal dust-transport cycle has been proposed to explain these observations: 1) During late southern spring and summer, bright dust is eroded from the surface (possibly ejected by a saltation triggering mechanism) and transported from the region by local dust storms (several were detected by Viking, and have been commonly observed from Earth). Removal of dust over a wide area results in the dark, distinct, Solis Lacus feature. 2) Following cessation of dust-storm activity, sedimentation from the atmospheric dust load occurs over the entire region, decreasing the contrast of the albedo feature with its surroundings. 3) The cycle may be renewed by dust-storm activity the following year. The retention of some albedo features throughout the year, plus the constancy of the regional thermal inertia, requires that the albedo features do not involve erosion or deposition of substantial deposits; cycling of, at most, a few tens of μm of dust is indicated. Differences in time of occurrence, severity, and longevity of dust-storm activity may lead to the observed year-to-year changes in Solis Lacus.

Dramatic seasonal variability is also characteristic of Syrtis Major (~5°S - 25°N, 275° - 300°W). The feature lies on the low-albedo slopes of a volcanic shield [8] (generally darker than ~0.2 in albedo), the darkest area (albedo ~0.1) being closely associated with a mass of dunes located near the crest of the shield. Thermal inertias of ~8 x 10^{-3} cal/cm^2/sec$^{1/2}$/°K, plus the observed dunes, argue strongly for a sandy surface. Syrtis Major increases in albedo immediately following global dust storms, then darkens steadily through the balance of the year until reaching its pre-storm albedo (also confirmed in [9]). The observed trend of bright and dark streaks is in response to winds generally directed upslope and to the west. The dust-transport cycle consistent with these observations is: 1) Enhanced deposition from global dust storms increases the regional albedo. 2) The relatively mobile surface coupled with effective regional winds (possibly reinforced by the global circulation) results in ejection of dust from the surface and net transport to the west during the remainder of the year, yielding a decreased regional albedo. 3) Beginning of another global dust-storm cycle begins the process again. Such a transport cycle provides a mechanism for significantly enhanced deposition in the neighboring low thermal inertia region, Arabia (as suggested in [10]).

Cerberus is located to the south of the Elysium volcanoes on the gentle slopes (< 0.5°) of Elysium Planitia, extending over about 10° of latitude and 20° of longitude. The feature is generally darker than ~0.2 in albedo, with the eastern portion being darker (minimum albedo of ~0.14) than that to the west (minimum albedo ~0.16). The albedo pattern is closely correlated with the regional thermal inertias, with the darkest areas having inertias of ~10 x 10^{-3} cal/cm^2/sec$^{1/2}$/°K, while the slightly brighter western region exhibits lower inertias of ~8. The entire Cerberus feature is surrounded by brighter (albedos to 0.30), lower inertia (~4) material. The pattern of wind streaks suggests relatively constant effective wind directions from the east, indicating that the gentle topography is not sufficient to significantly alter or enhance the global circulation [5]. Seasonal albedo variations closely mimic those observed in Syrtis Major, although the post-dust-storm darkening is not as pronounced, suggesting that the aeolian environment is less vigorous in Cerberus. The albedo and thermal inertia east-west asymmetry is consistent, however, with coarser material residing in the east and being transported westward by the global winds. Cerberus may therefore be acting as a source of sediment which is transported by saltation rather than in suspension. .

These observations indicate that very different levels of aeolian activity give rise to the noted seasonal variability of these regions: 1) Syrtis Major presents a picture of an extremely active aeolian environment. Deposition occurs only during and immediately following major dust storms, while during the rest of the year regional winds are apparently effective agents of dust ejection and transport. Syrtis Major thus acts as a dust source region through most of the year, possibly supplying the neighboring dust sink region of Arabia. 2) Cerberus may be thought of as a less-vigorous version of Syrtis Major, with definite removal of dust following global storms. A net westward flux of coarser material is evident, possibly encroaching onto surrounding Elysium Planitia. 3) In Solis Lacus, local dust storms result in net removal of dust from the area, while deposition occurs from the atmospheric dust load throughout the remainder of the year. Solis Planum serves as a source region of dust only during the limited period (dust storm season) when regional winds are capable of inducing dust ejection from the surface. Contributions to the global dust load may occur only during major dust storms.

REFERENCES

[1] Slipher, E.C., 1962, *A Photographic History of Mars, 1905-1961*, Northland Press, Flagstaff, AZ.
[2] De Mottoni, G., 1975, *Icarus 25*, 296-332.
[3] Sagan , C. et al., 1973, *J. Geophys. Res. 78*, 4163-4196.
[4] Thomas, P. and J. Veverka, 1979, *J. Geophys. Res. 84*, 8131-8146.
[5] Lee, S.W. et al., 1982, *J. Geophys. Res. 87*, 10025-10041.
[6] Lee, S.W., 1986, submitted to *Icarus*.
[7] Kieffer, H.H., et al., 1977, *J. Geophys. Res. 82*, 4249-4295.
[8] Schaber, G.G., 1982, *J. Geophys. Res. 87*, 9852-9866.
[9] Christensen, P.R., 1986, *Lunar Planet. Sci. Conf. XVII*, 121-122.
[10] Christensen, P.R., 1982, *J. Geophys. Res. 87*, 9985-9998.

WATER AND ICE ON MARS: EVIDENCE FROM VALLES MARINERIS; B. K. Lucchitta, U.S. Geological Survey, Flagstaff, Arizona 86001

An important contribution to the volatile history of Mars comes from a detailed study of Valles Marineris, where excellent stereoimages and a three-dimensional view of the upper Martian crust permit unusual insights: the subsurface in the equatorial region of Mars below about 1 km depth was not desiccated until relatively recently, even though desiccation is predicted by models of the equilibrium between water in the ground and the atmosphere [1].

The evidence that ground water and ice existed until relatively recently or still exists in the equatorial area comes from observations of landslides [3,4], wall rock [5], and dark volcanic vents [6,7]. Several observations suggest that landslides were lubricated by water. Three young slides generated an outwash fan and gave rise to a channel that has several bends and extends on a gradient of 4 m/km for a total distance of 250 km from its source [8]. Also, the material in this channel was capable of erosion at considerable distance from its source; it breached a bedrock ridge, carved flutes in the lower channel, and eroded its banks. Doughnut-shaped hills within this channel resemble moraines containing kettle holes, which on Earth are formed by the melting of blocks of ice.

Some landslides have lobes that angle backward from the main debris mass and flow downhill, others give rise to small sinuous valleys, and many small landslides are surrounded by levees like terrestrial mudflows. These observations also suggest that the landslide deposits contained fluids. A small channel debouches from a tributary canyon to Valles Marineris; apparently water discharged from the canyon walls, if canyon tributaries were indeed formed by sapping [9].

Valles Marineris landslides are different in efficiency from large catastrophic landslides on Earth. Whereas terrestrial landslides increase in efficiency of distance traveled with increasing weight [10], the large landslides in Valles Marineris retain the same efficiency regardless of weight [4]. One explanation for the difference might be that the Martian slides are lubricated by water, whereas most large terrestrial slides are dry-rock avalanches [11].

A comparison of landslide speeds also suggests that the Martian slides contained water. Among large catastrophic landslides on Earth, only the Huascaran slide [12] matches the Martian ones in speed [4]; the Huascaran slide contained much water and ice. Because all landslides in Valles Marineris are released from wall rock, some layers within the walls that are 7-10 km high must have contained these lubricating materials.

A relatively young, level deposit embaying eroded layered beds occurs in the lowest area of the central troughs of Valles Marineris [13]. The deposit looks like a dry lake bed or alluvial flat, which suggests that wet debris contributed to its formation. The wet debris was apparently derived from landslides or wall rock.

VALLES MARINERIS - WATER AND ICE

Lucchitta, B. K.

That Valles Marineris wall rock contained water or ice is further suggested by its difference from the interior layered deposits. Landslides having flow lobes that extend far out onto the chasma floors only debouch from wall rock or erosional remnants of wall rock. No such landslides come from the layered deposits, even where the layered deposits are as high and steep as the wall rock. Apparently, landslides formed from the wall materials flowed easily; those from the interior deposits generally did not [14].

Faults and fault zones in Valles Marineris also shed light on the problem of water content in the walls. Contrary to what is commonly seen on Earth, many fault zones in Valles Marineris are more resistant to erosion than the country rock. Spurs projecting into Valles Marineris developed along faults [5], and all the median ridges of wall rock paralleling chasma walls or separating chasmata from each other occur where faults and fracture zones are densely spaced. Apparently faults were lithified or intruded by dikes and thus are more resistant to erosion than the country rock. Conversely, the observation implies that the country rock is weaker relative to the faults. Such weak country rock would be consistent with wall rock composed of breccia [11] that is weakly cemented by ice near the free faces and is charged with water at some depth.

Another argument supports the idea that the wall rock contained water and ice. Dark deposits interpreted as volcanic-vent material [6,7] occur only at elevations lower than 6 km above Martian datum. The highest deposits are 3 km below the rim of adjacent plateau surfaces. This 6-km elevation appears to be the maximum height reached by extruding magmas and can be used to calculate relative densities of magma and wall-rock columns [16,17]. It appears that the material in the column of combined solid crust and mantle rock underlying the plateau must have been less dense than the material in the liquid magma column. Upper crustal rock composed of loosely consolidated breccia mixed with water or ice might fulfill such a requirement.

Because the main evidence for water and ice in the wall rock comes from landslides, their time of emplacement is important. The landslides in Valles Marineris date from the time of late eruptions on the Tharsis volcanoes [3] and thus were emplaced after the major activity on Martian outflow channels. Therefore, the concept of ground saturated by water and ice in the equatorial region is consistent with Carr's [15] hypothesis that confined aquifers developed in this region and gave rise to outflow channels. The concept also agrees with the presence of rampart craters in the equatorial area.

None of the above observations conclusively demonstrate that water or ice existed in the wall rock of Valles Marineris, but altogether the evidence is highly suggestive. Any models addressing the exchange of water with the atmosphere in the equatorial region of Mars must therefore take into account that, below a depth of about 1 km, this region was not entirely desiccated at least until landslide time.

References

1) Fanale F. R. (1976) Icarus, 28, p. 179-202.
2) Carr M. H. and Clow G. D. (1981) Icarus, 48, p. 91-117.
3) Lucchitta B. K. (1979) J. Geophys. Res., 84, p. 8097-8113.
4) Lucchitta B. K., Kaufman K. L., and Tosline D. J. (1981) NASA TM 84211, p. 326-328.
5) Lucchitta B. K. (1981) NASA TM 84211, p. 419-421.
6) Lucchitta B. K. (1985) Lunar Planet. Sci. XVI, p. 503-504.
7) Lucchitta B. K. (1986) Lunar Planet. Sci. XVII, p. 496-497.
8) Lucchitta B. K. (1984) Workshop on Water on Mars, Nov. 30-Dec. 1, 1984, p. 45-47.
9) Pieri David (1980) Science, 210, p. 895-897.
10) Scheidegger A. E. (1973) Rock Mechanics, 5, p. 231-236.
11) Hsü K. J. (1975) Geol. Soc. Am. Bull., 86, p. 129-140.
12) Plafker George and Erickson G. E. (1978) Rock slides and avalanches, Barry Voight, ed., Elsevier, Amsterdam, p. 277-314.
13) Lucchitta B. K. and Ferguson H. M. (1983) Proc. Lunar Planet. Sci. Conf. 13th, Part 2, 88, Supplement, p. A553-A568.
14) Lucchitta B. K. (1982) Repts. Planet. Geol. Prog.-1982: NASA TM 85127, p. 233-234.
15) Carr M. H. (1979) J. Geophys. Res., 84, p. 2995-3007.
16) Eaton J. P. and Murata K. J. (1960) Science, 132, p. 925-938.
17) Vogt P. R. (1974) Earth and Planet. Sci. Letts., 23, p. 337-348.

THE GREAT DUST STORM OF 1986 (?); L. J. Martin, Planetary Research Center, Lowell Observatory; and P. B. James, University of Missouri at St. Louis and Lowell Observatory

The title, of course, is hypothetical since this abstract was written when we were only beginning our observations and Mars was subtending only 13 seconds of arc. At the time of this meeting we will be less than halfway through our observing period and Mars will have been at opposition one week earlier. Mars' closest approach to Earth occurs on July 17th, when it is closer than anytime since 1971, the most recent year that this season was seen on Earthbased observations. It will also be the dust storm "season" (see figure), the first 1977 storm began at L_s 204°, which occurs this year on July 12th. If a storm breaks out before the meeting, we will give you as many preliminary details as possible. In any case, we will discuss current observations and what they are telling us about present atmospheric conditions and the recession of the South Polar Cap. Comparisons of this portion of the seasonal cycle with 1969 and 1971 Planetary Patrol observations and those from earlier years, as well as Viking observations, will help define both the differences and similarities of various Martian years. As the history of the Martian climate continues, we will endeavor to add to the data base.

This research is supported by the Lowell Observatory, the Perth Observatory, the University of Missouri at St. Louis, and the National Geographic Society. Telescopes and camera equipment were purchased under NASA grants.

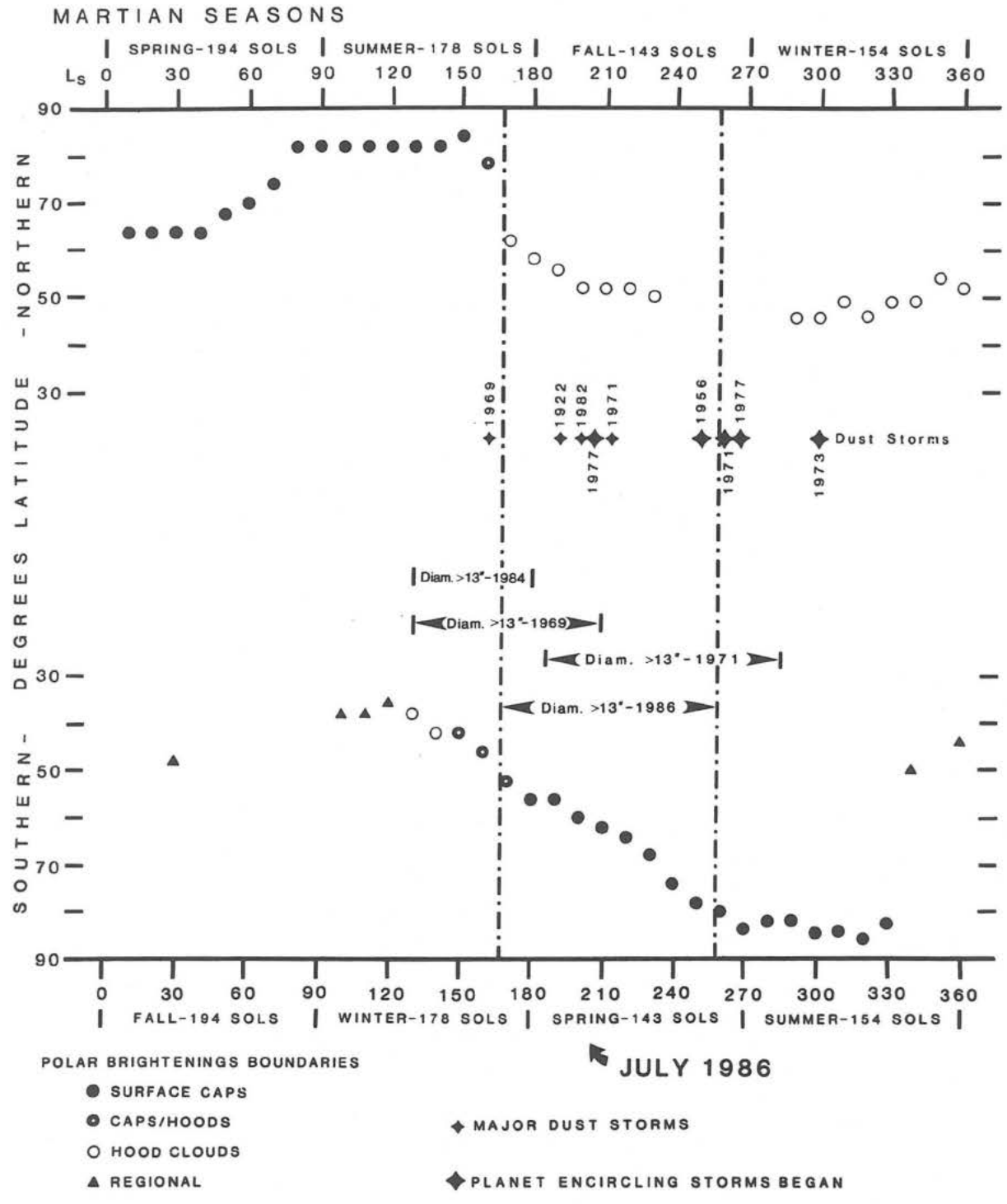
MARTIAN SEASONS
SPRING-194 SOLS
SUMMER-178 SOLS
FALL-143 SOLS
WINTER-154 SOLS
Ls 0 30 60 90 120 150 180 210 240 270 300 330 360
90 70 50 30
SOUTHERN- DEGREES LATITUDE -NORTHERN
1969
1922
1982
1977
1971
1956
1971
1977
1973
Dust Storms
Diam. >13"-1984
Diam. >13"-1969
Diam. >13"-1971
Diam. >13"-1986
0 30 60 90 120 150 180 210 240 270 300 330 360
FALL-194 SOLS
WINTER-178 SOLS
SPRING-143 SOLS
SUMMER-154 SOLS
JULY 1986
POLAR BRIGHTENINGS BOUNDARIES
SURFACE CAPS
CAPS/HOODS
HOOD CLOUDS
REGIONAL
MAJOR DUST STORMS
PLANET ENCIRCLING STORMS BEGAN

ABLATION OF MARTIAN GLACIERS

Henry J. Moore, U.S. Geological Survey, Menlo Park, CA., 94025
Philip A. Davis, U.S. Geological Survey, Flagstaff, AZ., 86001

Glacier-like landforms are observed in the fretted terrain of Mars in the latitude belts near ± 42° (1). It was suggested that sublimation or accumulation-ablation rates could be estimated for these glaciers if their shapes were known (2). To this end, we have obtained photoclinometric profiles (e.g. 3) of a number of these landforms (e.g. fig. 1). On the basis of our analyses of these profiles, we conclude that ice is chiefly ablating from these landforms that either are inactive rock-glaciers or have materials within them that are moving exceedingly slowly at this time. These conclusions are consistent with other geologic information.

For our analyses, we use a two-dimensional model of an isothermal glacier. The flow of material through a unit width of the glacier is assumed to obey the following flow law (4):

$$\bar{V} = A\tau^3 \, (h/5)$$

where: $\bar{V}$ is the average velocity of the material through a unit width of a section perpendicular to the bed of the glacier, h is the thickness of the material measured at right angles to the bed, τ is the stress on the bed, and A is the flow-law parameter.

The volume flow rate through a unit width, Q, is given by:

$$Q = \bar{V} \, h$$

The stress on the bed of a section of the glacier is estimated from the profiles (assuming an equilibrium condition) by using:

$$\tau = \rho g \bar{h} \, [(\Delta h / \Delta b) + \sin \theta]$$

where: ρ is the density of the material, g is the acceleration of gravity (3.72 m/s^2), $\bar{h}$ is the mean thickness of a section above the bed, Δh is the difference in thickness of each end of the section, Δb is the length of the section along the bed, and θ is the slope angle of the bed.

There are a number of problems with the glacier-like forms: 1. Their compositions are unknown. They may be chiefly ice, or they may contain large amounts of rock detritus (rock-glaciers). 2. If they are rock-glaciers, the flow laws are unknown. We assume flow like water-ice. 3. The flow-law parameter for water-ice is a strong function of temperature (4). We use 3.18 x 10^{-28} Pa^{-3} s^{-1} (ice at 210 K). 4. Densities are unknown and may range between 1,000 kg/m^3 (water-ice) and 1,800 kg/m^3 (rock-glaciers) or more. For the calculations below we use a density of 1,800 kg/m^3 (e.g., 5), but stresses for ice would be 1/1.8 times smaller than those of rock-glaciers and velocities and flow rates would be 1/5.8 times smaller. 5. The slopes of the glacier beds are inclined beneath at least part of the glaciers. 6. The undulatory form of the profile gives rise to variable stresses, average velocities, and volume flow rates. 7. Ice-glaciers are ephemeral, but rock-glaciers are not. Rock-glaciers contain ice and detritus; nearly complete ablation of the ice results in an inactive residue of detritus.

For the profile in figure 1, stresses on an assumed horizontal bed of the rock-glacier range from 70 to 23 kPa; near the tip, stresses decline from 36

kPa to zero (eg. table 1). Average velocities range from 135 to 3 μm/y; near the tip, velocities decline from 10 μm/y to zero. Volume flow rates peak at 15,400 cm^3/m y, but are smaller in the tip and head. If there is a bed sloping 1.7° beneath the rock-glacier (fig. 1), stresses on the bed range between 35 and 18 kPa and average velocities are between 1 and 9 μm/y. Volume flow rates peak at 1,000 cm^3/m y, but are smaller in the tip and head.

The changes in volume flow rates imply ablation or losses over the length of the glacier; because of the undulatory surface, however, calculated volume flow rates vary and do not yield a uniform ablation rate. For the rock-glacier with the horizontal bed, the maximum local ablation rate for a length increment of 592 m is 26 $\mu m/m^2 y$. Assuming uniform loss along the length, the ablation rate is 4.3 $\mu m/m^2 y$. For the rock-glacier with the inclined bed, the corresponding ablation rates are 1.4 and 0.2 $\mu m/m^2 y$, respectively.

The value of the flow-law parameter has a profound effect on the magnitudes of the calculated velocities, flow rates, and ablation rates. If the value for ice at 190 K is used, instead of 210 K, the velocities and rates would be about one one-hundreth of those in table 1; at 230 K, they would be about 40 times larger. In the isothermal case, such changes would not alter the qualitative conclusions, however.

Profile expectations for a rock-glacier that has a constant volume flow rate through all sections and those for an ice-glacier that is fed at the head and loses volume uniformly along its length (fig. 1) are much thicker near the tip than the actual one. Similar but smaller bulbous tips would be expected for a glacier having a sloping bed. The lack of a bulbous tip suggests that the glacier is no longer fed. Basal stresses for active rock-glaciers on Earth are greater than about 75 kPa (5), but those computed from the profile are less (see also 6). This finding suggests that, if the glacier is a rock-glacier, it is inactive.

Other information also suggests net ablation. Many of the lobate forms exhibit decreases in slope and slope reversals near their heads; some appear to be isolated mounds. Profiles across tongue-like forms undulate and inferred thicknesses are locally zero. Finally, some landforms suggest the former presence of lobate landforms that have been reduced or removed by ablation.

Net ablation of these glaciers requires sinks for the deposition of the ablated ice. Such sinks probably occur in the colder polar regions north and south of the glacier-like landforms (see also 7).

REFERENCES CITED

(1)Squyres, Steven W., 1978, Martian fretted terrain: flow of erosional debris: Icarus, v.34, p. 600-613.

(2)Moore, Henry, 1985, Sublimation rates required for steady-state glaciers on Mars, in Clifford, S. ed., Workshop on Water on Mars, LPI Tech. Rept. 85-03, Lunar and Planetary Institute, Houston, TX., p. 59-61.

(3)Davis, Philip A. and Soderblom, Laurence A., 1984, Modeling crater topography and albedo from monoscopic Viking Orbiter images: 1. Methodology: J. Geophys. Res., v. 89, no. B11, p. 9449-9457.

(4)Paterson, W.S.B., 1981, The Physics of Glaciers, 2nd ed., Pergamon Press, Oxford, England, 380 p.

(5)Wahrhaftig, Clyde and Cox, Allan, 1959, Rock glaciers in the Alaskan Range: Bull. Geol. Soc. Amer., v. 70, p. 383-436.

(6)Lucchitta, Baerbel K., 1984, Ice and debris in the fretted terrain, Mars: J. Geophys. Res., v. 89, Supplement, p. B409-B418.

(7)Squyres, S. W. and Carr, M. H., 1986, Geomorphic evidence for the distribution of ground ice on Mars: Science, v. 231, no. 4735, p. 249-252.

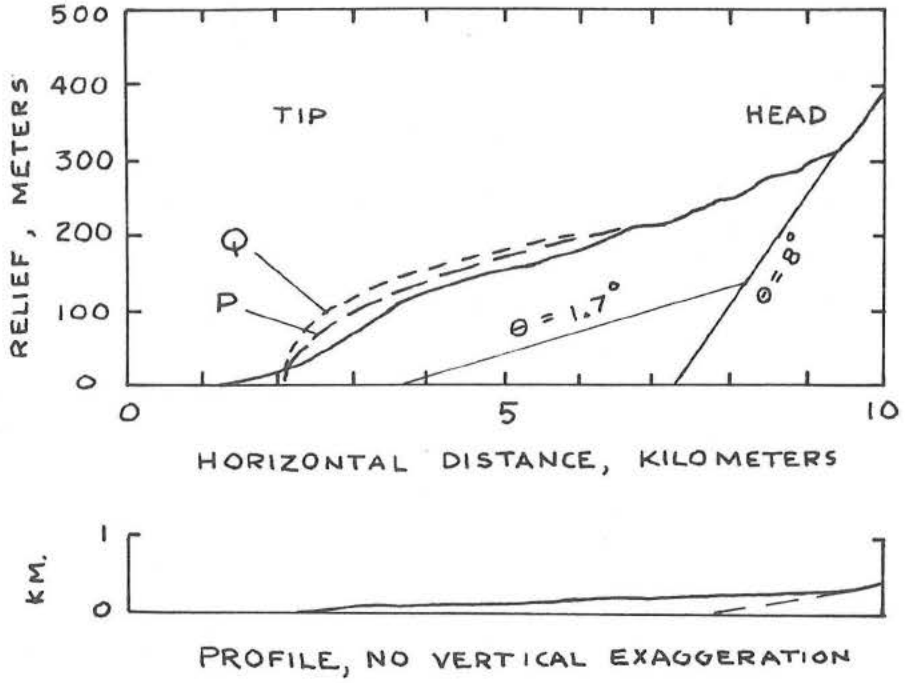

Figure 1. Photoclinometric profile of martian glacier (heavy-solid line). Assumed horizontal base extends to 7.2 km. Assumed sloping base indicated by $\theta = 1.7°$. Slope of mountain is 8°. Short-dashed line (Q) is form of an isothermal glacier that has a constant volume flow rate through all sections. Long-dashed line (P) is form of an isothermal glacier that is fed from its head and ablates uniformly along its length. Both Q and P have horizontal bases that extend to 7.2 km. Note that actual tip of glacier does not have a convex bulbous tip and that its surface undulates.

Table 1. Selected values of calculated mean thicknesses ($\bar{h}$), assumed slope of beds (θ), basal stresses (τ), average velocities ($\bar{v}$), and volume flow rates (Q) for sections having midpoints (D) for two models of martian glacier (fig. 1). Horizontal widths of sections are 592 m. A flow-law parameter for ice at 210 K was used in the calculations.

	Horizontal Base					Inclined Base				
D (km)	$\bar{h}$ (m)	θ (deg)	τ (kPa)	$\bar{v}$ (μm/y)	Q (cm^3/m y)	$\bar{h}$ (m)	θ (deg)	τ (kPa)	$\bar{v}$ (μm/y)	Q (cm^3/m y)
2650	48	0	18	0.6	0.3	48	0	18	0.6	0.3
3834	114	0	28	5.2	593	105	1.7	26	3.8	396
5018	152	0	26	5.2	782	107	1.7	18	1.3	139
6201	189	0	60	81.7	15,400	110	1.7	35	9.2	1,010
7977	138	8	38	15.5	2,140	118	1.7	33	8.8	1,040
8569	81	8	24	2.3	190	81	8	24	2.3	190

ICE OR LIQUID WATER IN THE MARTIAN REGOLITH? MORPHOLOGIC INDICATORS FROM RAMPART CRATERS;

P. J. Mouginis-Mark, Planetary Geosciences Division, Hawaii Institute of Geophysics, University of Hawaii, Honolulu, HI 96822*

Introduction: At the recent Lunar and Planetary Institute's Special MECA Session on geomorphic indicators of martian volatiles (March 1986), it became clear that considerable differences of opinion exist regarding the physical state (or even total absence) of the volatiles within the martian regolith that were responsible for the formation of the rampart crater lobate ejecta flows. Possible forms that this fluidizing medium might take include water ice or liquid water within the target material (1-4), or atmospheric gases interacting with suitable particle sizes within the ejecta curtain (5). Because rampart craters are distributed planet-wide, and occur in regional settings where both liquid water or water ice might be expected to occur (based on the distribution of channels and periglacial landforms) it has long been realised that the correct interpretation of crater morphology would provide the capability to document the spatial distribution and physical state of near-surface volatiles around the planet (cf. 1-4). Recognition of the correct volatile phase would have implications not only for the mode of formation of crater ejecta deposits, but also for other geomorphic processes such as channel network formation and terrain softening. This abstract reviews previously published interpretations on this subject, and considers some of the morphologic features that may be recognizable from the Viking Orbiter images, in an attempt to help resolve this unknown condition of the regolith and provide constraints on the global distribution of volatiles on Mars.

Global Observations:

Early analysis of martian craters (6) drew attention to the numerous craters that possess central peaks with summit pits. These pits are not associated with all fresh rampart craters of a given diameter, and led to the suggestion that the pits were formed by explosive decompression of strata containing subsurface volatiles. Such a situation suggested that in addition to the effects of the volatiles that created the lobate ejecta deposits, volatiles of another phase (possible liquid water as opposed to water ice) might be present. Circumstantial evidence from the analysis of craters (7) and volcanic landforms (8) in the Elysium Planitia region may support this interpretation, since an unusally large number of craters in this region possess pitted central peaks, possibly indicating that liquid water existed close to the surface as a result of a higher than usual thermal gradient.

Johansen (3) and recently Kragel (9) have suggested that the presence or absence of a distal ridge on an ejecta flow may be an indicator of water (ridge present) or ice (ridge absent) within the target material. Although there is a predominance of ridged craters at low latitudes and ridge-less craters at high latitudes (9) no corroborating models for ejecta emplacement, or theoretical or experimental data, were presented by these investigators to support their hypothesis that this difference in morphology was indeed associated with the physical state of water within the target.

Ejecta lobe thickness appears to be limited by some physical aspect of the deposit, inferred to be the maximum shear strength of the fluidized medium (10). No global study has been made of this variation in the upper limit for ejecta thickness, but the value appears to be quite uniform. For example, studies of craters on ridged plains materials between 40^{0}S and 30^{0}N and found no appreciable difference in the surface area (and, by inference, ejecta thickness) for a range of altitudes between +9 km to -2 km (11). This situation was felt to imply that the viscosity (and, hence, degree of ejecta fluidization) may have been constant for cratering events over a wide geographic area for an appreciable amount of martian history.

---

* Currently at NASA Headquarters, Code EEL, Washington DC

WATER OR ICE ON MARS?
Mouginis-Mark, P.J.

There are few close correlations between crater morphologies and target materials, but craters with two concentric ejecta lobes are most numerous in Acidalia and Utopia Planitia (two areas which have been independently identified as probable areas with periglacial landforms; 12). There also appears to be little variation in crater morphology as a function of age (and thus possible evolving atmospheric conditions on Mars). Craters that are apparently very young (inferred to be young due to the preservation of ejecta rays) still possess the same basic form of ejecta morphology as older craters on the same terrains (13).

Because there does not appear to be any strong morphological difference between the individual lobes associated with craters in the 5 - 10 km diameter range and craters in the 30 - 35 km diameter range, it is likely that the fluidizing medium and viscosity of these deposits was similar. Such an idea is borne out by the linear relationship between ejecta area vs. crater diameter curves (for craters 6 - 35 km in diameter; 10). This observation in turn would imply that no appreciable change in volatile state or concentration existed at the time of crater formation for ejecta originating at shallow depths (small diameter craters) and greater depths (large crater diameters).

Experimental Models:

Wohletz and Sheridan (14) suggested that terraced deposits seen on certain ejecta blankets resulted from surges in the emplacement of the ejecta as target water explosively vaporized during the impact event. However, their models did not consider the energy requirements to vaporize water ice as opposed to liquid water. Crater ramparts were thought to form when ejecta surges lost the fluidizing vapors and transported particles were deposited en masse.

No rigorous attempts at laboratory simulations of impact events into targets designed to simulate specific martian conditions have so far been attempted. Initial experiments using the Ames Gun have nevertheless shown that the final crater morphology, the break-up of the ejecta curtain into discrete fragments, and the morphology of the secondary deposits depend upon the viscosity of the target medium (15).

Crater Morphology:

While little positive information on volatile state can be gained from regional trends in the distribution of crater morphologies, a few high resolution (20 meter per pixel or better) Viking Orbiter images provide the capability to search for small morphological features that might distinguish between water and ice existing within the target material. For example, grooves on the ejecta lobes of the craters Bamburg (55 km dia.) and Arandas (25 km dia.) indicate that immediately after lobe emplacement, but prior to cessation of ejecta curtain deposition, the lobes had established sufficient physical strength to preserve these "scour marks" in their surface during the passage of the later ejecta materials (12, 16). A similar effects is also observed where pre-existing obstacles have created pressure ridges within the ejecta lobe on the crater-ward side of the obstacle. It appears unlikely that a very fluid, water-rich ejecta could retain these features after their formation, suggesting that ice might be a more acceptable target volatile.

Few examples of small-scale outflow of water can be seen in even the highest resolution (better than 20 meter per pixel) Viking Orbiter images. Some of the rare exceptions are the channel networks on the rim of Schiaparelli Basin (17), channels on the inner walls and abnormally smooth terrain within the ejecta blanket of Bamburg (16) and previously

undocumented channels on the inner walls of crater Cerruli. Were liquid water to be more commonly present within ejecta blankets at the time of their emplacement, deposits associated with seepage of water from the ejecta lobes are expected to be more frequently observable in the Viking images.

Summary and Speculations:

The absence of remobilized materials as a consequence of water sapping from the emplaced ejecta, and the formation (and preservation) of scour marks and pressure ridges within the still-forming ejecta blanket, suggest that the ejecta possessed appreciable mechanical strength at the time of emplacement. Numerical models would be needed to determine the effects of different volumeric amounts of liquid water versus water ice entrained within the ejecta, but these observations appear at this time to favor ground ice as the physical state for the fluidizing material responsible for creating the rampart crater lobes.

Boyce (2) suggested that in some regions of Mars, crater morphology may reflect a layer of water-rich material underlying an ice-rich permafrost. Such a situation might be responsible for the formation of the twin lobed craters, and thus mark the point where near-surface ice overlays liquid water. If this hypothesis is valid, it could explain the apparent anomaly whereby the inner, more viscous ejecta lobe was emplaced prior to the outer more fluid lobe (12). It is possible that a reanalysis of the highest resolution Viking Orbiter images could resolve this two-phase model for the regolith if suitable craters were imaged at 10 - 20 meters per pixel.

Clearly, however, these observations of ejecta morphology pertain to a only a few examples of martian craters, rather than comprise a general set of properties for the entire crater population. While these well imaged craters provide an insight into the physical state of the target materials, image resolution may still be insufficent to identify key landforms. As a result, it is concluded that making the morphology and geochemistry of fresh martian impact craters one of the prime targets for the ultra-high resolution camera and VIMS experiments to be flown on the Mars Observer may be the most appropriate method for identifying the state of volatiles within the regolith at the time of impact.

References:

1) Carr, M. H. et al (1977) J. Geophys. Res. v. 82, p. 4055-4065.
2) Boyce, J. M. (1979) NASA TM 80339, Rpts. Plan. Geol. Prog. 1978-1979, p. 114.
3) Johansen, L. A. (1979) NASA TM 80339, Rpts. Plan. Geol. Prog. 1978-1979, p. 123.
4) Mouginis-Mark, P. J. (1979) J. Geophys. Res. v. 84, p. 8011-8022.
5) Schultz, P. H. and D. E. Gault (1979) J. Geophys. Res. v. 84, p. 7669-7687.
6) Wood, C. A. et al (1978) PLPSC 9th, p. 3691-3709.
7) Hale-Erlich, W. S. (1986) LPS XVII, p.303-304.
8) Mouginis-Mark, P. J. (1985) Icarus, v. 64, p. 265-284.
9) Kargel, J. S. (1986) LPS XVII, p. 410-411.
10) Mutch, P. and A. Woronow (1980) Icarus v. 41, p. 259-268.
11) Mouginis-Mark, P. J. and E. Cloutis (1983) LPSC XIV, p. 532-533.
12) Mouginis-Mark, P. J. (1981) Icarus v. 45, p. 60-76.
13) Mouginis-Mark P. J. et al (1980) LPS XI, p. 762-764.
14) Wohletz, K. H. and M. F. Sheridan (1983) Icarus v. 56, p. 15-37.
15) Gault, D. E. and R. Greeley (1978) Icarus v. 34, p. 486-495.
16) Mouginis-Mark, P. J. (1979) PLPSC 10th, p. 2651-2668.
17) Mouginis-Mark, P. J. et al (1980). Proc. Conf. Multi-Ring Basins, Schultz & Merrill Eds., Pergamon, NY, p. 155-172.

SEASONAL WIND VARIATIONS IN THE MARTIAN SUBTROPICS. James Murphy, Conway Leovy, and James Tillman, Dept. of Atmospheric Sciences, University of Washington, Seattle, WA 98195

A recent analysis of winds at the Mutch Memorial Station (22.5N, 48W) will be presented and interpreted. During the late summer period from L_s 100 to L_s 180, there was a gradual transition from winds that are topographically controlled, diurnally repeatable, and predominantly southerly to a wind pattern reflecting reduced topographic influence and the predominance of northeasterly flow of the global Hadley circulation. The signature of the global westward propagating tides is also clear in these data.

During autumn and winter there are also transient disturbances in the period range 1 - 20 sols (Martian solar days). Two of the most prominent disturbances have coherent wind, temperature, and pressure fluctuations near the 2.5 and 3.4 day periods. By combining wind and pressure data we show that these are eastward propagating waves with zonal wave numbers two to four and phase speeds 5-15 ms^{-1}. We infer that they are the equatorward extensions of previously observed baroclinic waves at 48N. Pressure fluctuations at this period show strong interannual variations in amplitude.

Beginning in early autumn and continuing at irregular intervals through early winter are "surges" of strong northeasterly wind with little or no associated pressure fluctuation. These "surges" may arise from enhancement of the amplitude of global normal modes. They may also play an important role in the initiation of Martian global dust storms. Their precise mechanism remains unclear, however.

OPTICAL THICKNESS OF THE OLYMPUS CLOUD:

Y.NARUMI, Kyushu-Tokai University,Kumamoto 862,JAPAN.

Considering the seasonal cycle of water on Mars, it is very important to understand the nature of the water ice cloud on Mars, for example, the blue-white cloud over the Tharsis region, the polar hoods of the north and south polar regions. As the first approach to examine the nature of those clouds, we have estimated the optical thickness of the "Olympus cloud". In the afternoon of the Martian northern summer, a blue-white bright cloud has been often observed to appear near the summit of the Olympus Mons(20°N, 137°W). This cloud is usually called as the "Olympus cloud". The relative brightness of this cloud to the cloud-free point at the same location were determined from the photographic observations by Hida and Kwasan observatories in the 1982 apparition. Fig.1 shows the observed relative brightness of the cloud from the blue negatives(effective wavelength of 0.4μm) as a function of the Mars Local Time(MLT). Using the Discrete-Ordinate Method for radiative transfer to the inhomogeneous cloudy atmosphere, we calculated the reflected intensities from the top of the cloud having various optical thickness. Comparing those intensities with those from the cloud-free point, we estimated the diurnal variation of the optical thickness of the cloud.

The calculation scheme of the Discrete-Ordinate Method for the inhomogeneous cloudy atmosphere is based on Liou(1) and Moriyama(2). They calculated the reflected fluxes from the cloud. We expanded this scheme to the reflected intensity calculation using the Delta-M approximation for the strongly asymmetric phase function of ice cloud particles(Wiscombe(3)). The entire atmosphere is devided into ten homogeneous layers of 3km thick. Each layer includes the atmospheric gas(CO_2), dust particles, and ice cloud particles in different ratio from the other layers. The boundary and continuity conditions are as following: at the top of the atmosphere there is no diffuse downward intensity; at the interface of each homogeneous layer the upward and downward intensities have to be continuous; and at the bottom of the atmosphere, assuming an isotropic reflec-

tion surface with an albedo A_s, the upward intensities can be expressed in terms of the downward diffuse flux and the downward direct solar flux.

The scattering phase function of the Martian ice cloud particles is unknown, but it may be nonspherical. So that we approximated the laboratory data for the nonspherical ice particles by Sassen and Liou(4) with the semi-empirical theory of Pollack and Cuzzi(5). For the dust particles in the Martian atmosphere we adopted the phase function obtained from the Viking Lander Camera's observation (Pollack et al.(6)). We assumed the optical thickness of CO_2 gas and dust particles as 0.01 and 0.1, respectively and A_s=0.061 for λ=0.4 μm.

As the height of the Olympus cloud is unknown, we have examined three cases of the height distribution of cloud; (a) Low cloud case (cloud height is 0-15km), (b) Middle cloud case(9-24km), (c) High cloud case(15-30km). The calculated results show that the obtained optical thickness are scarcely affected by the height distribution of cloud. Fig.2 shows the estimated optical thickness from the Middle cloud case as a function of MLT. From Fig.2 it is found that the Olympus cloud appears near the local noon of Mars, and reaches the maximum optical thickness of about 0.8 in the early afternoon, then falls off slowly thereafter. The maximum optical thickness of about 0.8 is not contradict with the results from the Viking Orbiter observations(Christensen and Zurek(7)). We would like to estimate the optical thickness of the polar hoods and to examine the thermal effect of the polar hoods to the growth of the polar caps.

REFERENCES

1. Liou,K.N.(1975) J.Geophys.Res.,vol.80,3434-3440.
2. Moriyama,S.(1978) Atmospheric Environment,vol.12,1875-1887.
3. Wiscombe,W.J.(1977) J.Atmos.Sci.,vol.34,1408-1422.
4. Sassen,K. and Liou,K.N.(1979) J.Atmos.Sci.,vol.36,838-851.
5. Pollack,J.B. and Cuzzi,J.N.(1980) J.Atmos.Sci.,vol.37,868-881.
6. Pollack,J.B.,Colburn,D.,Kahn,R.,Hunter,J.,Camp,W.V.,Carlston,C.E., and Wolf,M.R.(1977) J.Geophys.Res.,vol.82,4479-4496.
7. Christensen,P.R. and Zurek,R.W.(1984) J.Geophys.Res.,vol.89,4587-4596.

Fig.1 Observed Relative Brightness of the Olympus Cloud
Hida and Kwasan Observatries(1982)

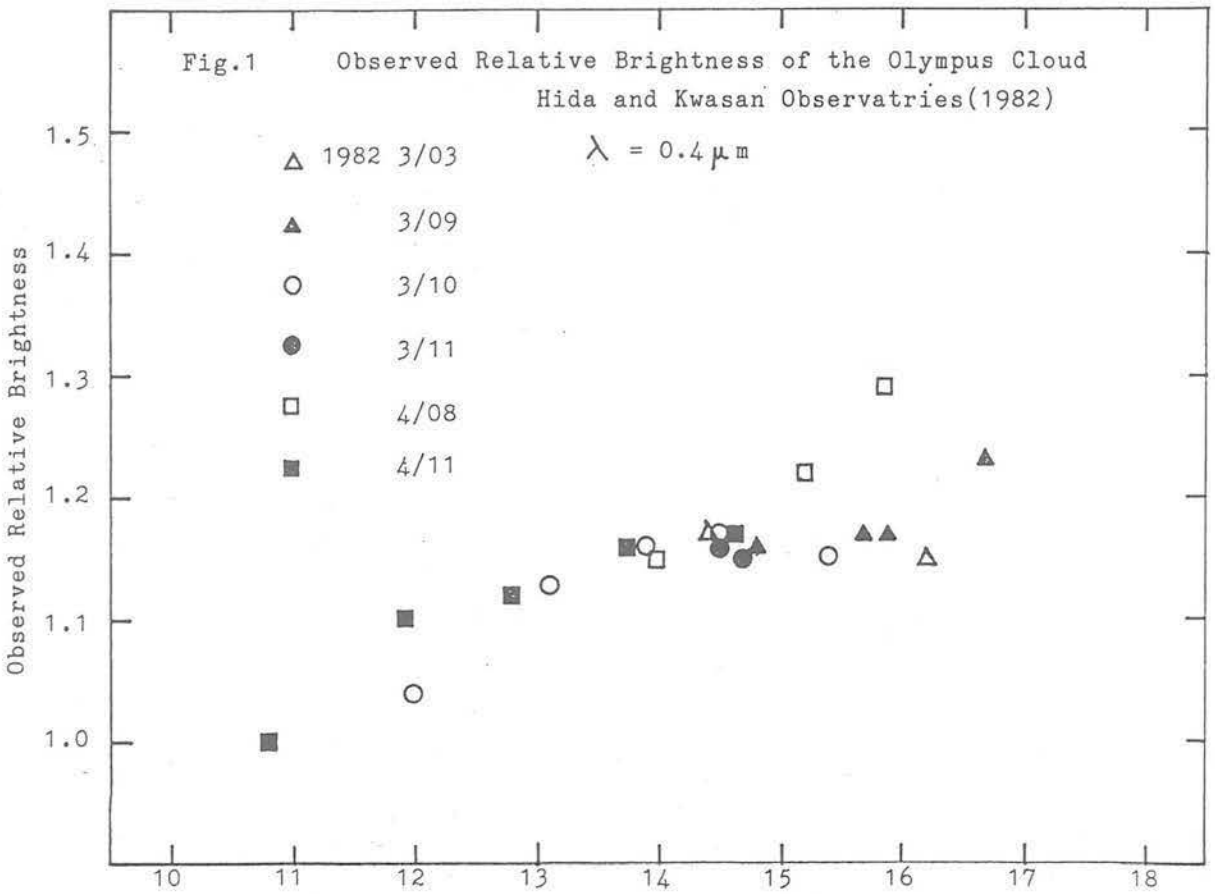

Fig.2 Estimated Optical Thickness of the Olympus Cloud
Middle cloud case (cloud height 9-24 km)

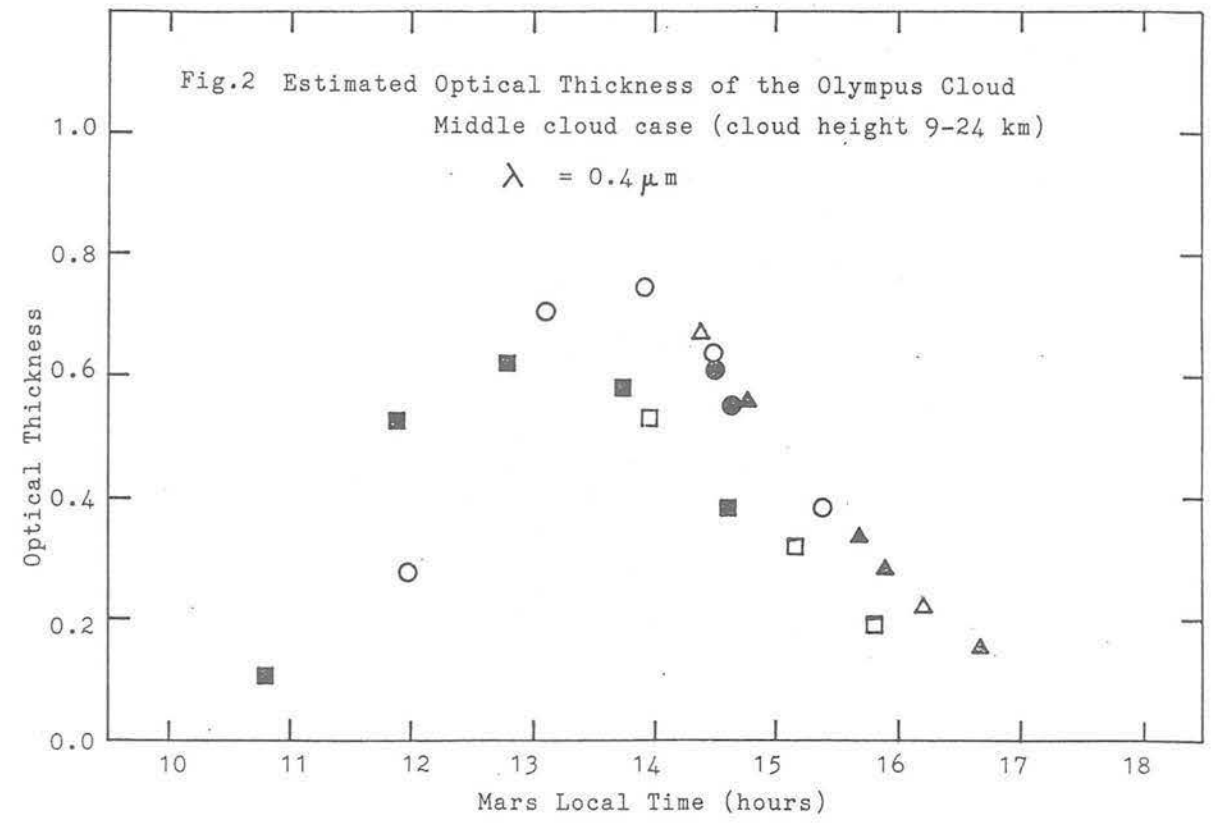

FORMATION OF THE LAYERED DEPOSITS IN THE VALLES MARINERIS, MARS, S.S. Nedell, Department of Geology, San Jose State University, San Jose, CA, 95192, and S.W. Squyres, Space Science Division, NASA Ames Research Center, Moffett Field, CA, 94035.

Thick sequences of layered deposits are found in the Valles Marineris (1-3). They exhibit fine, nearly horizontal layering, and are present as isolated plateaus of what may have once been more extensive deposits. Individual sequences of layered deposits are as thick as 5 km. We have argued previously that the morphology of the deposits is most consistent with origin in standing bodies of water (3). The rhythmic nature of the layering, their lateral continuity, horizontality, great thickness, and stratigraphic relationships with other units in the canyons all appear most consistent with deposition in a quiet aqueous environment. If standing bodies of water existed for any significant period of time in the Valles Marineris, they were almost certainly ice-covered. Here, we examine in more detail the conditions necessary for the existence of ice-covered Martian paleolakes, and consider mechanisms for sediment deposition in them.

Groundwater has been very important in shaping the Martian surface. There is ample evidence that the Martian regolith is highly porous and permeable, and at one time contained large amounts of liquid water (4). If a large tectonic depression such as the Valles Marineris cut deep into an aquifer system in the martian regolith, it would be natural for the canyons to become partially filled with water. As long as the subsurface aquifer system remained charged, water in the lakes could be replenished readily by seepage from the canyon walls.

It is unlikely that the Martian atmosphere was thick enough to have sustained mean annual temperatures above freezing after the earliest epoch of Martian history. Any standing water bodies would be expected to have a perennial ice cover. Perennially ice-covered lakes presently exist in the Dry Valleys of Antarctica. There the mean annual temperature is also well below freezing, and the ice on the lakes has reached an equilibrium thickness (5). As ice is lost from the upper surface of the lake by ablation, new ice forms on the lower surface, releasing latent heat as it does. This heat is the dominant term in the energy balance equation that gives the equilibrium ice thickness. Water in the lake is replenished in Antarctica by surface flow; on Mars this could be accomplished by ground water seepage. The rate of ablation exerts a strong influence on the equilibrium ice thickness, and on Mars it is poorly known. Based on reasonable estimates of ablation rates, the equilibrium thickness of ice on Martian lakes under the present climate might be 65 to 650 m (5). The depth of possible lakes is very poorly constrained, and could have ranged from very shallow depths to more than 5 km deep.

There are three ways that sediment could enter an ice-covered lake: down through the ice cover, up from the lake bottom, or in from the lake margins. We now consider each of these possibilities in turn.

Four processes that could have transported sediment downward through an ice cover are considered: (a) solar energy warmed individual particles, allowing them to melt through the ice; (b) sediment worked its way downward through vertical melt channels; (c) a layer of sediment deposited on the ice was thick enough to cause the ice layer to founder, dumping the sediment into the lake; and (d) a layer of sediment deposited on the ice cover led to a Rayleigh-Taylor instability, and sediment diapirs penetrated downward through the ice layer.

Simple energy calculations show that solar warming is inadequate to melt moderate-sized grains downward through the 5-meter ice cover of typical Antarctic lakes (6). It is therefore expected to be wholly inadequate on Mars, where the surface temperature and solar flux are still lower, and the equilibrium ice thickness may be one to two orders of magnitude greater.

Migration through vertical melt channels appears to be the primary sedimentation mechanism in some Antarctic lakes (7). Melt channels form when the ice thickness is less than about 3 m. In order for this process to have operated on Mars, surface temperatures and ablation

rates must have been high enough to thin the ice to only a few meters, and liquid water must have been stable at the surface for periods during the summer. Neither condition is likely to have been met, as there is no evidence that the Martian climate at the time of layer deposition was substantially warmer than it is at the present.

Foundering of the ice cover could have occurred if enough debris was loaded onto the ice surface so that the overall density of the ice-sediment layer became greater than that of the liquid below. As sediment accumulated on the ice surface, the ice layer would thicken continuously, since freezing at the lower surface of the ice would no longer balanced by ablation from the upper surface. We calculated, for a given thickness of the sediment layer to be dumped into the lake, how rapidly sediment must be piled onto the ice surface for foundering to occur. We take ice surface temperatures of 210 to 240 K, bulk sediment densities of 1.5 to 2.5 g cm^{-3}, and sediment layer thicknesses at foundering of 75 to 150 m (the thickness of a light layer and a light/dark couplet, respectively, measured in Candor Chasma). Sedimentation rates of 0.4 to 15 mm yr^{-1} are required, and will lead to foundering at ice thicknesses ranging from 0.5 to 2.8 km. A weakness of the foundering hypothesis is that the ice would not undergo substantial melting during the foundering event, and could subsequently reform as a continuous cover and continue to thicken. However, these calculations neglect the effect of a geothermal heat flow. If the geothermal heat flow had an Earth-like value, the equilibrium thickness of even a sediment-covered ice layer might be no more than $\sim$ 2 km. Foundering could then occur repeatedly, taking place each time the sediment thickness exceeded the critical value. For an equilibrium ice thickness of 2 km, continuous sedimentation and repetitive foundering with a bulk sediment density of 2.0 g cm^{-3} would produce a sequence of layers each 140 m thick.

Even if foundering did not take place, it is likely that a thick layer of sediment that accumulated on the ice surface would penetrate the ice by a Rayleigh-Taylor instability. The configuration of dense sediment over less dense ice would favor diapiric upwelling of the ice and sinking of the sediment. We consider the flow to be dominated by the rheology of the ice, and take an upper sediment layer of 75 to 150 m thick. For an ice temperature near freezing, the instability will grow in tens of years. For a temperature of 210 K, the growth time is of the order of 10^4 yr. Therefore, if a sediment layer thick enough to form one of the observed layers accumulated on an ice cover, it would probably penetrate it rapidly.

The limiting factor for sediment deposition by foundering or a Rayleigh-Taylor instability is the ability to accumulate substantial amounts of sediment on the ice surface. Global dust storms could conceivably be the source for the sediment, but there are significant problems with this hypothesis. The present Martian climate produces net deposition of dust at the poles, and this process would have had to be somehow reversed. Furthermore, sediment would have also presumably accumulated on the surrounding uplands as well as in the Valles Marineris. None is presently observed there. This difficulty could be overcome if there were repeated periods of deposition and erosion near the equator. Sediment built up on the uplands would be swept away during erosional episodes, while debris deposited on the ice would be trapped by foundering or a Rayleigh-Taylor instability, and preserved. Without a clearly plausible mechanism for massive, repeated sedimentation at low latitudes, however, origin of the deposits by downward migration through an ice cover remains speculative at best.

Volcanic material that originated beneath the lake might also be a source for the layered deposits. There are several arguments against formation of the deposits by subaerial volcanism. One would expect that accumulations of ash-fall debris would be widespread, yet there are no layered deposits on the uplands surrounding the Valles Marineris. The nature of the layering also does not support an ash-flow origin. Typical large terrestrial ash-flows form aprons of individual flows that taper away from central vents. Smaller and more abundant flows would produce irregular layering. In addition to there being no identifiable volcanic calderas, the layered deposits are characterized by fairly uniform layer thicknesses that extend laterally for at least many ten's of kilometers. These arguments would be largely eliminated if the volcanism

were subaqueous. Volcanic constructs may have been destroyed by slumping of material off cones as they were forming, or masked by floating pumice that eventually became water-logged and sank to the lake floor. Volcanic eruptions in water also would more evenly distribute effusive material. Even at fairly great depths, it seems that explosive volcanism could occur on Mars. On Earth, eruptions change from effusive to explosive activity, due to magma vesiculation, at water depths of 300 m for basaltic magma (8), and 500 m for silicic magma (9). The corresponding water depths for explosive eruptions on Mars are about 800 m and 1300 m, respectively. Although there is no direct evidence for it, the process of subaqueous volcanism is an attractive mechanism for explaining some aspects of the layered deposits.

Finally, the nearby canyon walls are an obvious source of sediment for the layered deposits. It is likely that the Valles Marineris formed as tectonic grabens that were substantially enlarged by removal of interstitial ground ice and collapse of the canyon walls. In a lacustrine environment, sediment would have been transported from the canyon walls into the deeper portions of the canyons by gravity flows, and deposited in nearly horizontal layers. This mechanism presents some geometric complications, and may not be able to account for all of the deposits. The material from the the collapsing canyon wall is sufficient to only partially fill the depressions that formed, yet the present deposits rise nearly to the level of the canyon rims in places. This problem could be alleviated if plateaus of layered deposits had cores of undisturbed canyon wall material, or if material were also added by volcanic eruptions or sediment transport downward through the ice.

We conclude that there are several geologically feasible mechanisms that could have led to formation of thick deposits in ice-covered paleolakes in the Valles Marineris. Present data are insufficient to choose conclusively among the various possibilities. Several types of data from the Mars Observer mission will be useful in further characterizing the deposits and clarifying the process of their origin. They should be considered important targets for a future Mars sample return mission.

REFERENCES

(1) McCauley, J.F. (1978) USGS Misc. Inv. Series Map I-897.

(2) Lucchitta, B.K. (1982) NASA Tech. Mem., 85127, 233-234.

(3) Nedell, S.S. and Squyres, S.W. (1984) in Workshop on Water on Mars, Lunar and Planetary Institute, 56-57.

(4) Carr, M.H. (1979) JGR, 84, 2995-3007.

(5) McKay, C.P., Clow, G.D., Wharton, R.A., and Squyres, S.W., (1985) Nature, 313, 561-562.

(6) McKay, C.P. and Clow, G.D. (1986) NASA Ames Research Center, personal communication.

(7) Nedell, S.S. et al., in preparation.

(8) Sigurdsson, H. (1982) Geol. Assoc. Canada, Short Course Notes, 2, 294-342.

(9) Moore, E.C. and Schilling, J.G. (1973) Contrib. Min. Petrol., 41, 105-118.

COULD ICY IMPACTS RECONCILE VENUS WITH EARTH AND MARS? T. Owen, Department of Earth and Space Sciences, State University of New York, Stony Brook, NY 11794.

The explanation of the origin of Earth's moon by a giant impact implies that the earliest atmosphere of our planet was lost. As Cameron (1) has emphasized, a long epoch of impacts resulting from its proximity to the main asteroid belt should also have removed much of the original atmosphere of Mars. This would explain that planet's surprisingly low volatile inventory as deduced from current observations (2). Venus, being larger than Mars and further from the asteroid belt, was spared this level of punishment and apparently also escaped a major, moon-forming impact. The abundances of noble gases in its atmosphere today may reflect the effects of a different mixture of volatile-carrying material that was present in the earlier phases of planetary accretion but not widely abundant after the time of the formation of the Earth's moon. Alternatively, Venus may simply have been subjected to a random event-collision with a planetesimal of unusual composition.

In either case, icy planetesimals from the outer solar system provide one possible source of suitable material (3). This idea gains support from the recent work of Mayer and Pletzer (4) and Bar-Nun et al. (5) which demonstrates that gases can be adsorbed by amorphous ice without forming clathrate hydrates. Under these conditions, the abundance ratios in the original gas mixture are preserved. Thus one expects argon, krypton and xenon to exhibit solar abundance ratios (as they do on Venus) while neon will not ordinarily be adsorbed. The neon on Venus would then have to be supplied by another source, presumably the early solar wind.

This hypothesis can be tested by observations of noble gases in comets. The recent encounters with Comet Halley may therefore provide the necessary information.

1. Cameron A. G. W. (1983) Icarus 56, p. 195-201.
2. Anders E. and Owen T. (1977) Science 198, p. 453-465.
3. Owen T. (1985) in Ice in the Solar System, Proceedings of a NATO Symposium, ed. J. Klinger (D. Reidel).
4. Mayer E. and Pletzer R. (1986) Nature, p. 298-301.
5. Bar-Nun A., Dror J., Kochavi E. and Laufer D. (1986) Phys. Rev. B (submitted).

SEISMIC EXPLORATION FOR WATER ON MARS

Thornton Page
Code SN, NASA Johnson Space Center, Houston, TX 77058

This proposal is intended to promote discussion under Topic III at the Symposium on Mars, Evolution of its Climate and Atmosphere. It is proposed to soft-land three seismometers in the Utopia-Elysium region and three or more radio-controlled explosive charges at nearby sites that can be accurately located by an orbiter. Seismic signatures of timed explosions, to be telemetered to the orbiter, will be used to detect present surface layers, including those saturated by volatiles such as water and/or ice.

The Viking Landers included seismometers, and the one on Viking 2 that did not fail showed that Mars is at present seismically quiet, and that the mean crustal thickness at 47°.96 N 225°.77 is about 14-18 km. (1) The new seismic landers must be designed to minimize wind-vibration noise, and the landing sites selected so that each is well founded on the regolith, not on rock outcrops or in craters. The expolsive charges might be mounted on penetrators aimed at nearby smooth areas. They must be equipped with radio emitters for accurate location and radio receivers for timed detonation.

Areas where subsurface water may be located on Mars were recently discussed at Lunar and Planetary Science XVII (2,3), and Utopia-Elysium is a prime contender, as noted earlier by Harold Masursky (4).

The Active Seismic Experiment worked well on Apollo 16, and the technique described by Kovach, Watkins, and Talwani (5) should apply equally well on Mars as on the Moon. They determined that the lunar regolith at the Apollo-16 landing site is 12.2 m thick.

Definite detection of water- or ice-bearing layers on Mars will be of value in tracing the history of Mars' climate and atmosphere, and in planning manned missions to the planet.

References: (1) D. L. Anderson in E. C. Ezell and L. N. Ezell, 1984, On Mars: Exploration of the Red Planet, 1958-1978, NASA SP 4212, p392

(2) B. K. Lucchitta, W. M. Ferguson, and C. Summers, 1986, Lunar and Planetary Science XVII Abstracts, p 498-499

(3) E. H. Christiansen and J. A. Hopler, 1986, LPS XVII Abstracts p 125-126

(4) H. Masursky in E. C. Ezell and L. N. Ezell, loc cit, p 342

(5) R. L. Kovach, J. S. Watkins, and P. Talwani, 1972, Apollo 16 Preliminary Science Report, NASA SP 315, p 10-1 to 10-14

THE THERMAL PROPERTIES OF MARTIAN SURFACE MATERIALS AT HIGH LATITUDES: POSSIBLE EVIDENCE FOR PERMAFROST D. A. Paige†, Jet Propulsion Laboratory, Pasadena, CA 91109 and H. H. Kieffer, U. S. Geological Survey, Flagstaff, AZ 86001

Thermal models for the distribution of martian permafrost indicate that subsurface water ice could presently be stable throughout the year at depths ranging from 10 to 100 cm at latitudes poleward of $\pm 40°$ (1). Proof for the existence of such deposits would have important implications for our understanding of the initial volatile inventory, atmospheric evolution, geology, and climate of Mars. Presented here are results of preliminary efforts to map the spatial distribution of surface and subsurface permafrost at high latitudes by using Viking IRTM surface temperature observations in conjunction with diurnal and seasonal thermal model calculations.

Solid water ice or hard-frozen ground can be distinguished from fine, unconsolidated surface materials on the basis of thermal inertia. Solid water ice has a thermal inertia of $I=50 \times 10^{-3}$ cal cm^{-2} $sec^{-1/2}$, whereas mid-latitude martian surface materials have thermal inertias ranging from 1×10^{-3} to 15×10^{-3} cal cm^{-2} $sec^{-1/2}$ (2). Thermal inertia can be inferred from remote sensing observations because it has a major influence on the amplitudes of diurnal and seasonal surface temperature variations. Since martian diurnal temperature waves penetrate a few centimeters into the surface, and seasonal temperature waves penetrate to at least a meter, surface temperature observations can be used to infer the presence of permafrost.

Figure 1 shows the boundaries of three relatively homogeneous regions in the north polar area that were selected for intensive study. They are all 2° in latitude by 30° in longitude. Region 1 lies within the north permanent water ice cap. Region 2 lies within the dark circumpolar sand sea. Region 3 lies within the north circumpolar planes. All highest quality IRTM observations that fell within these regions were selected. Emission angles for the observations were constrained to be less than 70°. The observations were binned by season at a resolution of 10 days and by Mars local time at a resolution of one hour.

Figures 2, 3 and 4 show the available measured IRTM 20μ channel brightness temperatures for these regions during one half of a Mars year. Seasonal and hourly temperature variations are multiplexed on the same plot. Each point consists typically of 1 to 20 separate observations, with standard deviations of less than 2K. During spring, all three regions are covered by seasonal CO_2 frost, which has a temperature of $\approx$ 148K. Measured brightness temperatures are generally higher than 148K during this season because of emission due to warmer dust and water ice clouds in the overlying atmosphere (3,4). During summer, when the seasonal CO_2 frost has disappeared, measured 20μ brightness temperatures are considered to be good approximations to actual surface temperatures because significant spectral contrasts between the four IRTM surface sensing channels are not observed during this season.

Also shown in Figs. 2, 3 and 4 are calculated diurnal surface temperature variations using the Viking Thermal Model (5). The model assumes constant thermal properties with depth and constant surface albedo with time. Atmospheric effects are ignored except for a small correction for the emissivity of the atmosphere at 15μ . The model also allows for the condensation and sublimation of CO_2 frost when appropriate. Assumed CO_2 frost albedos were adjusted so that the dates at which seasonal CO_2 frost disappeared at each location were in accord with the observations. In each case, the model was run for four Mars years to achieve stability over the annual cycle. Model-calculated diurnal surface temperature variations are plotted at 10 day intervals and can be compared directly with the available IRTM observations during the summer season.

For Region 1, it was possible to fit both the observed diurnal and seasonal temperature variations with a surface albedo of $A_s=0.43$ and a thermal inertia $I=40 \times 10^{-3}$. The derived thermal inertia is in good agreement north polar cap thermal inertias derived from heat balance considerations (3,4). This result implies that the bright regions of the north permanent polar cap consist primarily of dense water ice from the surface to great depths. The amount of dust and rock that may be imbedded within the ice cannot be determined from these observations.

For Region 2, it was not possible to satisfactorily fit both the observed diurnal and seasonal temperature variations with a single set of model input parameters. $A_s=0.22$ and $I=6.5 \times 10^{-3}$ gives a reasonable

fit to the general seasonal temperature variations, but the amplitudes of diurnal surface temperature variations during early summer are underestimated. Despite this discrepancy, it can be argued that I=6.5 $\times 10^{-3}$ represents an upper limit for the thermal inertia of the uppermost few centimeters of the sand dune deposits. This surprisingly low value implies that the dunes are not frozen solid, and lends support to the the notion that they could presently be active (6).

For Region 3, it was again not possible to satisfactorily fit both the observed diurnal and seasonal temperature variations with a single set of model input parameters. A_s=0.30 and I=15 $\times 10^{-3}$ gives a reasonable fit to the general seasonal temperature variations, but again, the amplitudes of diurnal surface temperature variations during early summer are underestimated. Differences between observed and model calculated surface temperatures at midnight diminish as the summer season progresses, giving good agreement at the end of the season. Attempts to fit the early summer observations with lower thermal inertias yielded calculated late summer surface temperatures that were much lower than observed.

Two distinct arguments can be made for the existence of martian permafrost on the basis of these observations. The first is that annual average temperatures of regions 2 and 3 are ≈165K and ≈168K respectively. This means that temperatures at great depths are well below required permafrost temperatures of ≈198K (1).

The second is that the observed thermal behavior of Region 3 implies the existence of high thermal inertia material below the surface. If I=15 $\times 10^{-3}$ is an overestimate for thermal inertias at diurnal skin depths, then I=15 $\times 10^{-3}$ is an underestimate for for thermal inertias at seasonal skin depths. This reasoning can be tested quantitatively by developing a more flexible thermal model that can treat non-constant thermal properties with depth.

Although permafrost is not the only plausible martian surface material with high thermal inertia, polar thermal mapping may turn out to be a powerful tool for determining the distribution of permafrost deposits and understanding their behavior. At this point, the circumstantial case for permafrost deposits in the north polar region of Mars is very strong indeed.

REFERENCES

1. Farmer, C. B. and P. E. Doms, *J. Geophys. Res.* 84, 2881 (1979).
2. Palluconi, F. D. and H. H. Kieffer, *Icarus* 45, 415 (1981).
3. Paige, D. A. and A. P. Ingersoll, *Science* 228, 1160 (1985).
4. Paige, D. A., Ph.D. Thesis, California Institute of Technology (1985).
5. Kieffer, H. H. *et. al., J. Geophys. Res.* 82, 4249 (1977).
6. Tsoar, H., Greeley, R. and A. R. Peterfreund, *J. Geophys. Res.* 84, 8167 (1979)

† National Research Council Resident Research Associate

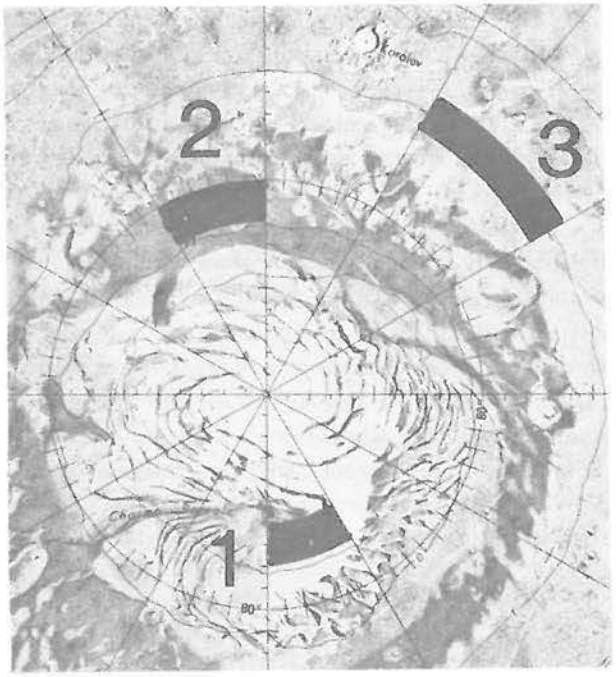

Figure 1. Three regions in the north polar area.

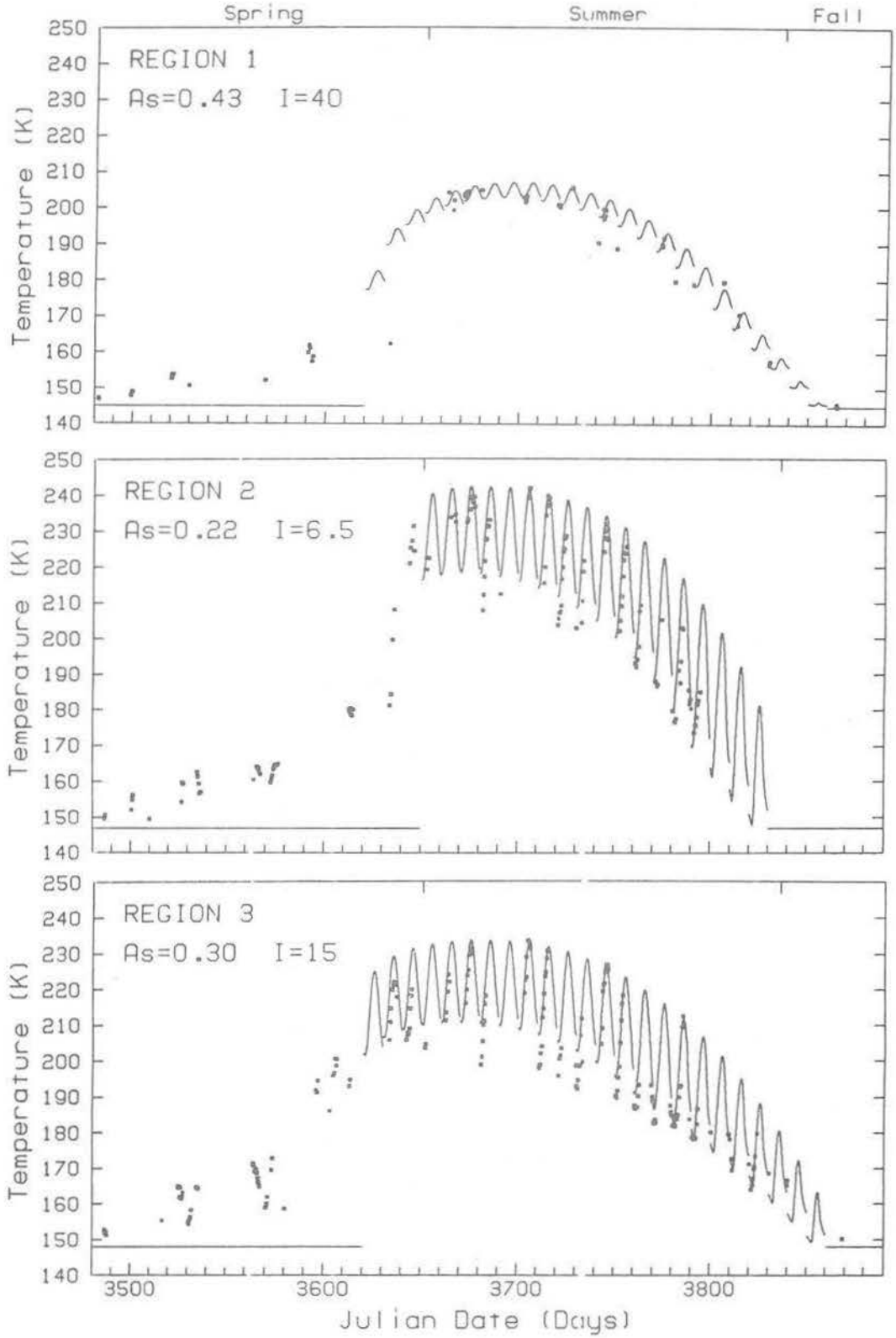

Figures 2, 3 and 4 Ten-day averaged diurnal surface temperature variations for three regions in the north polar area. (Dots) IRTM 20μ channel observations. (Lines) Thermal model calculations.

GEOMORPHIC EVIDENCE FOR ANCIENT SEAS ON MARS

by
Timothy J. Parker, Dale M. Schneeberger, David C. Pieri, and R. Stephen Saunders
Jet Propulsion Laboratory, Pasadena, CA

The discovery of large outflow channels on Mars has posed complex and outstanding problems with regard to their formation. Most channels empty into large, seemingly featureless plains with little apparent evidence of the depositional morphologies to be expected with the debouchment of enormous volumes of sediment, as implied by the physical scale of the outflow channels. Hypotheses have never reconciled volumes and locations of proposed source regions with the observed sizes and implied discharges of the channels, nor have they adequately accounted for the apparent lack of obvious depositional features at outflow channel mouths.

The inability to identify fan or delta deposits at the mouths of the martian outflow channels at available resolutions does not preclude their existence (1), since such deposits are difficult to identify even in terrestrial examples of catastrophic outflow - for example, the Channeled Scablands of the Pacific northwest (2) and the Pleistocene glacial lake basins of the northern Great Plains (3). Apparently catastrophic deposition spreads material over a much larger outwash area than that of a typical river. On Mars this effect would be more pronounced due to the lower gravity (4).

The debouchment areas of major outflow channels and fretted terrains present an intriguing array of subtle morphologies, which, taken as a group, could plausibly argue for formation in a near-shore lacustrine environment. Some of these features are illustrated in figures 1-3, and are described briefly below.

Figure 1 depicts a region in southwest Cydonia Mensae (32^0 lat., 17^0 lon.), north of the lowland/upland boundary escarpment comprised of clusters of massifs and knobs, probably outliers of cratered upland material, and smooth lowland plains. Surrounding the clusters and linking many isolated knobs is a system of curvilinear ridges and arcuate terrain boundaries which tend to separate the knobby terrain and massifs from the smooth plains, the concave sides of the arcs facing toward the plains. This relationship is strikingly similar to terrestrial examples of islands linked by coastal barriers and tombolos and is of comparable scale.

Figure 2 depicts a degraded, 45 km crater at 33^0 lat., 23^0 lon., 300 km from the lowland/upland boundary escarpment in Acidalia Planitia. The crater rim has been modified into a loose, broken chain of knobs with low, roughly concentric debris aprons. This style of debris-aproned knob, or stepped massif, represents a morphology unique to the northern lowlands and may represent pre-flood material modified during a rise in base level during flooding of the northern lowlands. The debris aprons are rounded in plan, typically non-lobate, and could have formed either by wave action or mass wasting processes, or both. Further, they appear to have a smooth, nearly horizontal upper surface, often displaying sharp demarcations at slope inflections. These differ from massifs with debris aprons described elsewhere (5,6) in which the debris apron is often lobate in plan with a distinctly striated upper surface. Curvilinear ridges may occur in direct association with the stepped massifs, forming links between individual knobs, and appear to grade into the upper surfaces of the debris aprons.

Actual shorelines or strandlines would have to be very broad in order for them to be identified as separate features at typical Viking resolution, rather than as boundaries between morphologic units. Though very high resolution images (<15 m/pixel) are available, few coincide with areas in which this hypothetical shoreline might be expected. Figure 3 illustrates the best example of possible shoreline/strandline features we have found thus far. Figure 3a is a low resolution (200 m/pixel) mosaic of fretted terrain in west Deuteronilus Mensae, showing at least three zones parallel to the lowland/upland boundary, suggestive of increasing modification northward. The southern-most zone consists of sharply defined highland plateau material (zone "A"). The middle zone (zone "B") consists of well defined plateau material with a surface smoother than that of zone "A". The northern-most zone consists of rounded, softened plateau remnants and "striped" or mottled terrain (zone "C"). The floors of the canyons or "frets" also display at least 3 different zones, offset southward with respect to the plateau surface zones. Zone "A" consists of flat canyon floors bounded by prominent debris aprons. Zone "B" consists of flat floors lacking debris aprons. Zone "C" consists of striped or mottled terrain separated from zone "B" by an arcuate boundary. Figures 3b-e are part of a 9 m/pixel image mosaic centered at 46^0 lat., 346^0 lon., of part of the west canyon of figure 3a. In this mosaic, the northern extent of zone "B" of both the plateau and canyon floor have been resolved into polygonally patterned ground, the individual polygons measuring several tens to a few hundred meters across, similar or somewhat larger in scale than terrestrial ice-wedge polygons.

Several bands, visible along the canyon wall and within the degraded 10 km crater to the west, appear to be topographically conformal features and may be strandlines. No polygonal terrain is visible north of the lowest of

these bands where it separates the middle zone from the northernmost zone of the fretted terrain. The scale of these bands is similar to broad terrestrial strandlines and beach ridges.

These hypothetical lakes or a shallow sea or ocean may have persisted for a time period significant with regard to the erosion of promontory and bounding topography (e.g., flat-topped mesas and fretted terrain). While our assertions may appear provocative, they are consistent with very conservative estimates of martian global water inventories (7, 8), as well as with an emerging realization that thin, heavily sediment-laden flows may have spread out from channel mouths across the northern plains for hundreds of kilometers (9, 10, 11).

(1) Baker, 1982, University of Texas Press, 198 p.
(2) Baker, V. R. and Nummedal, C., eds., 1978, Washington, D. C., NASA Office of Space Science, Planetary Geology Program, 186 p.
(3) Kehew, A. E., and Lord, M. L., 1986, Geol. Soc. Am. Bull., V. 97, p. 162-167.
(4) Pieri, D. C., 1980, NASA TM 81979, p. 1-160.
(5) Carr, M. H., 1977, Journ. Geophys. Res., V. 82, p. 4039-4054.
(6) Squyres, S. W. and Carr, M. H., 1984, in Workshop on Water on Mars, Lunar and Planet. Inst., p. 80.
(7) Anders and Owen, 1977, Science, V. 198, p. 453-465.
(8) Pollack and Black, 1979, Science, V. 205, p. 56-59.
(9) Jons, H.-P., 1985, Proc. Lunar Sci. Conf. 16th, p. 414-415.
(10) Jons, H.-P., 1986, Proc. Lunar Sci. Conf. 17th, p. 404-405.
(11) McGill, 1985, Proc. Lunar Sci. Conf. 16th, p. 534-535.

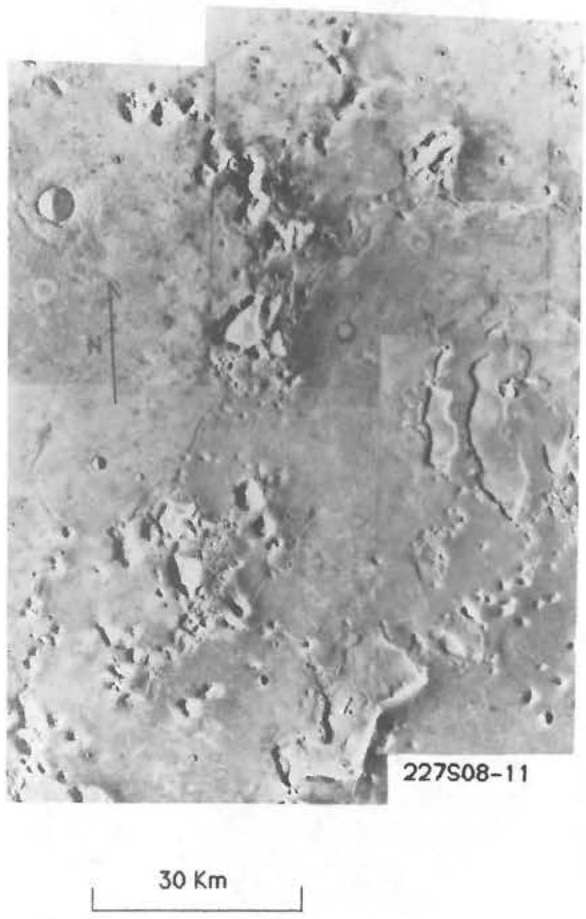

Figure 1

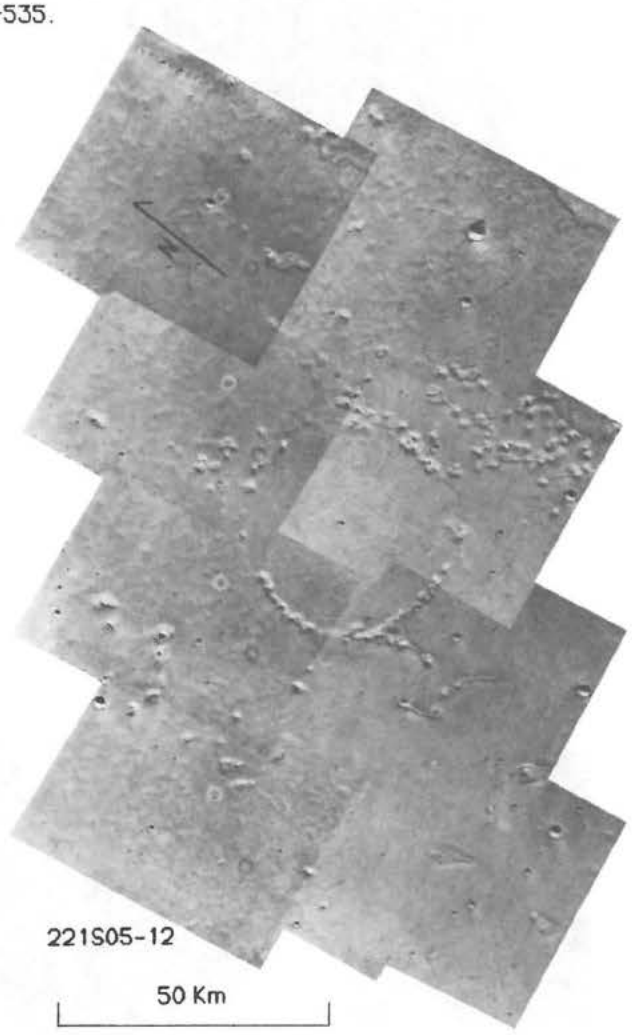

Figure 2

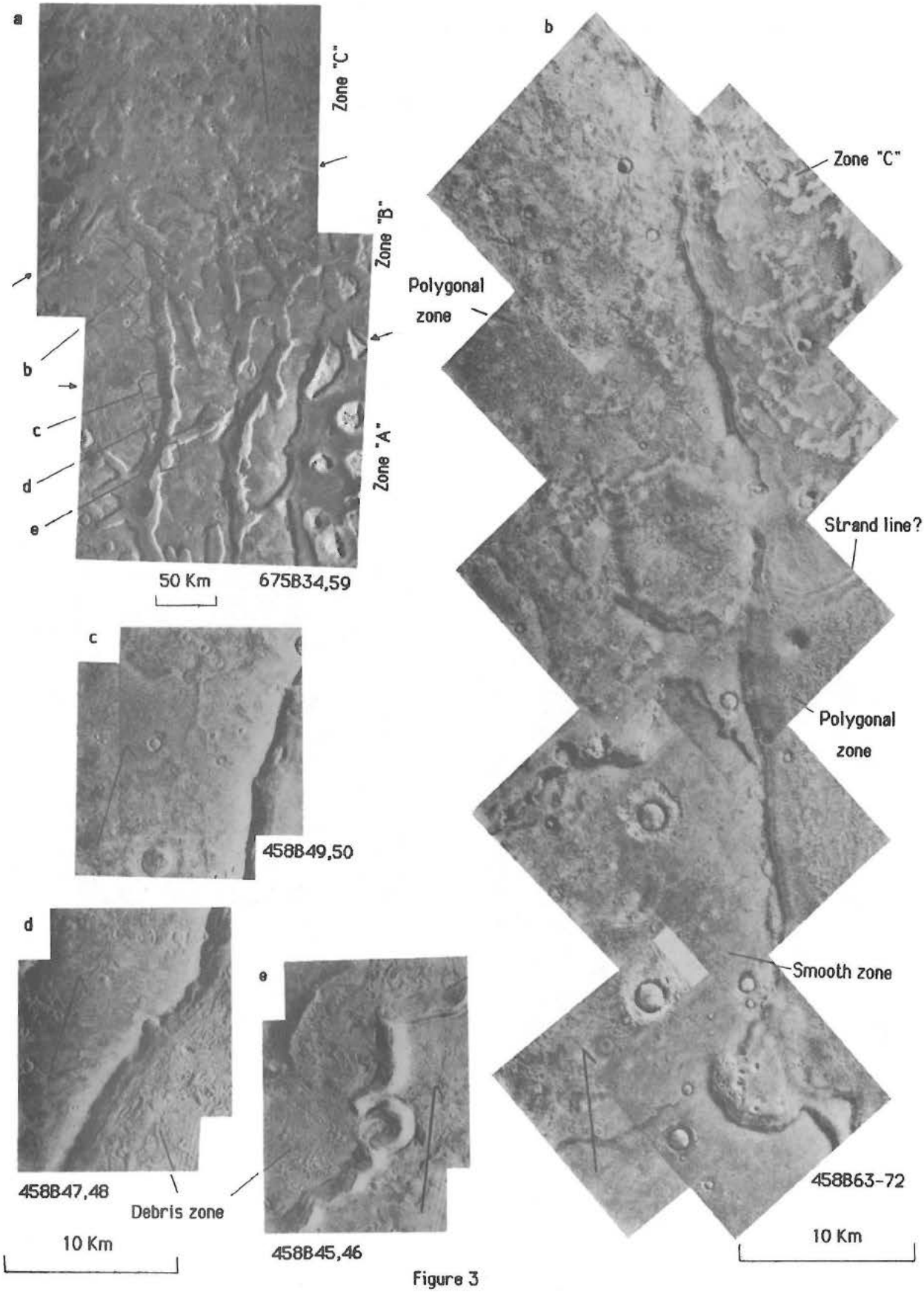
a
Zone "C"
Zone "B"
Zone "A"
b
c
d
e
50 Km
675B34,59
b
Zone "C"
Polygonal zone
Strand line?
Polygonal zone
Smooth zone
458B63-72
10 Km
c
458B49,50
d
458B47,48
Debris zone
10 Km
e
458B45,46

Figure 3

VOLATILE INVENTORY OF MARS-II: PRIMORDIAL SOURCES AND FRACTIONATING PROCESSES. R. O. Pepin, School of Physics and Astronomy, University of Minnesota, Minneapolis, Minnesota 55455.

The small differences in relative elemental abundances of noble gases in the atmospheres of Earth and Mars are smooth functions of mass, and may imply a fractionation relationship between them(1,2). Both planetary atmosphere patterns are roughly similar to elemental noble gas ratios in carbonaceous chrondrites, with the conspicuous exception of Xe: the meteoritic $^{130}Xe/^{84}Kr$ ratio is ∿20x higher. The three reservoirs are isotopically distinct. Abundances of the Xe isotopes on Earth and Mars are very different from AVCC (Average Carbonaceous Chondrite) Xe. Both appear to have been generated by gross mass fractionation of meteoritic components: Mars from AVCC-Xe(3) and Earth from U-Xe, an inferred composition closely related to AVCC-Xe but without a nucleogenetic heavy-isotope contribution that is abundant in the carbonaceous chondrites(2,4). Martian and terrestrial Kr compositions differ from each other and from AVCC-Kr(3,5), and Ar on Mars has an extraordinarily low $^{36}Ar/^{38}Ar$ ratio(6). Finally, relative elemental and isotopic abundances in the solar nebula, the presumed primordial source for most of the noble gases in contemporary meteoritic and planetary reservoirs, were different from the composition of these reservoirs to varying degrees, based on estimates of "cosmic"(7,8) and solar wind(9-13) abundances. It is clear that understanding the origin and evolution of noble gas distributions in meteorites and planetary atmospheres, and their implications for the past and present volatile inventories of these reservoirs, requires knowledge of the processes that generated these contemporary abundance patterns from primordial sources, and identification of the astrophysical environments in which they could reasonably have operated. A model that shows some promise in this direction is outlined below.

Sources. Two primordial noble gas sources are assumed: the early solar nebula with "cosmic" (∿solar wind) composition, here called solar composition; and pre-solar, probably carbonaceous grains carrying traces of exotic nucleogenetic noble gases (e.g., Ne-E, s-process Kr and Xe, H[CCF]-Xe and L-Xe).

Processes. Several reports in the literature have pointed out an apparently fundamental process of mass fractionation in the take-up, presumably by adsorption, of ambient Ne, Ar, Kr and Xe on various carbonaceous substrates synthesized in the laboratory in air or a noble gas atmosphere(14-16 and references therein), or on natural terrestrial sedimentary materials such as shales(17-19). The fractionation, which is strikingly uniform considering the wide range of physical conditions under which it has been produced, is primarily elemental --no consistent isotopic effects have been reported in nonplasma environments. The noteworthy characteristic of this absorptive fractionation is that it generates on the substrate, from an ambient atmosphere of solar composition, elemental abundance ratios that begin to resemble the AVCC pattern, although still too rich in Ne and Ar relative to Kr(14-19).

The other primary process invoked in the model is mass fractionation of minor atmospheric species during early episodes of hydrodynamic hydrogen escape from planetary bodies and large planetesimals. Hunten et al.(2) have recently shown that this process, given an enhanced EUV flux from the young sun(20) and the availability of large but not unreasonable amounts of hydrogen in the accreted planets, could have generated the U-Xe ↔ Earth-Xe isotopic fractionation and the apparent Mars ↔ Earth noble gas elemental fractionation. This is also the case for the AVCC-Xe ↔ Mars-Xe isotopic fractionation(3). Hunten et al., while demonstrating the possible applicability of fractionation in hydrodynamic escape to planetary atmospheres, did not attempt to develop a general model to reconcile the various observations of fractionated mass distributions

within the context of a single scenario for evolution of meteoritic and planetary noble gases.

Astrophysical settings: [1] Planetesimals large enough ($\geq 10^{24}$-10^{25} g) to acquire and retain atmospheres against thermal escape for at least limited periods, probably $\leq 10^6$-10^7 years; and [2] the accreted terrestrial planets. The planetesimal atmospheres are solar in composition, possibly generated by internal outgassing but more probably captured from the surrounding nebula. (Gases in dust grains comprising the planetesimals would probably have experienced elemental fractionation during their earlier adsorption from the nebula, thus leading to nonsolar abundances in atmospheres derived from grain outgassing). This astrophysical setting is taken from a recent model by Donahue(21) for production of noble gas distributions in planetary atmospheres. The Donahue model involves accretion of the planets from two planetesimal populations, one with atmospheres of solar composition and the other with atmospheric Ne and Ar depleted by Jeans (thermal) escape. It can account reasonably well for relative Ne:Ar:Kr elemental abundances and for Ne isotopic compositions in planetary atmospheres. But because of the very steep mass dependence of Jeans escape, predicted $^{36}Ar/^{38}Ar$ ratios are much too low. The model is unable to accommodate the variations in Kr-Xe elemental and isotopic compositions in different planetary reservoirs, nor does it speak to meteoritic elemental and isotopic compositions(21). In the present model, fractionation in Jeans escape is replaced by fractionation during hydrodynamic escape of hydrogen, which is much less sensitive to mass, in both planetesimal and planetary environments. The hydrogen is assumed to be generated by reduction of H_2O during impact or internal differentiation, or by photodissociation of surficial H_2O.

Scenarios, assumptions, and results. Planetesimals, surfaced with carbonaceous grains carrying the nucleogenetic noble gas components, are warmed by internal processes to at least the temperature of liquid water. In an episode of hydrodynamic escape driven by an enhanced but declining solar EUV flux(20), atmospheric species lighter than Xe are depleted and fractionated. The escape episode is terminated, probably within $\leq 10^6$ years, by cooling and concomitant cut-off of the hydrogen supply. Residual atmospheric gases experience a second stage of elemental fractionation during adsorption on cooling grain surfaces prior to final dissipation of the atmosphere. These adsorbed gases represent the so-called "planetary" noble gas component. Together with the nucleogenetic components, which are presumed not to have outgassed from pre-solar grains during thermal/hydrothermal activity on the parent bodies, they comprise the noble gas inventory of the carbonaceous chondrites. With appropriate choices for the parameters of the hydrodynamic escape episode, and with certain assumptions concerning isotopic compositions of solar noble gases in cases where they are not well known (e.g., Ar, Kr and Xe), this scenario is capable of reproducing the AVCC elemental and isotopic noble gas pattern.

A more complex sequence of events is required to account for the mass distribution of noble gases in planetary atmospheres. Here we focus on Mars; with variation of parameters, the model is also applicable to Earth. (Venus needs more thought, and perhaps a unique, solar-dominated gas component). AVCC gases have contributed to the Mars volatile inventory, but a second component is mandated by the isotopic composition of martian [≡SNC] Kr. A satisfactory choice is simply a carrier of gases derived by adsorptive fractionation ("AF") of solar gases (resulting in elemental but not isotopic fractionation), on dust grains in the nebula or on a hydrogen-poor parent body whose solar atmosphere was not fractionated by hydrodynamic escape.

A model scenario for Mars is then as follows. The AF and AVCC gas carriers are supposed to have accreted into proto-Mars, in proportions such that ~40%

of the Kr was contributed by AVCC material. These gases are at least partially retained within the growing planet. The final stage of accretion involved primarily AVCC carriers, with impact energies sufficient to generate an AVCC-like primordial atmosphere, rich in H_2 or water vapor, by projectile outgassing. At this stage the nebula has cleared, and the high solar EUV flux begins to drive a prolonged ($\sim 10^8$ year) and severe episode of hydrodynamic escape which greatly depletes (Xe to a few % of its initial abundance, lighter gases to larger extents) and mass-fractionates the primordial atmosphere. The residual, severely fractionated AVCC-Xe generated in this episode remains in the contemporary martian atmosphere. Hydrodynamic escape may have been interrupted temporarily by exhaustion of the surficial H_2 supply, but resumes as H_2 produced in internal differentiation is outgassed from the body of the planet(22), sweeping with it the AF+AVCC noble gases incorporated at an earlier stage of accretion. At this time the solar EUV flux is assumed to have decreased to the level where only gases lighter than Kr are depleted and fractionated. This scenario, with suitably chosen parameters for the escape episode, can account for all characteristics of present-day noble gas abundances on Mars (including a low $^{36}Ar/^{38}Ar$ ratio) except one: the low Xe/Kr ratio. Here it is necessary to introduce a purely ad hoc assumption: that during differentiation processes under conditions of high pressure in the martian mantle, Xe contributed by the AF+AVCC carriers partitions very efficiently into mantle- or core-forming phases and is therefore retained in the planet's interior. The same assumption is required for Earth.

For the particular choices of hydrodynamic escape functions and parameters (2) that yield the requisite noble gas fractionations in this model, the hydrogen losses needed to implement the process seem reasonable: the equivalent of a few tens of meters of water in the planetesimal environment, and 20-30 kilometers of water on Mars. The latter loss estimate, while very large, is in fact only about one-quarter of the initial martian water inventory if the Dreibus-Wänke two-component mixing model for Mars(22) is correct.

REFERENCES. (1) Pepin R. O.(1986)Lunar and Planetary Science XVII, 656. (2) Hunten D. M., Pepin R. O. and Walker J. C. G.(1986)Mass Fractionation in Hydrodynamic Escape, preprint, submitted to Icarus. (3) Swindle T. D., Caffee M. W. and Hohenberg C. M.(1986)GCA, in press. (4) Pepin R. O. and Phinney D. (1978)Components of Xenon in the Solar System, preprint, submitted to The Moon and Planets. (5) Becker R. H. and Pepin R. O. (1984)EPSL 69, 225. (6) Wiens R. C., Becker R. H. and Pepin R. O.(1986)EPSL 77, 149. (7) Cameron A. G. W. (1982), in: Essays in Nuclear Astrophysics, pp.23-43. (8) Anders E. and Ebihara M.(1982)GCA 46, 2363. (9) Bochsler P. and Geiss J.(1977)Trans. Int. Astron. Union XVIB, 120. (10) Frick U. and Pepin R. O.(1981)Lunar and Planetary Science XII, 303. (11) Becker R. H., Rajan R. S. and Rambaldi E. R.(1983)Abstracts from Workshop on Past and Present Solar Radiation, Lunar and Planetary Institute, Houston, TX, 2. (12) Becker R. H., Pepin R. O., Rajan R. S. and Rambaldi E. R. (1986)Light Noble Gases in Weston Metal Grain Surfaces, abstract submitted for 49th Meteoritical Society Meeting, New York, September. (13) Becker R. H. and Pepin R. O.(1984)EPSL 70, 1. (14) Frick U., Mack R. and Chang S.(1979)Proc. Lunar Planet. Sci. Conf. 10th, 1961. (15) Niemeyer S. and Marti K.(1981)Proc. Lunar Planet. Sci. Conf. 12th, 1177. (16) Yang J. and Anders E.(1982)GCA 46, 861. (17) Canalas R. A., Alexander E. C. and Manuel O. K.(1968)J. Geophys. Res. 73, 3331. (18) Phinney D.(1972)EPSL 16, 413. (19) Bernatowicz T. J., Podosek F. A., Honda M. and Kramer F. E.(1984)J. Geophys. Res. 89, 4597. (20) Zahnle K. J. and Walker J. C. G.(1982)Rev. Geophys. Space Phys. 20, 280. (21) Donahue T. M.(1986)Fractionation of Noble Gases by Thermal Escape from Accreting Planetesimals, Icarus, in press. (22) Dreibus G. and Wänke H.(1985)Meteoritics 20,367.

MARTIAN TECTONICS: A REVIEW; R. J. Phillips, Dept. of Geological Sciences, Southern Methodist University, Dallas, TX 75275

Mars appears to play an intermediate role in the tectonic style of the five large bodies of the inner solar system. The tectonic style of Mars is dominated by vertical motion, perhaps more so than any of the terrestrial planets. The imprint of this tectonic activity has left a surface widely faulted even though younger volcanism has masked the expression of tectonism in many places. Geological activity associated with Tharsis and, to a lesser extent, Elysium Provinces is responsible for a significant portion of this faulting (1, 2, 3, 4), while the origin of other features is enigmatic. The tectonic imprint of Tharsis is seen over at least 180 degrees of longitude.

The origin and evolution of the Tharsis and Elysium Provinces, in terms of their great elevation, volcanic activity, and tectonic style has sparked intense debate in the last 15 years in the planetary geosciences community. Central to these discussions are the relative roles of three basic modes of imparting stress to the lithospheric layer; flexural loading, flexural uplift and isostatic loading. These mechanisms predict stress fields that are quite distinct, so that the orientation and type (e.g., graben or wrinkle ridge) of tectonic features mapped on the surface are a guide to the stress mode. In turn, the stress history points to the evolution of the geological feature in question. A caveat in all of this work is that the present-day gravity field and topography must be used to constrain ancient stress fields. This is appropriate if the history of mass movement in the interior has been dominated by vertical motion. Indeed, the fact that the present-day fields can predict ancient structural features suggests that this has largely been the case.

What we are learning is that these different modes of stress have operated at different times in the history of the Tharsis and Elysium Provinces. Thus it becomes crucial to map the tectonic features associated with each stress mode and decipher their relative age of formation. Confounding this task is whether or not there have been distinct centers of faulting (5) that have migrated geographically with time, beyond the spatial resolution of the spherical harmonic stress modeling.

A specific model for the Tharsis Province is as follows (6): The first stage of formation is characterized by flexural uplift. Evidence for this event is found in circumferential graben in the Claritas Fossae region. Following this is an episode of isostatic loading that produced many of the normal faults in the immediate Tharsis region and is probably associated with large-scale volcanic construction. The last major stage is flexural loading, which produced radial graben on the periphery of Tharsis. Major questions concerning this model include: What is the load that caused the flexural failure and what is the mechanism for (essentially) permanent uplift? The former question arises because it is difficult to identify the volcanic load of the correct relative age and magnitude to account for the flexural faulting. Two possibilities are: (a) effective loading due to loss of buoyant isostatic support due to interior cooling and (b) transfer of magma to the surface and the subsequent effects of membrane stress (7). Permanent uplift is a more speculative topic. Possibilities here are:

(a) massive intrusion into the crust (2) and (b) large blow-off of pyroclastic material from an early volatile-rich martian mantle (8), leading to uplift required to maintain mechanical equilibrium.

Analysis of stress models for the Elysium Province suggests that the tectonics of that region have been influenced by flexural uplift and by the stress field associated with Tharsis (4). There is no tectonic evidence for flexural loading, however. There is ample evidence of flexural lithospheric failure on Mars due to local loading, and studies of the location of circumferential graben around large shield volcanoes, for example, have led to estimates of lithospheric thickness (4, 9).

Other tectonic features on Mars have no obvious association with Tharsis or Elysium, and we are challenged to devise plausible models. The role of large impacts in setting a tectonic fabric needs to be evaluated (e.g., 10). We still do not have a plausible model to explain the north-south dichotomy.

REFERENCES

(1) Banerdt, W. B., et al., JGR, 87, 9723-9733, 1982.
(2) Willemann, R. J., and D. L. Turcotte, JGR, 87, 973-9801, 1982.
(3) Sleep, N. H., and R. J. Phillips, JGR, 90, 4469-4489, 1985.
(4) Hall, J. L., et al., JGR, in press, 1986.
(5) Plescia, J. B., and R. S. Saunders, JGR, 87, 9775-9791, 1982.
(6) Phillips, R. J., and N. H. Sleep, to be submitted to JGR, 1986.
(7) Phillips, R. J., and A. A. Finnerty, LPSC XVII, Lunar and Planetary Institute, Houston, 658-659, 1986.
(8) McGetchin, T. R., and J. R. Smyth, Icarus, 34, 512-536, 1986.
(9) Comer, R. P., et al., Rev. Geophys., 23, 61-92, 1985.
(10) Schultz, P. H., et al., JGR, 87, 9803-9820, 1982.

PARTITIONING OF CARBON DIOXIDE BETWEEN THE ATMOSPHERE AND LITHOSPHERE ON EARLY MARS; J.B. Pollack, J. Kasting (NASA Ames Research Center, Moffett Field, CA 94035), and S. Richardson (Iowa State University, Ames, Iowa, 50011)

There is limited geological evidence that Mars may have had a clement climate in its early history, perhaps one characterized by surface temperatures exceeding the freezing point of water (1,2). The most likely means of achieving a warmer, wetter climate is by an efficient greenhouse effect produced by a high pressure, carbon dioxide dominated atmosphere (1,3). In a comparison paper (4), we show that CO_2 partial pressures at the surface ranging from 0.75 to 5 bars are required to raise the surface temperature above 273K, with this range of pressure depending on the choice of orbital location, latitude, season, and surface albedo. Here, we examine geological processes that remove and add atmospheric carbon dioxide, assess the feasibility of retaining a several bar CO_2 atmosphere for extended periods of time ($\sim 1 \times 10^9$ years) at an early epoch on Mars, and discuss the ultimate fate of such an atmosphere.

Carbon dioxide in the present atmosphere of the Earth has a residence time of only about 10^4 years due to the chemical weathering of continental Ca and Mg containing silicate rocks that ultimately convert atmospheric carbon dioxide into carbonate rocks (5). If the surface temperature on early Mars was above the freezing point of water, at least at certain seasons and places, the chemical weathering of rocks would undoubtedly cause a rapid loss of atmospheric carbon dioxide, thereby tending to greatly diminish the greenhouse effect responsible for the clement climate. We have estimated the time scale for the removal of an initially massive CO_2 atmosphere by chemical weathering by appropriately scaling chemical weathering rates for the Earth and using empirical relationships for the dependence of these rates on pressure (6), temperature(7), and precipitation (7). We also allow for differences in the cation content of silicate rocks and the fractional area covered by standing bodies of water on the two planets and consider constraints imposed by heat balance considerations on the rate of evaporation and hence precipitation and by physical weathering on the rate of chemical weathering. According to our calculations, a several bar CO_2 atmosphere would have a residence time of 10^7-10^8 years due to chemical weathering. Although this time scale is a lot longer than that for the present Earth's atmosphere (due mostly to the larger mass of the putative early Martian atmosphere), it is still short compared to the time scales of greatest interest ($\sim 1 \times 10^9$ years).

Although carbon dioxide has a short residence time in the Earth's present atmosphere, its loss is approximately balanced by the outgassing of CO_2 from the Earth's interior. Much of the outgassed CO_2 may be derived from carbonate rocks that have been subducted into the Earth's interior, where they are thermally decomposed. An analogous process may have existed on early Mars: global scale volcanism may have led to the efficient decomposition of carbonate rocks when hot lava came in contact with these rocks and especially when magma buried them to great enough depth where temperatures exceeded their phase stability boundaries. We have been able to estimate the time scale for such recycling from simple energy considerations: the interior heat flux at the surface is due to a combination of thermal conduction and latent heat released from surface magmas. Constraining the rate of volcanism to be a prescribed fraction of

the surface heat budget and using theoretical estimates of the surface heat flux for early Mars (8), we find that the time scale for recycling CO_2 by lava burial is comparable to the time scale for chemical weathering. Hence, through such a recycling mechanism, a large CO_2 atmosphere could have been maintained on early Mars for an extended period of time.

Ultimately, the recycling rate would have greatly declined due to both a decrease in the rate of surface lava production (due to a decline in the surface heat flux) and to its assuming a more regional character (hence carbonate rocks in only localized regions would be recycled). Therefore, during an intermediate epoch in Martian history, chemical weathering would have assumed a dominant role and the large greenhouse effect would have disappeared. However, it is conceivable that large amounts of CO_2 may have been reintroduced into the Martian atmosphere for comparatively short times ($<<1 \times 10^9$ years) during some portions of its later history at times of extensive volcanism that temporarily recycled CO_2 back into the atmosphere.

If chemical weathering played a key role in controlling the amount of CO_2 in the early Martian atmosphere and ultimately in removing much of it, then geologically significant quantities of carbonate rocks should have resulted. Even after liquid water could no longer exist in most places and at most times at the surface, transient pockets of liquid water may have continued to provide an environment in which atmospheric CO_2 could have been transformed into carbonate rocks, although at a much reduced rate (9). Thus, a search for the signature of carbonate rocks on the surface of Mars would be quite useful. Such searches might be conducted during the present opposition of Mars during the summer of 1986 and, ultimately, at much higher spatial resolution, with the VIMS experiment of the Mars Observer spacecraft.

It has not escaped our attention that the above scenario, if true, could have profound inplications for the possible occurrence of life on early Mars and its ultimate survival.

REFERENCES

1. J.B. Pollack, Icarus, 37, 479, 1979.

2. P.H. Schultz, MECA abstracts, p.16, Aug. 1985.

3. R.D. Cess, V. Ramanathan, and T. Owen, Icarus, 41, 159, 1980.

4. J.F. Kasting, this volume.

5. H.D. Holland, "The Chemistry of the Atmosphere and Oceans", 1978.

6. J.C.G. Walker, P.B. Hays, and J.F. Kasting, J. Geophys. Res., 86, 9776, 1981.

7. R.A. Berner, A.C. Lasaga, and R.M. Garrels, Amer. J. Sci, 283, 641, 1983.

8. G.F. Davies and R.E. Arvidson, Icarus, 45, 339, 1981.

9. R. Kahn, Icarus, 62, 175, 1985.

IMPLICATIONS OF ISOTOPIC SIGNATURES OF NOBLE GASES FOR THE ORIGIN AND EVOLUTION OF TERRESTRIAL ATMOSPHERES.

A.S.P.Rao, Dept. of Geology, Osmania University, Hyderabad-500007, India.

The author (1,2,3) has proposed successive accretion model for the origin of terrestrial planets based (a) on the sequence of zones of condensation of solar nebula (b) on the condensation sequence of minerals, iron and nickel in different P-T regimes of the solar nebula and (c) on the sequence in the nucleation of iron cores of the terrestrial planets. Any model proposed for the origin of the terrestrial planets should also be capable of explaining the origin and evolution of the terrestrial atmospheres. The origin and evolution of the atmospheres are intimately related to the sizes and masses, thermal histories and tectonics of the terrestrial planets and the interactions of the degassed volatiles with the lithospheres of the planets. According to the successive accretion model the quantities of volatile rich-bodies (similar to carbonaceous chondrites (6) low temperature assemblages-LTA) captured by the terrestrial planets were controlled by the masses and sizes of the terrestrial planets. For example, larger planets (Earth and Venus) must have captured all most all the available volatile rich-materials while smaller planets (Mars & Mercury) had captured only negligible quantities of volatile rich-bodies during the final stages of their formation.

A comparision of the abundances of ^{40}Ar and ^{4}He (radiogenic) in various planetary atmospheres provides clues on the tectonics and outgassing histories of the planets and the comparision of primordial noble gases (^{20}Ne, ^{36}Ar, ^{84}Kr, ^{132}Xe) in the planetary atmospheres provides clues on the quantities of volatile rich materials captured by each of the planet. Finally the absolute amount of degassed Co_2 of a planet provides clues regarding the quantity of noble gases (primordial) that accreted to planets in form of carbonaceous chondrites, the host for the primordial noble gases (6). A comparision of the noble gases (primordial) contents of Mars, Earth and Venus clearly shows that their absolute abundances of gases (^{36}Ar, ^{20}Ne etc.) are intimately related to the amounts of degassed Co_2 into planets atmospheres.

^{36}Ar was found to be about 75 times more abundant (Table-I) in the Venus atmosphere than in the Earth's atmosphere and Mars is depleted in ^{36}Ar content by a comparable factor relative to the Earth (Table-I). Surprisingly the pressures of degassed Co_2 are 90, 80 and 0.1 bars in the atmospheres of Venus, Earth (if all the Co_2 locked up in the sediments is put in the atmosphere) and Mars respectively.

The greater the amount of degassed CO_2 the greater will be the amount of ^{36}Ar in the atmosphere of the planet. This model also can explain the 200 times more ^{4}He in the atmosphere of Venus than that in the Earth's atmosphere. This may also probably indicate that no significant quantities of ^{4}He escaped from the Venus atmosphere.

The successive accretion model for the formation of the planets can explain the nearly constant $^{20}Ne/^{36}Ar$ ratio (4) (Mars, Earth and Venus) and also accounts for the $^{36}Ar/^{132}Xe$ variation (see table-I) taking into account the Xe locked up (5) in the Earth's sedimentary rocks and Mar's regolith. This ratio $^{36}Ar/^{132}Xe$ is an indicator of interactions between Xe and water formed terrestrial rocks of a planet.

The ^{40}Ar content of Venus is only four times less than than of the Earth indicating that degassing history of Venus (inspite of single plate, water poor mantle and slightly smaller size) is some what similar to that of the Earth. Similarly the atmosphere of Mars compared to the Earth and Venus is diffi-cient in ^{40}Ar due to small mass and paucity of K-rich material.

This paper maintains that the quantities of primordial noble gases that were captured into the outer layers of the terrestrial planets were controlled by the sizes and masses of the planets and the successive accretion model proposed by the author can explain the key trends (several orders of magnitude increase in ^{20}Ne and ^{36}Ar from Mars to Earth to Venus and a constant $^{20}Ne/^{36}Ar$) in the primordial noble gas contents of the planetary atmospheres.

REFERENCES

1) Rao,A.S.P.(1967) Meteorites and geochemistry (Abstr). In 30th Annual meeting of the meteoritical Soc.,California, p.130.
2) Rao,A.S.P. (1984) Varying densities of terrestrial planets (Abst) In Lunar planet Sci., Abs.XV, p.663-64, L.P.I.,Houston.
3) Rao,A.S.P.(1982) Volatiles as invaluable clues to planeto-genesis (Abst). In Conf. on planetary Volatiles, p.85-86, Alexandria.
4) Pollack, J.B. and Black,D.C.(1982) Icarus 51, 69-198.
5) Fanala,F.P. and Cannon,W.A.(1971) Earth Planet.Sci.Lett. 11, pp.362-368.
6) Lewis,R.S., Gros,J. and Anders,E. (1977) J.Geophy.,Res.82, pp.779-792.

TABLE-I*

Absolute Abundance of ^{36}Ar (g/g) and Nuclide Ratios of Noble Gases in Planetary Atmospheres and Extraterrestrial Samples (4)

Object	^{36}Ar	$^{36}Ar/C$	$^{20}Ne/^{36}Ar$	$^{36}Ar/^{84}Kr$	$^{36}Ar/^{132}Xe$
Venus	2.5×10^{-9} ($\pm$0.3)	9.4×10^{-5} ($\pm$1)	0.15[b] ($\pm$0.04)	50-1200	>3000
Earth	3.5×10^{-11} ($\pm$0.003)	1.3×10^{-6} ($\pm$0.6)	0.57 ($\pm$0.003)	48 ($\pm$0.5)	1300[c] ($\pm$15)
Mars	2.1×10^{-13} ($\pm$0.6)	4.1×10^{-7} (1— 20)	0.43 (0.15-1.0)	31 (10-90)	280 (100-900)
CCI	1.6×10^{-9}	5.0×10^{-8}	0.27	109	114
CCII	6.9×10^{-10}	2.8×10^{-8}	0.30	74	89
CCIII V	7.7×10^{-10}	1.4×10^{-7}	0.19	99	126
CCIII O	1.6×10^{-9}	2.9×10^{-7}	0.03	154	242
CC4	1.8×10^{-10}	1.3×10^{-7}	0		126
Ureilites	7.4×10^{-9}	2.5×10^{-7}	0.01	94	148
Aubrite	2×10^{-11} 2×10^{-9}		16	2300	17,000
E chondrite	1.5×10^{-11} 1.2×10^{-8}	4.2×10^{-9} 3.3×10^{-6}	0.003-0.2	64-450	70-2700
Lunar soil	5×10^{-7} 1.3×10^{-6}	10^{-2}	8 $\pm$ 3	1650 $\pm$ 500	10,500 $\pm$ 5000
"Brownlee" dust	8×10^{-8} ($\pm$0.5)		9 $\pm$ 3	125	500 $\pm$ 200
Sun	3×10^{-5}	4.8×10^{-2}	35	2500	25,000

* Table-II from reference (4) is partly reproduced.

CRATER EJECTA MORPHOLOGY AND THE PRESENCE OF WATER ON MARS; P. H. Schultz, Brown University, Department of Geological Sciences, Providence, Rhode Island 02912

Introduction: Various approaches have been used to establish the presence of buried ice or water on Mars. A popular and frequently referenced diagnosic indicator has been the multi-lobed or rampart-bordered martian ejecta facies (1,2,3 among others). The implicit premise has been that fluidized ejecta facies indicates the presence of water; in fact, fluidized ejecta only indicate fluid-like emplacement. Laboratory experiments (4,5) have shown that rampart-bordered ejecta facies and ejecta flow lobes can develop without the presence of water. These results do not disprove the notion that subsurface water/ice exists but reveal the non-uniqueness in interpretations owing to a variety of controlling variables. The purpose of this contribution is to review the possible effects of projectile, target, and environment on the cratering process.

Atmospheric Effects: Laboratory experiments performed at the NASA-Ames Vertical Gun Range (AVGR) have documented the effects of an atmosphere on ejecta emplacement at small scales. For vertical impacts into compacted pumice, a systematic change in ejecta morphologies is observed with increasing atmospheric pressure (4,5): vacuum-like ($P_0 < 0.05\ P_0$); contiguous rampart (0.1-0.3 P_0); multiple flow lobe (0.3-0.6 P_0); and radially scoured (0.7-1.0 P_0). These changes are accompanied by an increasingly distorted ejecta curtain and the development of a basal ejecta flow.

Further studies reveal the effects of atmospheric density impact velocity, and *in-situ* ejecta size. Reduced atmospheric density (He) still results in rampart-bordered ejecta facies in the appropriate pressure range (0.1-0.3 P_0) without significant distortion of the ejecta curtain. Impact velocity (from 0.03 km/s to 6.5 km/s) has little effect on ejecta morphology; therefore, ejecta curtain modification and the distinctive ejecta patterns reflect late-stage processes, decoupled from early-time impact velocity effects. An important variable, however, is the average *in-situ* grain size in the target. A shift in the modal grain size from 50 μ to 100μ also changes the onset of characteristic ejecta patterns to larger atmospheric pressures. A modest amount of fine-grained material (20% pumice) with coarser grained No. 24 sand, however, results in rampart-bordered ejecta facies at 1 P_0.

This brief summary indicates that Mars-like ejecta facies can be produced in the laboratory without the presence of water and principally depends on atmospheric pressure and ejecta size. The dynamic process responsible for the ejecta patterns has been revealed through stereo-photography and 1/4-space experiments wherein airflow patterns are revealed by splitting the evolving ejecta curtain in half. As summarized elsewhere (5,6), the outward movement of the wall of ejecta creates a partial vacuum within the crater cavity. At late-stages, this pressure difference results in a toroidal airflow that pursues the ejecta curtain. With increased atmospheric pressure, the relatively simple toroidal circulation breaks into tongues of air-ejecta. The process can be successfully scaled to much broader scales if the Froude number similitude is preserved and the Reynolds number is high enough (6).

Atmospheric pressure appears to establish the toroidal winds; air drag establishes limits on the size of ejecta that can be entrained. The latter effect requires that the combination of ejecta size, ejecta velocity, and drag coefficient must be properly simulated between the laboratory and martian conditions (8). If an impact-generated airflow is established but the ejection velocity is too low or ejecta size is too large, then ejecta emplacement will not be modified significantly. Such considerations indicate that at present atmospheric conditions, martian craters 5 km in diameter with a sufficient fraction (20%) of ejecta smaller than a few centimeters should result in craters with contiguous ramparts. Small craters do not result in sufficiently high ejecta velocities nor excavate (generate) sufficiently fine-grained ejecta. Larger craters or impacts into finer grained

substrates will result in multi-lobed or even radial facies. As crater size increases, however, the effects of atmosphere scale height and secondary cratering reduce the role of the atmosphere (6).

Effects of Volatiles: The possible effect of high water content on ejecta emplacement has been studied in the laboratory both directly (9) and indirectly (10). A difficulty in directly equating the presence of water with fluid-like ejecta flow is the fate of ballistic water in the martian atmosphere. The low velocities (cm/s) for near-rim ejecta in the laboratory preserve the splosh-like behavior, whereas the high-velocities (50 m/s) for ejecta around a 5 km-diameter martian crater result in aerodynamic dispersal and atomization. During ballistic ejection, the distinction between drag-decelerated ejecta and drag-decelerated atomized water becomes less apparent. During emplacement, the inner near-rim lobe may reveal the effects of decreased viscosity due to the presence of water, whereas the outer facies records a more complex behavior reflecting atmospheric interactions and air entrainment (8,11).

Recent laboratory experiments have explored the possible effects of impact-induced vaporization by using powdered dry-ice on the surface at the point of impact (7,12). High-frame-rate photography (8,000-35,000 fps) reveals enhanced vaporization and ionization in the presence of an atmosphere or for oblique impacts. Early-time (< 10% completion) modification of the ejecta curtain does not persist to late time, and contiguous ramparts are produced. This is primarily because impact-induced vapor is jetted vertically and expands. The expanding vapor cloud scours the pre-impact surface well in advance of the ejecta plume. Although decoupled from the plume, the presence of the dry-ice resulted in a decreased ejection angle during the early stages of crater growth. Burial of the dry-ice has little effect on ejecta emplacement and does not result in a two component curtain as suggested in (13).

Discussion: For a given size crater between 5 and 20 km in diameter, a relatively contiguous rampart-bordered ejecta facies is believed to reflect the presence of relatively coarse ejecta sizes. Multiple rampart-bordered ejecta lobes around craters of the same given size reflect an increased fraction of smaller ejecta. Strong radial grooves indicate an even greater contribution by smaller ejecta. This sequence from contiguous rampart to multiple rampart to radial grooves reflects the increased entrainment of ejecta in the recovery airflow pattern created by the advancing ejecta curtain. The different emplacement styles correspond to a factor of 10-20 in ejecta size. Transitions from one ejecta emplacement style to another also can be produced by different atmospheric pressure, thereby perhaps accounting for craters of identical size but different ejecta morphologies only 50 km apart on the same geologic unit. It is important to note that the possible range in atmospheric pressures due to time variations (factor of 5) or to elevation (factor of 7) is small compared with the potential range range in target-controlled ejecta sizes. Because the effect of such variations is reflected in shifts in ejecta emplacement styles with crater size, a given region still may exhibit the same range in ejecta morphologies. Ejecta size is controlled by *in-situ* particle size and impact-induced comminution. The former control reflects local geologic history; the latter reflects processes including effects of impact velocity, total impact energy, and target-entrapped volatiles.

This discussion suggests that contradictions in interpreting martian crater ejecta morphologies reflect oversimplifying the process as a singular consequence of buried water. It seems entirely possible that most ejecta facies could be produced without the presence of liquid water. However, the combination of extraordinary ejecta fluidity, absence of secondaries, and high ejection angles all would point to the combined effects of atmosphere and fluid-rich substrates (11). Moreover, recent experiments revealing the broad scour zone associated with rapid vapor expansion may account for numerous craters in the circum-polar regions with subtle radial grooving extending 10 crater radii away with faint

distal ramparts. Thus certain crater ejecta morphologies may yet provide fundamental clues for the presence of unbound water.

References: 1) Johansen, L.A. (1979) NASA TM 80339, 123-125; 2) Masursky, H. (1982) In the *The New Solar System* (J.K. Beatty, *et al.*, eds), p. 90; 3) Horner, V.M. and Greeley, R. (1986) *Lunar and Planetary Science XVII*, 358-359, LPI, Houston; 4) Schultz, P.H. and Gault, D.E. (1981) *Third International Colloq. on Mars, LPI Contrib. 441*, p. 226-228; 5) Schultz, P.H. and Gault, D.E. (1984) *Lunar and Planetary Science XV*, 732-733, LPI, Houston; 6) Schultz, P.H. and Gault, D.E. (1982) *Geol. Soc. Sp. Paper 190* (L.T. Silver and P.H. Schultz, eds), p. 153-174; 7) Schultz, P.H. and Gault, D.E. (1986) *Lunar and Planetary Science XVII*, 779-780, LPI, Houston; 8) Schultz, P.H. and Gault, D.E. (1979) *J. Geophys. Res. 84*, 7669-7687; 10) Wohletz, K. and Sheridan, M. (1983) *Icarus 56*, 15-37; 11) Schultz, P.H. and Singer, S. (1980) *Proc. Lunar and Planetary Science XI*, 2243-2259; 12) Schultz, P.H. and Gault, D.E. (1985) *Lunar and Planetary Science XVI*, 740-741, LPI, Houston; 13) Mouginis-Mark, P. (1981) *Icarus 45*, 60-76.

PHOBOS AND DEIMOS: A BASE FOR SAMPLING THE MARTIAN PAST; S.F. Singer, George Mason University, Fairfax, VA 22030

The Martian satellites are of unique interest: as platforms for detailed Mars exploration and for later Mars habitation, as low-cost accessible sources of materials for propellants and construction, and as objects of intrinsic scientific value. Their origin is a mystery---whether captured or formed in place, perhaps remnants of an original larger body, or perhaps unmodified examples of primitive planetesimals.

A manned Ph.D. mission can accomplish the scientific and resource objectives sooner and at lower cost than either a long series of unmanned missions directed from the Earth or a series of manned landings on the Martian surface. The Ph.D. mission can direct a series of unmanned rover vehicles to all parts of the surface and recover samples, including cores, for analysis in a Deimos-based laboratory. This sequential experimentation permits exploration of the most promising, and perhaps most difficult, terrain for a study of the geologic, climatic, and possibly biologic history of the planet Mars. Data on past climates could shed light on climate processes on the Earth. It is widely believed that Mars was initially wet and warm, providing an environment suitable for the development of life forms. The discovery of fossil life or cryptolife would represent a major scientific achievement.

The Ph.D. mission promises to be no more difficult or costly than proposed manned missions to the Moon or to earth-crossing asteroids. To fit into an early timeframe, it would use chemical propulsion plus aerobraking, but would build on the experience of the U.S. and Soviet space stations to deal with the habitat and zero-g problems of a 2-year round trip.

MARS GLOBAL ATMOSPHERIC OSCILLATIONS:TRANSIENTS AND DUST STORM RELATIONS JAMES E. TILLMAN, Viking Computer Facility, Dept. of Atmos. Sci., AK-40 University of Washington, Seattle, WA 98195

The existence of transient global oscillations in the atmosphere of Mars was first reported by Tillman in 1981 at the Third International Mars Colloquium, Pasadena Calif Aug. 30 to Sept 2, 1981 and published by Tillman 1984. At these presentations, the transient events were associated with global dust due to their diurnal and semi-diurnal variations, the latter indicating relatively deep dust distributions. One problem with this interpretation is that the events decay in a few sols, an uncharacteristically short time for deep, global scale dust storms. It was also mentioned that their characteristics, taken with those of the surrounding diurnal harmonics, might be related to the presence or absence of global dust storms later in the winter of a given year.

Hamilton and Garcia, 1986, describe the existence of short period normal mode oscillations in the Earth's Atmosphere with periods of from 7 to 50 hours. These include many different modes of interaction, direction of propigation and global symmetry. They also predict the frequency of oscillation for three different types of modes for Mars. Of these, Two Kelvin modes with periods of 23.2 and 11.9 hours may explain many of the characteristics of the transient events. Since the calculated frequencies are very close to that of the diurnal and semi-diurnal, and the events are only a few cycles long and highly non-stationary, it is difficult to distinguish between the Kelvin and solar heated dust oscillations by a casual examination of the pressure traces. However, initial analysis indicates that the periods may not be harmonics of a sol and may be global Kelvin waves. Alternatively, on the basis of frequency alone, gravity and gravity-Rossby waves may be responsible for the oscillations.

An important characteristic of the global storms is that in the case of the 1977 A storm, the buildup occurred in about two sols, Tillman, 1984, and the 1977 B storm reached its maximum in about 7 sols. Examination of the pressure data during the buildup indicates that the period of the apparently diurnal and semi-diurnal oscillations may deviate from an exact harmonic during the buildup while remaining close to a harmonic during the many tens of sols of the storm. If confirmed by more detailed analysis, this would mean that the major dust storms are initially triggered by global oscillations which are then followed by solar-heated, dust induced tides. Details of these analyses will be discussed along with speculations about the relation of such global oscillations to the presence or absence of dust storms.

References:

(1) Tillman, James E., Martian Meteorology and Dust Storms from Viking Observations, Case for Mars II Conference, July 10 -14, Boulder, Colo., 1984 and published in Case for Mars II, V 62, Science and Technology, American Astronautical Society, ed. Christopher P. McKay, 333-342, 1985.

(2) Hamilton, Kevin and Rolando R. Garcia, Theory and Observations of the Short Period Normal Mode Oscillations of the Atmosphere, submitted, J. Geophys. Res., 1986.

VERTICAL O_3 DISTRIBUTION AS A DIAGNOSTIC FOR EDDY DIFFUSION PROFILE; A. L. Tyler and D. M. Hunten, Lunar and Planetary Laboratory, the University of Arizona

This paper illustrates the dependence of the vertical distribution of O_3 on the height variation of eddy diffusion coefficient. O_3 abundance is a valuable diagnostic for other climatological parameters. In addition, the sensitivity of O_3 distribution to eddy diffusion may aid in determining the role of surface oxidation and recombination processes and lead to a better understanding of the volatiles released or adsorbed cyclically in the Martian regolith.

In spite of rapid photolysis of the predominantly CO_2 Martian atmosphere by solar UV, observations of CO and O_2 near the surface indicate these constituents have mixing ratios less than 0.1% (1). The rate of production of CO and O is exactly the rate of CO_2 photolysis, and because the 3-body recombination reaction:

$$CO + O + M \rightarrow CO_2 + M$$

is negligibly slow, most O atoms are instead converted to O_2 by:

$$O + O + M \rightarrow O_2 + M$$

If no other recombination process were operating, the observed 0.1% would be produced in less than five years. Much effort has been spent attempting to explain the stability of the minor constituents against rapid increase by UV photolysis of CO_2.

Common to all current Mars aeronomy models explaining this phenomenon is that CO_2 is reformed from CO by odd hydrogen photochemistry via the reaction:

$$CO + OH \rightarrow CO_2 + H$$

Extensive modelling has shown that various combinations of rapid downward transport of photolysis products to the region of recombination below 20 km and odd hydrogen catalysis recycling CO and O_2 to CO_2 in the presence of enhanced H_2O_2 can fit the limited observational constraints (2-5).

None of the constituents of major aeronomical interest (O_2, CO, H_2O, H_2O_2, O_3) have been measured in-situ in the lower atmosphere. It has been necessary to make assumptions about the vertical profiles of these

necessary to make assumptions about the vertical profiles of these constituents and the eddy diffusion coefficient. The figure illustrates these points with three computed profiles (7) of eddy coefficients and the corresponding ozone distribution. Additional calculations are in progress.

Vertical O_3 Distribution as a Function of Height Variation in Eddy Diffusion Coefficients (K_Z)

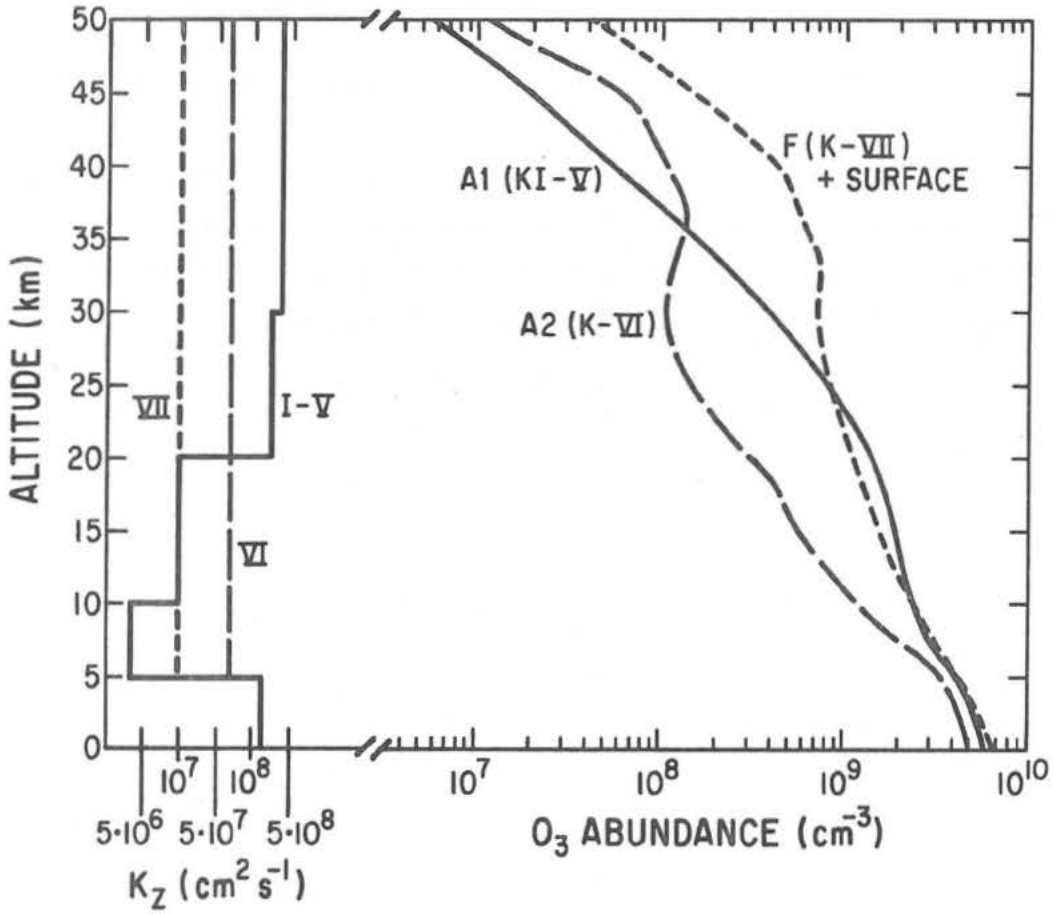

O_3 profiles computed by Kong and McElroy (6) are plotted on the right side of the figure and correspond to the respective eddy diffusion profiles at the left.

VERTICAL O_3 DISTRIBUTION

Tyler, A. L.

Simultaneous measurements of pressure, temperature and vertical profiles of H_2O vapor, O_3, CO, and O_2 are needed before atmospheric processes can be well understood. In particular, a stellar occultation experiment which provides a high resolution vertical profile of H_2O in absorption and a dayglow limb emission detector to measure the 1.27 μm emission of $O_2(^1\Delta_g)$, the photolysis product of O_3, can provide direct evidence for the magnitude of the vertical profile of the eddy diffusion coefficient. The payload chosen for Mars Observer will not make all these measurements but a future opportunity (Mars Aeronomy Observer) is likely.

(1) U. von Zahn and D. M. Hunten (1982) Proc. 'The Planet Mars', Leeds, (ESA SP-185) 37-45.

(2) T. D. Parkinson and D. M. Hunten (1972) J. Atmos. Sci., 29, 1380-1390.

(3) D. M. Hunten (1974) Rev. of Geophys. Space Phys., 12, 529-535.

(4) M. B McElroy and T. M. Donahue (1972) Science 177, 986-988.

(5) M. B. McElroy and J. C. McConnell (1971) J. Atmos. Sci., 28, 879-884.

(6) T. Y. Kong and M. B. McElroy (1977) Icarus 32, 168-189.

WATER ON MARS . H. Wänke and G. Dreibus, Max-Planck-Institut für Chemie, Saarstrasse 23, D-6500 Mainz, F.R.Germany.

With the assumption that the SNC-meteorites are indeed Martian rocks, these meteorites allow very definite conclusions about the bulk composition of Mars. Figs. 1 and 2 show correlations of the moderately volatile K and of the volatile Br with the refractory element La. As to a first approximation one can assume C 1-abundances for the refractory elements for all terrestrial planets, these correlations clearly indicate higher abundances of moderately volatile and volatile elements on Mars as compared to the Earth. In the case of Br, the difference may actually be smaller as on the Earth the oceans represent such an ideal reservoir for Cl and Br that today the major portions of the whole terrestrial inventory of Cl and Br reside in the oceans.

According to the two component model for the formation of terrestrial planets as introduced by Ringwood (1,2) and slightly modified by Wänke (3), the composition of these planets can successfully be described as mixtures of:
Component A: Highly reduced and free of all elements with equal or higher volatility than Na, but containing all other elements in C 1-abundance ratios.Fe and all siderophile elements and even Si partly in metallic form. And
Component B: Oxidized and containing all elements - including the volatiles - in C 1-abundances. Fe, all siderophile and lithophile elements as oxides.

From the analytical data of SNC-meteorites (4,5), Dreibus and Wänke (6,7) concluded that the mixing ratio of component A/component B for Mars is 60:40, compared to a ratio of 85:15 for the Earth. They further concluded that Mars accreted almost homogeneously contrary to the inhomogeneous accretion of the Earth, as proposed by Jagoutz et al. (8) and in more detail by Wänke (3).

On Mars because of the homogeneous accretion almost all H_2O added (from component B) reacted with metallic Fe (and, of course, with other metallic phases like Si of component A) and was reduced to H_2 which escaped. The huge quantities of H_2 will not only have greatly accelerated the extraction of gaseous species from the interior of the planet but also have furthered the removal of these species from the gravity field of the planet due to hydrodynamic escape by keeping the mean molecular weight of the atmosphere low. Hence, in their estimate of the amount of H_2O left on Mars after accretion, Dreibus

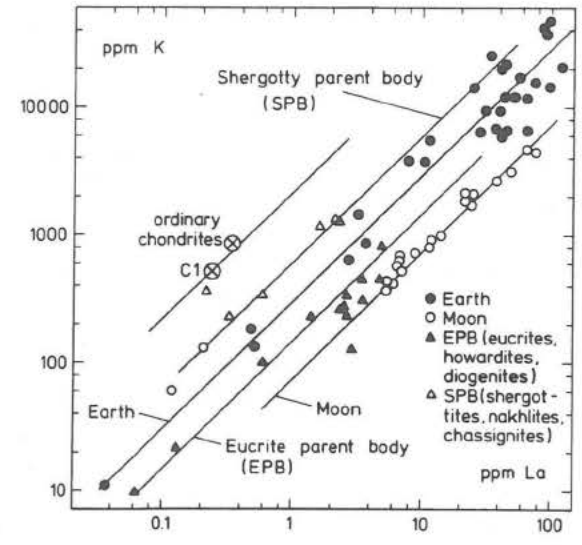

Fig. 1

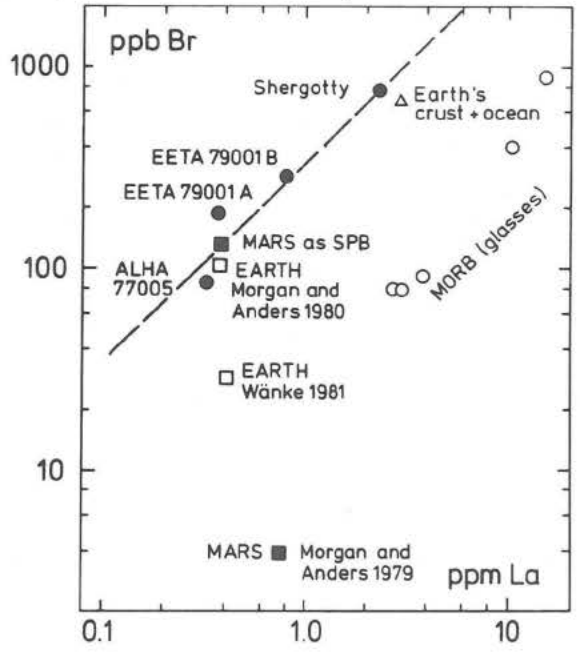

Fig. 2

Morgan and Anders, 1979 (19); Morgan and Anders, 1980 (20); Wänke, 1981 (3)

and Wänke (7) assumed that at the end of accretion the concentration of H_2O and other volatiles at the surface of the planet was zero. From the Br/La concentration (Fig. 2), they could calculate the absolute amounts of Cl, Br and I on Mars using C 1-abundance ratios of Cl/Br and I/Br. In this way, they found for Mars an absolute Cl concentration of 34 ppm. Assuming the composition of component B to be identical to that of C 1-meteorites, 320 ppm Cl were actually added to the planet, of which all except the 34 ppm was lost during the accretion process together with H_2 and other gases, yielding a depletion factor for Cl of 0.11.

During accretion even the relatively small Mars was heated to temperatures which probably led to partial melting of the silicates (9). Nevertheless we have to expect that the solid or liquid phases of the planets' interior were in solubility equilibrium with the temporary atmosphere during the accretion process. The solubility of HCl in basaltic melts exceeds that of H_2O by about a factor of 200 (10), yielding for H_2O a depletion factor of 0.11:200 = 5.5×10^{-4}. C 1-chondrites contain about 20% H_2O, however, the preterrestrial H_2O content is only 4.5% (11), the rest is mainly terrestrial contamination. Hence, in order to find the composition of component B which we assume to be identical to C 1-chondrites, we devide the C 1-values by 0.85. During accretion the hydrogen of the hydrocarbons of the C 1-material will at an intermediate stage also be present in form of H_2O. For the following, we will therefore use a C 1-concentration of 7.1% H_2O as deduced from the H abundance of 7900 ppm (12). With this value we find that 3.3 % H_2O was added to Mars during accretion. Together with the depletion factor of 5.5×10^{-4}, we find that a total of 18 ppm H_2O was retained in the interior of the planet corresponding to 23 ppm H_2O in the mantle. Making the unrealistic assumption of a 100% release, this would yield a water layer of 80 m covering the whole planet.

From SNC-meteorites a value of 247 ppm K for bulk Mars is obtained (6,7), leading to a total of $1840 \times 10^{-8} cm^3/g$ ^{40}Ar produced in 4.5×10^9 years. The observed amount of ^{40}Ar in the Martian atmosphere corresponds to $48 \times 10^{-8} cm^3/g$. Hence, if we neglect a possible loss of ^{40}Ar from the atmosphere into space, we find a release factor for ^{40}Ar of 0.026. Assuming the release factor of H_2O to be identical to that of ^{40}Ar, we derive at a water layer of 2.1 m or a total of 0.3×10^6 km^3. The low ^{40}Ar concentration in the Martian atmosphere leading to the very low release factor may be in part due to removal of ^{40}Ar from the atmosphere by energetic impacts in geologic time (13). Hence the release factor would in fact be higher than 0.026 and consequently the amount of water at the surface of Mars would become higher, too.

The assumptions made above may not be as unrealistic as they might sound at first sight. Because of the even smaller Cl abundance on Earth compared to Mars only a small fraction of the total H_2O of the Earth could be explained in this way. However, the Earth probably accreted inhomogeneously. According to the model of Wänke (3), the accretion of the Earth started with the highly reduced and volatile-free material of component A. After the Earth had reached about 60% of its present mass more and more of the oxidized component B was added. However small amounts of metal still present were responsible for the extraction of highly siderophile elements (Ir, etc.).Towards the very end of accretion metal became unstable, hence, even the highly siderophiles remained in the mantle in their C 1-abundance ratios. The concentration of 2.8 ppb Ir in the Earth's mantle equal to 1.9 ppb Ir for the whole Earth, corresponds to 0.39% C 1-material. With a C 1 H_2O content of 7.1%, we find that 280 ppm H_2O were added to the Earth after metallic iron respectively Ni became unstable. These 280 ppm remained in form of water while of the much larger amounts of the water ($\sim$ 1%) added before metal became unstable almost all was converted

Wänke, H. and Dreibus, G.

to H_2. Hence, we would expect a total H_2O content of the Earth of about 300 ppm. The contribution of the crust (mainly the oceans) to the bulk Earth H_2O content is already close to 300 ppm so that very little would remain for the contribution of the mantle. However it seems likely that this contribution is indeed much smaller as generally assumed. Of the total halogen inventory of the Earth more than 90% were found to be concentrated in the crust. A similar distribution is expected for water.

The large amounts of H_2 generated during accretion may have removed most of the primordial rare gases delivered by component B so that even these gases were contributed predominantly by the 0.39% C 1-material added at the very end of accretion. The 0.39% C 1-material would bring 0.29 x 10^{-10}cm^3/g ^{132}Xe to the bulk Earth compared to 0.16 x 10^{-10}cm^3/g ^{132}Xe present in the atmosphere. Most of the Earth's ^{132}Xe inventory is certainly in the atmosphere, nevertheless a surprisingly good agreement, considering the large uncertainties in our exercise. In the case of ^{36}Ar only 16% of the 210 x 10^{-10}cm^3/g ^{36}Ar in the Earth atmosphere could be derived by 0.39% C 1-material. However we have the strong suspicion that in respect to rare gases the C 1-chondrites of today do not represent the material actually added at the accretion stage of the terrestrial planets. As about 90% of the radiogenic ^{40}Ar produced during the 4.5 x 10^9 yrs was obviously lost from C 1-chondrites by diffusion a similar loss of ^{36}Ar may be inferred. Preferential diffusion loss of Ne, Ar, and Kr relative to Xe would also explain the striking difference of Kr/Xe-ratios in Earth and Mars as compared to that in C 1-chondrites (Fig. 3). In this way, the "Xe problem" might be solved (14-18).

Ref.: (1) Ringwood A.E. (1977) Geochem. J. 11, 111. (2) Ringwood A.E. (1979) On the origin of the Earth and Moon, Springer, N.Y. (3) Wänke H. (1981) Phil. Trans.R.Soc. Lond. A303, 287. (4) Burghele A. et al. (1983) LPS-XIV, 80. (5) Laul J.C. et al. (1985) LPS-XVI, Supp. A, 17. (6) Dreibus G. and Wänke H. (1984) 27th In. Geol. Con. Vol.11, VNU Sci. Press, 1. (7) Dreibus G. and Wänke H. (1985) Meteoritics 20, 367.(8) Jagoutz E. et al. (1979) LPSC-10th, 2031. (9) Kaula W.M. (1979) JGR 84, 999. (10) Anderson A.T. (1975) Rev. Geophys. Space Phys. 13, 37. (11) Kaplan I.R. (1971) in Handbook of Elemental Abundances in Meteorites. B. Mason (ed), 21, Gordon. (12) Anders E. and Owen T. (1977) Science 198, 453. (13) Watkins H. and Lewis J.S. (1984) Workshop on Water on Mars, LPI Tech, Rep. 85-03, p. 93. (14) Canalas R. A. et al. (1968) JGR 73, 3331. (15) Fanale F.P. and Cannon W.A. (1971) EPSL 11, 362. (16) Bernatowicz T.J. and Podosek F.A. (1978) in Terr. Rare Gases, E.C. Alexander & M. Ozima (eds) 99. (17) Podosek F.A. et al. (1980) GCA 44, 1875. (18) Wacker J.F. and Anders E. (1984) GCA 48, 2373. (19) Morgan J.W. and Anders E. (1979) GCA 43, 1601. (20) Morgan J.W. and Anders E (1980) Proc. Natl. Acad. Sci., USA, Vol. 7, No. 12, Geophys. 6973.

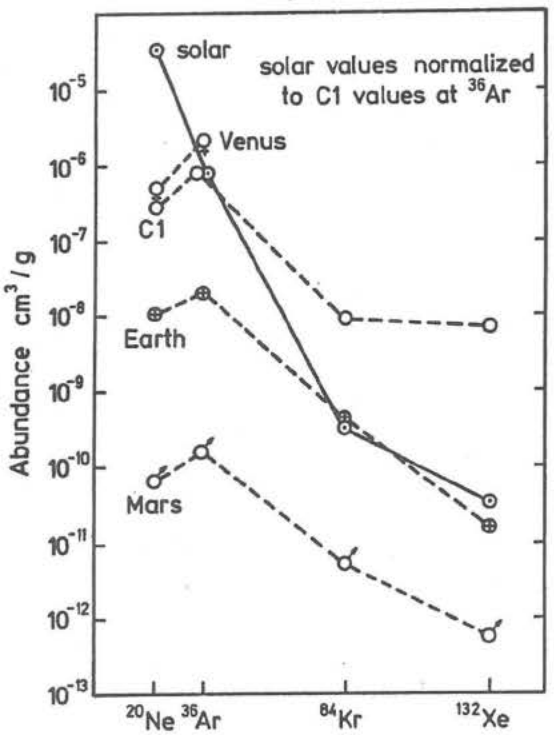

(Fig. 3)

MARS REGOLITH VERSUS SNC METEORITES: EVIDENCE FOR ABUNDANT CRUSTAL CARBONATES?

Paul H. Warren
Institute of Geophysics, University of California, Los Angeles, CA 90024

The 1.3 Ga old SNC (shergottites, nakhlites, and Chassigny) igneous meteorites are widely believed to come from Mars [1-3], problems with spalling large, little-shocked rocks off a Mars-sized planet notwithstanding. Although Clark [4] noted that Viking XRF analyses indicate that the martian regolith is remarkably similar to shergottites, he also noted that Ca contents are far lower in the regolith. Indeed, irrespective of the provenance of SNC's, the low Ca/Si ratios of the martian soils require an explanation. Fig. 1 shows Mg/Fe vs. Ca/Si for SNC's and for the composition that Clark [4] derived to be representative of the regolith at both landing sites, based on averaged data for deep, loose fines [7] (analyses of shallow "duricrust" samples are scarcely different). Mg/Fe is used instead of Mg/(Mg+Fe) in order to facilitate interpretations of error bars and possible mixing lines. Fig. 1 shows error bars derived, conservatively, by simply summing the errors estimated by Clark [4]. Viking data are imprecise for most elements, but among 16 analyses reported from two sites [7], Ca/Si ranged from 0.192 to 0.213. The correlation among SNC meteorites on Fig. 1 indicates that all SNC meteorites with low Mg/Fe have high Ca/Si relative to the martian regolith.

Clark's [4] main conclusion was that the Viking geochemical evidence is consistent with the hypothesis that SNC meteorites come from Mars. He addressed the Ca/Si disparity only briefly, as follows: "Calculations show mineralogic starting composition can be similar if pigeonite increases at the expense of augite (constant total pyroxene). The inferred composition is then consistent with all 10 measured elements (Mg, Al, Si, K, Ca, Ti, Fe, Sr, Y, Zr) bearing on this question. An alternative explanation for Ca-deficiency is chemical weathering to produce insoluble sulfate deposits." Clark [4] is justified in doubting that the SNC's are entirely representative. Their young ages suggest that they come from the northern hemisphere, which (including both Viking sites) is dominated by relatively young volcanic plains, whereas the heavily cratered highlands that comprise the remaining 60% of the surface are 3-4 Ga old. The upper regolith is probably well mixed on a global scale by dust storms. The highlands have obviously been exposed to weathering longer; and a key weathering mechanism on early Mars may have been hydrothermal alteration of impact melts, mainly in the heavily cratered highlands [8]. Thus, the fines analyzed by Viking may comprise more material ultimately derived from the ancient highlands than from young volcanic terrains — and the highlands may be altogether different from the young volcanic terrain that putatively supplied the SNC meteorites.

However, there remain limits to the compositions that can plausibly be invoked for the unsampled crust. Assume, for the sake of argument, that the regolith materials analyzed by Viking were derived without secondary fractionation (such as differential chemical weathering; or concentration of certain elements into sedimentary rocks) from the igneous crust. It should be possible to estimate the composition of the "missing" crust (= southern highlands?) by simple mass-balance calculations. Such calculations imply that the Ca/Si ratio for the "missing" crust must be low (<0.20), whether "H" (the fraction of the Viking regolith assumed to come from the "missing" crust) = 1% or 99%, because even an average SNC meteorite has a higher Ca/Si ratio than the regolith. Likewise, because the Viking composition is so extremely rich in Fe relative to Si, any reasonable assumption about H leads to a "missing" crust composition that is Fe-rich, with molar (Fe+Mg)/Si = 0.3-0.5.

A Ca/Si ratio of less than 0.20 does not appear realistic for any major fraction of the martian igneous crust. As illustrated by Fig. 2, not only SNC meteorites, but igneous rocks from Earth, its Moon, and the parent asteroid of the eucrite meteorites — igneous rocks from all these sources, seldom have Ca/Si <0.2, except for granitic types with molar (Fe+Mg)/Si <0.3, or else ultramafic types with molar (Fe+Mg)/Si >1.2.

MARS REGOLITH - SNC'S = CARBONATES?

Warren, P. H.

In terms of Ca/Si, the crust of Mars is presumably at least comparable to the crusts of the Moon and the Earth. Yield of crustal Ca-feldspar from planetary differentiation is probably a function mainly of: (a) pressures that prevail in the outer few hundred km of the planet, because high pressures stabilize garnet and other phases that compete with feldspar for Ca and Al; and (b) availability of Na and K, which compete with Ca for whatever crustal Al is available. In terms of internal pressures Mars is intermediate between Earth and its Moon. SNC meteorites are also intermediate in terms of crustal Na and K [2]. Thus, barring an incredibly Ca-poor highlands, the fines analyzed by Viking cannot be derived from the igneous crust without secondary (post-igneous) Ca/Si fractionation.

Secondary Ca/Si fractionation might develop as a result of differential chemical weathering leaving rinds of Ca-rich material covering exposed igneous rocks; as a result of deposition of Ca-enriched sedimentary rocks; or both. Aside from Clark's [4] brief suggestion of "insoluble Ca-sulfate deposits," Gooding (pers. comm., 1986) has suggested that Ca/Si fractionation occurs because igneous rocks weather primarily into Ca-poor clay minerals. Weathering on Mars is of course poorly understood. Some studies [9, 10] suggest that major Ca-bearing minerals on Mars tend to weather into Ca- or Ca,Mg-carbonates, but atmospheric SO_2 may de-stabilizes surface carbonates [11]. A problem with any differential weathering model is that physical weathering tends to convert all weathering products into fines. Consider first the Ca-rich weathering rind hypothesis. Based on landform degradation rates, the rate of aeolian erosion during recent martian history has been estimated [12] to be of the order 1-100 m Ga^{-1}. Physical weathering by heating/cooling cycles may be particularly effective on Mars, where the soil surface temperature varies by about 90 K every 25 hours [9, 13]. Attempts to scrape material from Mars rocks showed the surfaces to be strong and scratch-resistant [14]. Barring the remote possibility that chemical weathering on Mars races ahead of physical weathering (i.e., chemical weathering has produced far more rind material than has been mobilized by physical weathering), rind models cannot plausibly account for the low Ca/Si ratios of the Viking soil analyses.

Another type of differential weathering model would be to sequester Ca-rich weathering products into different sediments from Ca-poor weathering products. Conceivably sorting by grain size and/or shape would tend to deposit the Ca-rich materials deeper than the Ca-poor materials, leading to a low Ca/Si ratio for the regolith. The question then arises, what could be the Ca-rich material? Clark and Van Hart [11] argue that sulfates in the martian crust must be mainly Mg-sulfate, not Ca-sulfate. The soils analyzed by Viking have remarkably high contents of SO_3, ranging from 5.9 to 9.5 wt% [7]. If crustal Ca were largely associated with sulfate, these soils should have high, not low, Ca/Si ratios. In fact, neither the Viking analyses [7] nor analyses of soil from the analogous Dry Valleys of Antarctica [15] manifest any correlation between Ca/Si and sulfate. If, on the other hand, the Ca carrier were a clay mineral, such as prehnite, it would probably not sort apart from the Ca-poor weathering products (presumably also clay minerals).

I suggest that the Ca "missing" from the Viking soils is sequestered as Ca-carbonate. Based on the Ca/Si disparity between the average Viking regolith composition and compositions of otherwise comparable igneous rocks, particularly Shergotty, Zagami, and EETA79001-B (Figs. 1-2), the mass of Ca sequestered into $CaCO_3$ is most likely roughly 3% of the mass of material that has been eroded off of igneous rocks, i.e., 3% of the combined total mass of regolith plus sedimentary rocks (assuming that Mars contains few igneous rocks formed by "recycling" of sedimentary rocks). Addition of CO_3 to the Ca implies that, by this reckoning, $CaCO_3$ amounts to roughly 8% of the combined total mass of regolith plus sedimentary rocks. In addition to $CaCO_3$, martian carbonates probably include minor $MgCO_3$ and comparatively negligible $FeCO_3$. Note that $MgCO_3$ fractionation would enhance the effect of $CaCO_3$ fractionation in terms of Fig. 1.

Other recent suggestions that abundant carbonates exist in the martian crust have

been motivated by considerations of the CO_2 budget [5,6]. The CO_2 in the atmosphere, the polar caps, and adsorbed onto surfaces of silicates in the regolith [16], combined does not seem to account for the total CO_2 that has been degassed since the origin of Mars. Kahn [5] also points out that the present surface atmospheric pressure of Mars, about 7 mbar, is close to the triple point of H_2O, 6.1 mbar. Liquid water facilitates carbonate formation, and Kahn suggests that the present mass of the martian atmosphere is buffered by liquid water. Kahn suggests that CO_2 occurs mainly in carbonates formed in the regolith in association with transitory pockets of liquid H_2O, melted by heat from solar insolation. However, on Mars solar insolation can only generate temperatures above 273 K in the upper few cm of the regolith (and only in low-lattitude, low-elevation regions), and high sulfate contents found in the regolith by Viking may be inconsistent with near-surface $CaCO_3$ [11].

An alternative model is that carbonates formed during an early stage of martian history by precipitating from open ponds of water. These ancient "limestones" and/or "marlstones" would be coherent, and would have formed mainly in areas of low elevation. The bulk of such formations could easily have since been buried by complementary, Ca-depleted material. Note that additional shallow carbonates might still form in association with Kahn's [5] transitory liquid water pockets. The key requirement is to segregate a considerable mass of Ca-carbonate apart from the homogeneous, wind-stirred upper regolith analyzed by the two Viking landers. Formation of the equivalent of a global shell of Ca-carbonate 20 m thick would suffice to remove 1000 mbar of CO_2 from the martian atmosphere. Carbonate formation may have irreversibly depleted what was once a far more massive CO_2-dominated atmosphere. Warming by the greenhouse effect from such an atmosphere may have once allowed liquid water to exist on Mars [5,6].

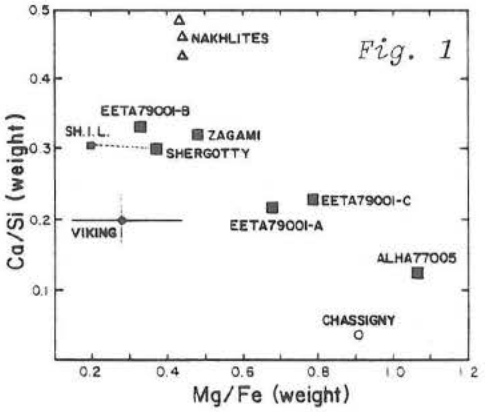

Fig. 1

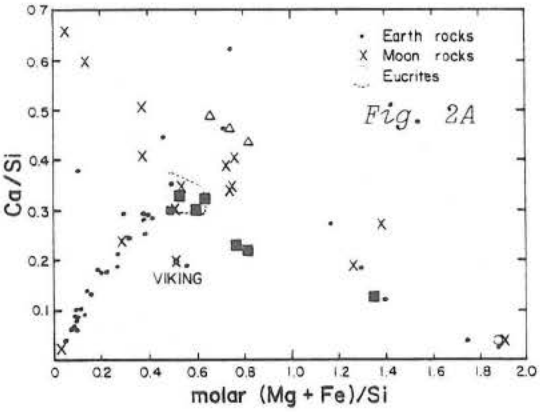

Fig. 2A

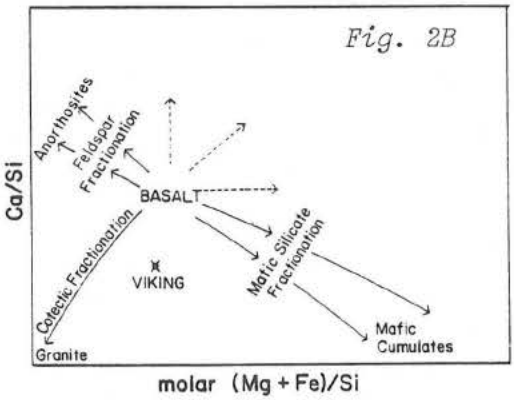

Fig. 2B

[1] Wood C. A. & Ashwal L. D. (1981) Proc. LPS Conf. 12, 1359. [2] Burghele A., et al. (1983) Lunar Plan. Sci. 14, 80. [3] McSween H. Y., Jr. (1985) Rev. Geoph. Sp. Phys. 23, 391. [4] Clark B. C. (1983) Lunar Plan. Sci. 14, 117. [5] Kahn R. (1985) Icarus 62, 175. [6] Haberle R. M. (1986) Nature 318, 599. [7] Clark B. C., et al. (1982) JGR 87, 10059. [8] Berkley J. L. & Drake M. J. (1981) Icarus 45, 231. [9] Gooding J. L. (1978) Icarus 33, 483. [10] Booth M. C. & Kieffer H. H. (1978) JGR 83, 1809. [11] Clark B. C. & Van Hart D. C. (1981) Icarus 45, 370. [12] Arvidson, R., et al. (1979) Nature 278, 533. [13] Gooding J. L. (1986) 207-229 in The Solar System (ed. Kivelson M.), Prentice. [14] Moore H. J., et al. (1979) JGR 84, 8365. [15] Gibson E. K., et al. (1983) JGR 88, A912. [16] Fanale F. P., et al. (1982) Icarus 50, 381.

ADSORPTION ON THE MARTIAN REGOLITH: SPECIFIC SURFACE AREA AND MISSING CO_2. Zent, A. P., F. P. Fanale and S. E. Postawko, Planetary Geosciences Division, Hawaii Institute of Geophysics, University of Hawaii, Honolulu, Hi. 96822

Estimates of the total amount of outgassed CO_2 on Mars range from 140 mbar to 3000 mbar (1, 2). Only 8 mbar is currently in the atmosphere, less than 10 has escaped to space (3), and no more than a few mbar are in the permanent south polar cap reservoir (4). In the absence of a recycling mechanism, the remainder must be stored in the regolith, either as carbonate rock or in the adsorbed state. Because the problem of maintaining liquid H_2O (necessary for sufficiently fast carbonate production) is formidable, we have examined the adsorptive behavior of Mauna Kea palagonites, a low temperature weathering product of basaltic glass and a good spectral and chemical analog for the Viking soils. We hope to improve estimates of the maximum CO_2 capacity of the regolith, and thereby constrain the amount of carbonate which is necessary to make up the difference.

CO_2 adsorption measurements have previously been obtained on ground basalt (5) and nontronite (6). We expanded this data set by measuring the adsorption of CO_2 on Mauna Kea palagonite at martian conditions of temperature and P_{CO_2}. Initial results have been reported elsewhere (7). The measured surface area of the palagonite was 59.06 $m^2\ g^{-1}$, while for the nontronite it was 47.0 $m^2\ g^{-1}$, and for the basalt 5.8 $m^2\ g^{-1}$. The adsorption isotherms, in terms of g of $CO_2\ g^{-1}$ of adsorbent, were divided by the specific surface area of each adsorbent to get the equation in terms of g of $CO_2\ m^{-2}$. Although on a gram per gram basis there is a two order of magnitude difference between the adsorptive capacity of the three minerals considered, the minerals differ by less than a factor of three on a gram per squre meter basis at martian conditions (Figure 1). For the purposes of this study, we assume that an equation can be written which describes CO_2 adsorption on any basalt or basaltic weathering product in terms of temperature, P_{CO_2} and the specific surface area of the material, without regard to mineralogy. The advantage of this is that while many guesses at the mineralogy of the martian regolith are available, at least one indirect measurement of the surface area of the martian regolith has been made (8).

We employed a least-squares fitting routine to find coefficients for the adsorption expression, and tested it's predictive ability against available adsorption data for all three mineralogies. The average error in the equation is on the order of 10%. The equation which describes CO_2 adsorption is

$$\rho_a = A_s \times \delta\ P^{\gamma}\ T^{\beta} \qquad (1)$$

where $\delta = 5.9629 \times 10^4$ g $CO_2\ m^{-2}$, $\gamma = 0.364391$, and $\beta = -3.83415$. A_s is the specific surface area of the material in m^2, and P is in mbar. The value of ρ_a is in g adsorbate / g adsorbent. Because available measurements indicate at specific surface area of approximately 17 $m^2\ g^{-1}$ (8), we can use equation (1) to move toward a point model of CO_2 adsorption on the martian regolith.

Fanale et al., (1982), (4), presented a model of the martian climate in which they considered regolith adsorption to be the primary CO_2 reservoir. They presented results based on two types of regolith mineralogy, basalt and nontronite, and described cap formation of atmospheric pressure as a function of obliquity. Because their model does not include any other CO_2 reservoir, it forms an implicit test of the ability of the regolith to store all of the necessary CO_2 in the adsorbed state. We have reconfigured the model, eliminating explicit assumptions of mineralogy, and substituting equation (1) for adsorption, with a specific surface area of $17 m^2\ g^{-1}$. We fixed orbital parameters at current values, and used the thermal constants presented in the original model (4). Our independent variables were the total CO_2 inventory (ΣCO_2), and the depth of the

regolith. Only a limited combination of these variables is compatible with the present atmospheric pressure(6.0 - 8.5 mbar), lack of permanent polar deposits of CO_2, and absence of carbontes (Figure 2).

Our results indicate that at least 450m of regolith, in diffusive contact with the atmosphere, are necessary to store the minimum CO_2 inventory of 140 mbar. Further, if the planetwide average depth of the accessible regolith is 1 km or less, then the maximum CO_2 inventory compatible with the absence of carbonates is only 240 mbar.

We conclude that, while it is not strictly necessary to invoke carbonates as a CO_2 reservoir, it is likely that between 350 and 2700 g cm^{-2} of CO_2 is stored as carbonate rock assuming the upper limit of ΣCO_2 = 3000 mbar, and the lower limit, ΣCO_2 = 500 mbar. Such a carbonate inventory would represent roughly 2 to 14 wt. % of the regolith column, assuming the regolith depth were 100m. If the regolith were assumed to be 1 km, the lower and upper limits would be 0.3 to 3 wt. % of the regolith.

REFERENCES

1. Anders, E., and T. Owen, (1977), Science, Vol. 198, pp.453-465.
2. Pollack, J. B., and D. C. Black, (1979), Science, Vol. 205, pp.56-59.
3. Pollack, J. B. and Yung, Y. L., (1980), Ann. Rev. Earth Planet. Sci., Vol. 8, pp.425-487.
4. Fanale, F. P. et al., (1982), Icarus, Vol. 50, pp.381-407.
5. Fanale, F. P. and Cannon, W. A., (1971), Nature, Vol. 230, pp.502-504.
6. Fanale F. P. and Cannon, W. A., (1978), J. Geophys. Res., Vol. 83, pp.2321-2325.
7. Zent, A. P. and F. P. Fanale (1986), [Abstr.] Lunar and Planet. Sci. XVII, p. 962., LPI, Houston, Tx.
8. Ballou, E. V., et al. (1978), Nature, Vol. 271, pp.644-645.

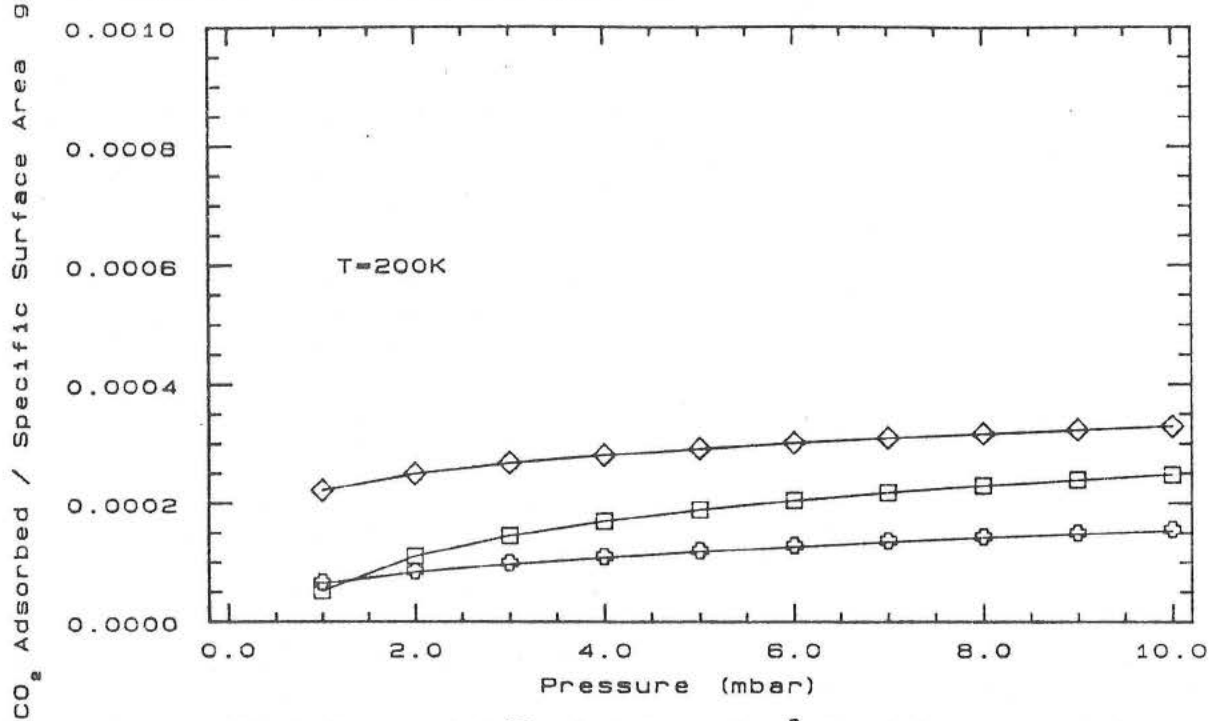

Fig. 1 - The amount of CO_2 adsorbed on each m^2 of particulate surface area for three mafic materials at martian pressures and T=200K. The uppermost curve is for palagonite, the middle for basalt and the bottom for nontronite. When surface area is accounted for the adsorptive capacities of these materials differ by two orders of magnitude.

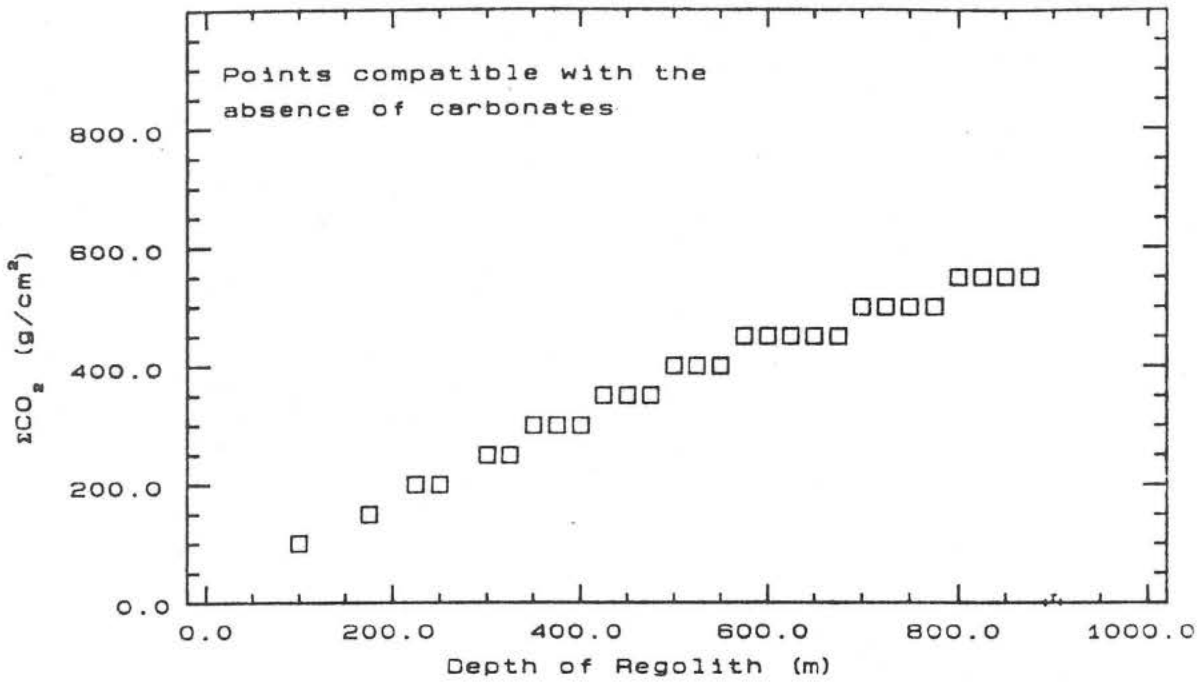

Fig. 2 - The combination of $\Sigma\ CO_2$ and regolith depth compatible with (1) the present atmospheric pressure, (2) the absence of polar caps, and (3) the absence of carbonates. For comparison, $\Sigma CO_2 = 600\ g\ cm^{-2} \sim 240$ mbar.

THERMAL PROPERTIES OF CHANNELS IN THE AEOLIS QUADRANGLE: TOPOGRAPHIC TRAPS FOR AEOLIAN MATERIALS. James R. Zimbelman, Lunar and Planetary Institute, 3303 NASA Road 1, Houston, Texas, 77058.

High spatial resolution thermal data (with individual spot sizes down to 2 by 5 km) for the Elysium and Aeolis quadrangles of Mars have been compiled for comparison with surface features visible in orbiter images (1,2). Data for the Aeolis quadrangle (0^{o} to 30^{o}S, 180^{o}W to 225^{o}W) were used to determine the physical properties of channel materials in an attempt to constrain the processes active during the formation of the channels. The results, however, point to the dominance of aeolian materials in characterizing the thermal properties of the surface materials within the channels. The channels apparently act as topographic traps for transportable aeolian materials, similar to the trapping of dark aeolian materials within craters (3). This conclusion indicates that remote sensing results sensitive to properties of the uppermost several centimeters of the surface may not be directly related to the processes that produced the channel morphology in the Aeolis region.

Two prominent channels are located within the Aeolis quadrangle. Ma'adim Vallis cuts a slightly sinuous path over 900 km long through cratered plains typical of the southern hemisphere of the planet, more or less following the 183^{o}W meridian from 28^{o}S to 16^{o}S latitudes (Fig. 1). Al-qahira Vallis follows a rectilinear path, presumably reflecting tectonic control of zones of weakness within the crust, for over 600 km from approximately 22^{o}S, 200^{o}W to 14^{o}S, 195^{o}W (Fig. 2). Both channels vary in width from approximately 10 km near their headward ends to 15 - 25 km near their distal ends. Both channels flow down a $1/2^{o}$ slope that encompasses the 3 km drop in elevation from the heavily cratered southern highlands to the sparsely cratered northern plains. These channels are large enough to be resolved from their surroundings by the thermal data and they represent the only channel material mapped by Scott and Carr (4) in the Aeolis quadrangle. A digitized version of the Scott and Carr map is included in the Mars Consortium data sets (5). The digitized locations of channel material were used to determine the thermal properties of this unit (2,6).

The distribution of thermal inertias for the channel material (Fig. 3, top) is distinct from the bimodal distribution obtained for 1.7×10^{6} km^{2} of the Elysium and Aeolis quadrangles (Fig. 3, bottom). The channel material has thermal inertias ranging from 3.5 to 12.5 ($\times 10^{-3}$ cal cm^{-2} $s^{-1/2}$ K^{-1}) with a modest mode near a value of 8. This distribution is quite distinct from the low thermal inertias obtained for units in the northern plains while it is similar to the thermal inertias obtained from all of the units in the southern highlands (2). There is no indication of an increase in thermal inertia with distance down the channels, unlike the results from the Kasai Vallis area (7). The channel thermal inertias are in good agreement with thermal inertias obtained for dark intracrater deposits all over the planet (3), except that the channel material does not include the very high thermal inertias (up to 26) observed for some intracrater deposits. The modal value of 8 corresponds to an effective grain size of 0.5 mm representative of medium sand, assuming the surface materials are homogeneous and unconsolidated (8). Low resolution orbiter images (684A01,3,5,7) show the presence of dark materials collected within the channels along much of the channel lengths. The contrast of this material at different visual wavelengths is consistent with the spectral properties

of dark patches and splotches found elsewhere on Mars (9). These results all support the interpretation that dark aeolian material has accumulated between the the topographic confines of the channel walls. This aeolian material need only be 10s of cm thick to completely mask the underlying materials from remote observation at thermal wavelengths. Other portions of the planet might be less dominated by aeolian materials, possibly allowing the properties of channel wall and floor materials to be directly measured.

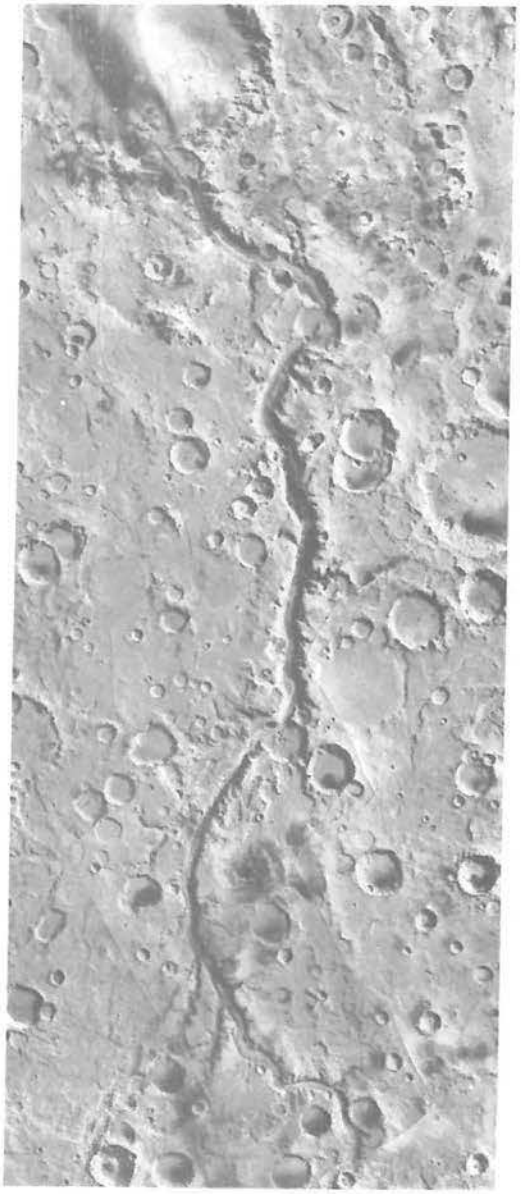

Fig. 1. Ma'adim Vallis. Note the dark material extending north from the mouth of the channel. Area shown is 340 km wide (14°S to 28°S, 180°W to 186°W). Photomosaic is from (10).

Fig. 2. Al-qahira Vallis. Note the rectilinear pattern of the channel. Area shown is 400 km wide (14°S to 23°S, 194°W to 201°W). Photomosaic is from (10).

THERMAL PROPERTIES OF CHANNELS IN AEOLIS

J.R. Zimbelman

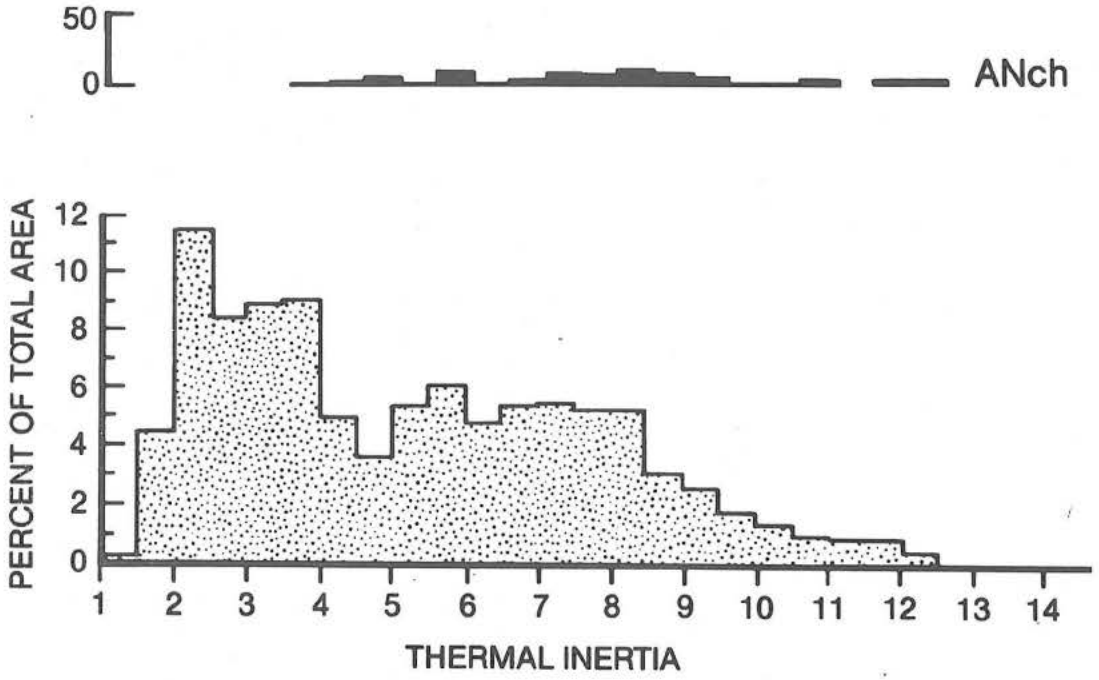

Fig. 3. Thermal inertias for channel material (top, solid) and all of the 1.7×10^6 km^2 measured within the Elysium and Aeolis quadrangles with high resolution thermal data (bottom, stipled). Vertical axis on channel distribution is the number of $1/4^o$ by $1/4^o$ latitude-longitude bins having the thermal inertias indicated by the horizontal axis. Note the wide distribution of thermal inertias (in units of 10^{-3} cal cm^{-2} $s^{-1/2}$ K^{-1}) for the channel materials. The bimodal cumulative distribution results from predominantly low thermal inertias on the northern plains and predominantly high thermal inertias on the southern highlands. The unit name ANch inidcates that the age of the channels is from (A)mazonis to (N)oachian (4). Thermal data are from (2,6).

REFERENCES: 1) Leshin, L.A. and J.R. Zimbelman, Lunar Planet. Sci. XVII, 474-475, 1986. 2) Zimbelman, J.R. and L.A. Leshin, submitted to Proc. 17th Lunar Planet. Sci. Conf., 1986. 3) Christensen, P.R., Icarus 56, 496-518, 1983. 4) Scott, D.H. and M.H. Carr, USGS Map I-1083, 1978. 5) Kieffer, H.H. et al., Proc. Lunar Planet Sci. 12B, 1395-1417, 1981. 6) Zimbelman, J.R. and L.A. Leshin, Lunar Planet. Sci. XVII, 965-966, 1986. 7) Christensen, P.R. and H.H. Kieffer, J. Geophys. Res. 84, 8233-8238, 1979. 8) Kieffer, H.H. et al., J. Geophys. Res. 82, 4249-4291, 1977. 9) Thomas, P., Icarus 57, 205-227, 1984. 10) U.S.G.S., Map I-1215 (MC-23 SE), 1979.

AUTHOR INDEX